CRANFIELD UNIVERSITY

SCHOOL OF APPLIED SCIENCES

MSc ADVANCED MATERIALS

Academic Year 2010 - 2011

SIMON MEANA

PROCESS DESIGN FOR THE FABRICATION OF A PZT STRESS-ENHANCED FIBRE COMPOSITE FOR HUMAN ENERGY HARVESTING

Supervisor: Dr. Chris Shaw and Dr. Stephen Wilson

September 2011

This thesis is submitted in partial fulfilment of the requirements for the degree of Advanced Materials
(NB. This section can be removed if the award of the degree is based solely on examination of the thesis)

ABSTRACT

In the modern world in which we live, we are surrounded by portable electronic devices limited in terms of time and energy, by the batteries they need and utilize. There are abundant types of energies in the environment which, in fact, represent an infinite source, such as the one produced by human. We might take advantage and utilize this energy in our favour and thus, we could have an extra source of power for our portable electronic devices.

This thesis aims to discuss a design method for the fabrication of an active fibre composite (AFC) capable of producing electric energy from body movements, such as the stretching of the thigh when walking or the stretching produced in the thoracic cavity when breathing. These types of movements would exert a bending stress and a force of around 1 N in the composite. An AFC is a composite composed by a polymer matrix, which contains piezoelectric fibres inside, able to produce electric energy when submitted to stress (and vice-versa) and some electrodes which are responsible of conducting the electricity between the fibres and either the battery or directly the electronic device.

As a result of this research, a promising method has been proposed in order to fabricate the composite utilizing SBX^{TM} liquid resist emulsion, PZT5A piezoelectric fibres and an interdigitated electrode (IDE). For this IDE, three techniques have been attempted: evaporation, sputtering and screen-printing, made from a combination of gold and chromium, aluminium and from silver epoxy respectively.

In this thesis, two polymers namely PDMS and SBX have been considered as a matrix, SBX being more adequate. Two different ways to align the fibres in the polymer matrix were proposed, aligning with designed masks and with a rig frame. Tests results and graphs have been generated with regard to the behaviour of SBX in terms of shrinkage when casted and the relation between the rotational speed and thickness when spun. This investigation also contains data with relation to the curing and development of the SBX, in addition to mechanical tests done to different samples with a Deben Microtester. Eventually, some ideas have also been included on how to arrange carbon or glass fibres around the PZT fibres in a later stage, so as to enhance the stress by applying increased stress in different places along them.

ACKNOWLEDGEMENTS

I would like to thank first to both of my supervisors: Dr. Stephen Wilson because his pragmatic vision of the project was key to buck my ideas up and to Dr Christopher Shaw because his dedication to this project, his comprehension and because his tricky questions were key to push this project forward and to promote my curiosity in order to look for my own way to carry on the research. I very much enjoyed discussing with him the issues and knowledge I gained during the thesis. I would also like to have some words for Andrew Stallard and Matthew Taunt. I will especially not forget their kindness and help they offered me when I asked for materials, tools or doubts about AutoCAD. I also have grateful words to my parents. To my father, Manolo Meana, although he was not always aware, he always knew how to challenge me to push forward. To my mother, Irene Garay, for her infinite faith on me was the source of energy that I needed to overcome whatever type of problem, no matter how difficult it was. Without her it would have been impossible for me to achieve what I have achieved and to become who I am nowadays. To all the members of my family, because they always motivated me in different ways, opening my eyes and making me realise of all the possibilities within my reach. Finally, to all the members of the R-club: Alejo, Antonio, Cyril, David, Javier C., Javier S., Javier M., Marina, Pierre, Sarah and Bea. They were my family at Cranfield and it would have been an utterly different thing without them. My grandfather, Simon Garay, used to say: surround yourself with better people than you in different aspects because you will learn from them how to improve and become a better person. I am glad to say that the RClub made his words to have sense.

TABLE OF CONTENTS

LIST OF FIGURES

LIST OF TABLES

LIST OF EQUATIONS

1 INTRODUCTION

1.1 Aim & Objectives

1.1.1 Aim

To create a knowledge base for the design of a new flexible energy harvesting prototype able to produce electricity from low frequency movements by incorporating enhanced localised stress points within the design in order to supply energy afterwards to a small portable device.

1.1.2 Objectives

- To collate a state-of-the-art understanding through a review of the latest scientific literature on wearable energy-harvesting textiles and related technologies
- To identify a feasible and useful material for the composite to be created.
- Come up with a feasible fibre arrangement in order to get the maximum energy from the fibres.
- Implement a process design and a test programme for the composites.
- Gather reproducible stress data to support the localised stress design.
- Field-test the chosen composite as a prototype.

Design specifications

- Forces applied must be equal or less than 1 N which is a hypothesis of approximately the maximum force that can be done with the thigh or when breathing.

- The thickness of the composite must be around 1mm or less so as not affect the comfort of the individual.

1.1.3 Enhancing the stress

One of the motivations of this project is to enhance the stress applied on the PZT fibres. Three arrangements were thought to be good for this purpose. The

arrangements shown in Figure 1 and Figure 2 would require flexible and stiff fibres so that to be embedded around the PZT fibres. As it can be seen in these cross-section figures, the idea is to take advantage of stresses perpendicular to the direction of the PZT fibres, indicated by red arrows, so as to increase the stress on them either by applying compressive stresses such as in Figure 1 or a bending stresses such as in Figure 2, indicated in both cases with blue arrows.

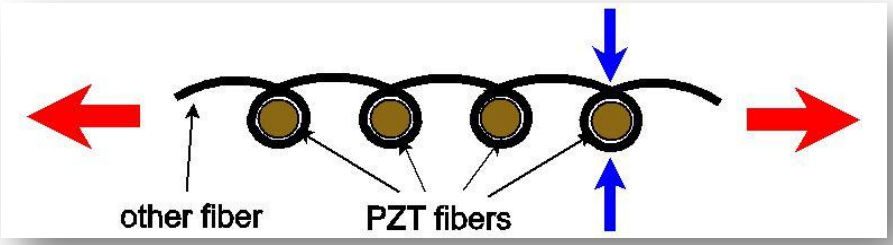

Figure 1: Fibre arrangement 1

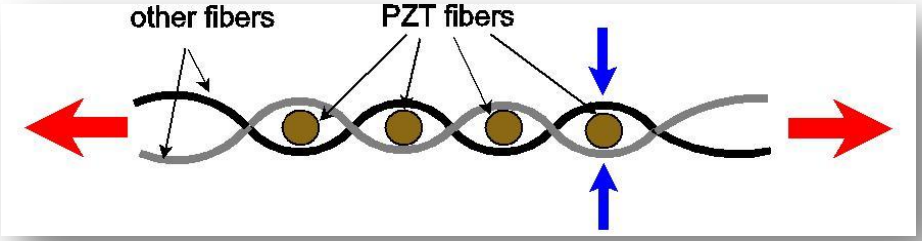

Figure 2: Fibre arrangement 2

The third fibre arrangement (Figure 3) was meant to be for a multilayer composite. Fibres are aligned in right angle to the PZT fibres and would submit them to different bending stresses along them, as shown by the blue curved lines in Figure 3. Rigid fibres such as carbon fibres could be utilized to do so, always remembering that they are conductive and, consequently, they have to be isolated from the PZT fibres.

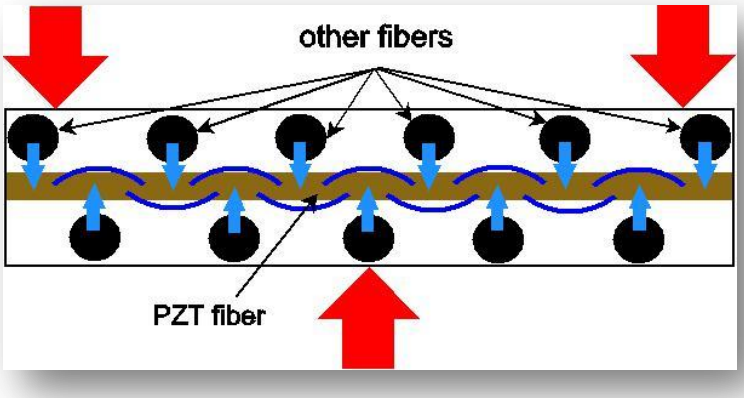

Figure 3: Fibre arrangement 3

This option was the selected for the process to be built around it, as it seemed the more feasible way taking into account factors such as the alignment and how to make contact with the electrodes.

2 LITERATURE REVIEW

2.1 Energy Harvesting

Energy harvesting, so-called energy scavenging or power harvesting is the term to refer to the energy recovering from the environment transforming it, for instance, to electrical energy (1). Though it could apparently seem that the human being has been only trying to get electricity to recover these natural resources, in fact, it is not. Several activities from our life involve the conversion of some kind of natural power to mechanical energy, for instance, a very simple example is that when sailing, the wind power is converted to kinetics energy for the boat. There are a lot of actions and processes around us in which energy is spent and part of this energy could be recovered. The most common energies to scavenge come from are wind, temperature or concentration gradients, water power. Large devices have been made in order to adapt these energies to somewhat useful for use by means of wind farms, solar panels and water plants. However, besides these large-scale exploitations where amounts of power are involved, there is an increasing interest in small process where no

such powers are involved, as for example, recovering the kinetics energy lost when we stop the car. Small devices are needed in order to do so and micro-electronics as well.

Nevertheless one question arises, why is it of interest these micro-devices? Mainly two big reasons can be stated (1).

1. Infinite source of energy would mean indefinitely energy provision to whatsoever attached to it (e.g. sensors), subjected of course to the efficiency and life of the device.
2. It would lead to the inconvenience and cost of changing batteries and it would also then reduce the waste produced by this (environment friendly)

It is because of this that a global research effort is currently underway to produce more efficient of these electronic systems for sensing and communications. The expansion of use of portable electronic devices has resulted in larger supply requirements for the batteries to reach. These batteries add weight and volume to the device and moreover the necessity of recharging them. Although there is an effort on making the batteries life last longer, the increasing energy that these electronic devices are demanding makes difficult to reach the purpose.

Clear progress is being made in several areas, namely ultra-low power integrated electronics (2) (Gaurbio, et al, 2009), efficient power storage such as batteries and super-capacitors (Barrade et al, 2010) (3) and in energy harvesting techniques (4). This last one represents an unlimited power source and a different approach to enhance the batteries or even get rid of them in a future.

Future systems will undoubtedly operate with a much lower power budget and hence a major part of the total effort is focused on creating autonomous and semi-autonomous power supplies, for example through recovery of small amounts of electrical energy from random sources as it may mean that conventional batteries could be dispensed with completely for some

applications or that their useful lifetimes could be very much longer. Some wireless sensor networks, for instance, demand very low power in order to work. Energy harvesters could give enough energy to these devices so that to be autonomous.

From the point of view of a more sustainable world, energy harvesters are a good solution for the future. They get their energy from the surrounding environment reducing the impact on it. Current efforts are done in producing electricity from forms like flowing water, wind, sunlight, kinetic energies from mechanical processes, etc.

We could include these forms of energy in four types of sources: thermal energy, optical energy, acoustic energy and mechanical energy.

Optical energy is probably one of the most abundant in the world. We just have to think about the large amount of radiation from the sun reach the earth. In order to harness this energy, very often photovoltaic cells are used. To scavenge energy from a thermal source, a gradient of temperatures is needed. In the case of an acoustic source, then a transducer capable to transform pressure differentials into electricity is needed. The last of the sources, mechanical energy, is probably the one which gives more paths to get energy from. This is because it relies on external vibrations, especially sinusoidal cyclic vibrations. Four general methods exist to transform energy from mechanical vibrations: Using electromagnetic transducers, electrostatic transducers, magnetostrictive and piezoelectric transducers.

C.A. Featherston, et al (5) discuss that piezoelectric represent one of the best options. They comment that while piezoelectric transducers do not have moving parts, the rest of them (electromagnetic, magnetostrictive and electrostatic) do have, making them more vulnerable to faults and breakages meaning maintenance work.

In the paper of Blackstone ultrasonics (6) they compare magnetostrictive transducers against piezoelectric transducers for ultrasonic applications.

Although both of them showed high frequencies, they concluded that piezoelectrics are much more efficient than magnetostrictive. The reason was, mainly, because the latter needs from two steps: transforming from mechanical energy to magnetic one and afterwards from magnetic to electricity whilst piezoelectric transducer does it immediately.

2.1.1 Bodily Harvesting

Our body can be compared with a machine that is the whole day working. Our day-to-day tasks imply an expenditure of energy which we recover by eating. The human body consumes minimum around 4 kJ/kg*h (7). It means that an average person weighing 70 kg spends at the end of day the amount of 6720 kJ equivalent to 77.77W. This is confirmed by Starner (8) where he says that the energy expended while sleeping is 81W. In his work, we can see that the body is able to generate power as high as 1600W. The body can consume energy quite rapidly in daily activities. In Table 1 it is shown the energy expenditure for some of them. However, there is also quite energy wasted in vibrations, heat, etc. This energy could be partially recovered by wearable electronics. In order to do so, different approaches have been taken and tried.

Activity	Kilocal/hr	Watts
Sleeping	70	81
Lying quietly	80	93
Sitting	100	116
Standing at ease	110	128
Conversation	110	128
Eating a meal	110	128
Strolling	140	163
Driving a car	140	163
Playing violin or piano	140	163
Housekeeping	150	175
Carpentry	230	268
Hiking, 4 mph	350	407
Swimming	500	582
Mountain climbing	600	698
Long-distance running	900	1048
Sprinting	1400	1630

Table 1: Energy associated to different day-to-day activities

Body heat, blood pressure, finger motion, breathing, walking and so on are good action to take advantage of the energy involved. Walking is likely the best to try because, a priori, is the one where more energy can be obtained. In Figure 4 we can see that up to 67 W are used in the simple act of walking. In his paper, T. Starner (8) states that up to 5-8 W out of this 67 may be recovered.

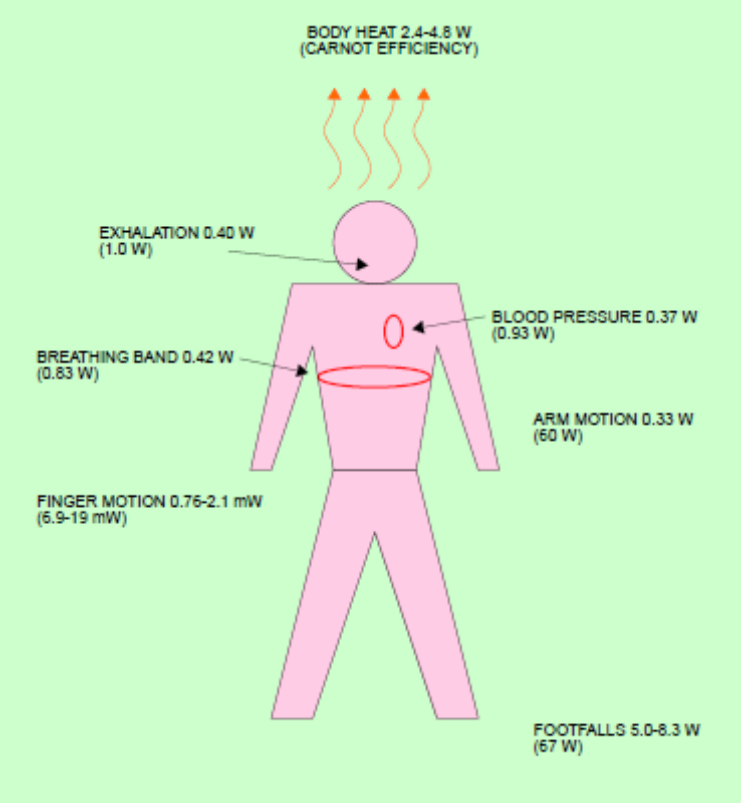

Figure 4: Energy expended in specific bodily movements (8)

Further investigation, stepping in a wide range of possibilities to scavenge energy from different activities in which the human body is involved, was realized by Paradiso and Staner (9). Details about the energy involved and efforts and prototypes done in each case so that to harvest every type of energy are given. To mention some activities they pay attention to, here are some examples: Power from blood and pressure, inertial microsystems, energy from typing, energy for arm motion and breathing.

2.2 Piezoelectricity

The term ‘piezoelectric’ comes from the Greek word ‘piezein’ meaning ‘squeeze’ or ‘press’. Piezoelectricity is the effect by which some materials generate an electric potential in response to an applied mechanical stress (10). It was first discovered by Pierre and Jacques Curie in 1880.

Piezoelectric materials may be separated into two groups: ferroelectric and non-ferroelectric, typified by polymers and ceramics. Inside the group of ceramics we can find crystalline structures with piezoelectric properties such as Perovskite crystals, Rochelle salt and quartz.

They are used typically as transducers from mechanical energy to electrical energy or vice-versa. One of the first applications was sonar (11), where a piezoelectric crystal generates an acoustic wave from an electrical impulse, this sound wave is reflected when hits an object and, the reflected pressure wave is reconverted into an electrical signal. Comparing the time delay between the sent and received electrical signals, it is possible to know the distance at which the object is.

As it can be seen these ceramics has been used since long time ago. Though perhaps we do not realize, they are in common items that we normally use. For instance, when we press the button of a classic cigarette lighter, we are generating friction by rubbing against a piezoelectric crystal, producing a high voltage that leads to a spark (12). Piezoelectric materials can be found in different fields such as the automotive (airbags), medicine (ultrasonic therapy), computers (hard disk) and consumer (smoke detectors) (11). Examples of commercial piezoelectric crystals are potassium niobanite ($KNbO_3$), barium Titanate ($BaTiO_3$) and lead titanate ($PbTiO_3$).

On the other hand, there are the piezoelectric polymers. The most common piezoelectric polymer, and probably the most efficient, is polyvinylidene fluoride (PVDF). It is a semi-crystalline polymer and has a really high molecular weight (around 10^5 corresponding to 2000 chemical repeating units (13). Provided its strong dipoles within the polymer chain, it has piezoelectric characteristics. Depending upon the type of chain conformation, three forms of PVDF are known: alpha, beta and gamma phases. Its Curie temperature is around 110ºC(5). One of the best advantages from the piezoelectric polymers is their flexibility. They can accommodate up to 2% of strain or even higher compared to the 0.1% of ceramics on average. Moreover, they are cheap; the cost of producing polymers is very low compared to other materials. Some piezoelectric

polymers can be a great deal less expensive than crystals. Nevertheless, due to their low electromechanical coefficients constants, it is needed stress over large areas so as to produce a considerable amount of energy. In Table 2 , it can be seen that the piezoelectric constant, for instance, from PVDF is around 2 and 17 times less compared to some piezoelectric ceramics (PZTs). In terms of energy that can be produced, they are above natural crystals but below ceramics. In Figure 9, they are compared to some specific PZT fibres. Having said this, piezoelectric polymers do not represent, currently, the most efficient way to produce energy from bodily movements. In the project done by Guillot et al (1), a piezoelectric polymer sensor was tested equally as PZT fibres and a ceramic fibre composite. Their result was that assessing the energy produced per volume, 30 PZT fibres and the composite sensor they used generated about 7 times and 49 times respectively more energy than the PVDF polymer sensor.

2.2.1 Lead Zirconate Titanate (PZT)

PZT (a lead zirconate titanate ceramic) has the perovskite crystal structure (Figure 6). Its composition depends upon the quantity of Zirconium (Zr) and Titanium (Ti) but always under the formula $Pb(Zr_xTi_{1-x})O_3$ (14). Then, changing this x factor the crystalline structure can be modified and, hence, its properties. In Figure 5, the phase diagram for PZT can be seen.

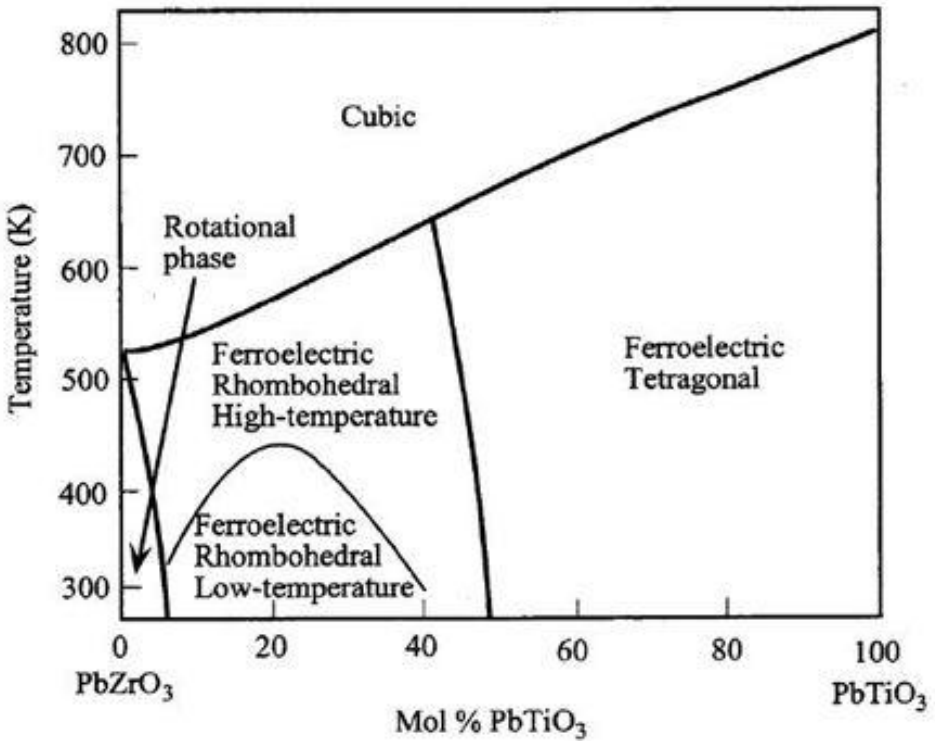

Figure 5: PZT phase diagram (14)

One of the more efficient piezoelectric materials and most commonly used in piezoelectric transducers are lead zirconate titanate ceramics, due to its widespread commercial availability and their high electromechanical coupling coefficient 0.5-0.7(15) (the coefficient of quartz is around 0.1). Natural materials such as the Rochelle salt, quartz and tourmaline present low piezoelectric properties (16). Therefore, ferroelectric ceramics like PZT or barium titanate are of interest given their enhanced piezoelectric effect and reflected in their good performance per cost. PZT's Curie temperature is typically between 300 and 400ºC (17).

The reason why it has piezoelectric properties is because a mechanical stress moves the cations Ti^{4+} or Zr^{4+} from the center of the unit cell, creating as they move a dipole and, then, electrical energy. In Figure 6, it can be appreciated how the cation in the center has been moved up polarizing the crystalline structure.

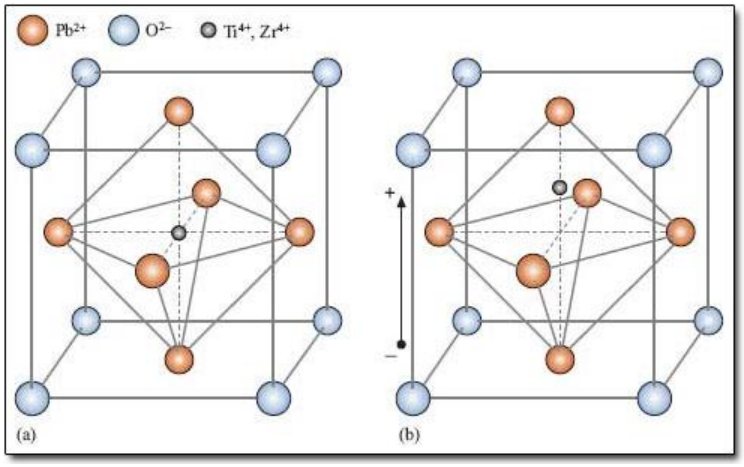

Figure 6: Molecular structure of a PZT (18)

2.2.2 Piezoelectric fibres

Fibres give one of the best advantages over monolithic materials: anisotropy. They allow composites to have different structures and to select the direction of either actuation or sensing that we would like to have. In addition to this, fibres allow us to utilize materials in a manner where they would not perform as a structural component. Thus, they can reduce brittle fracture problems that are likely to occur in monolithic materials or just let us to fabricate something rather more flexible and resistant to failure if used, for example, as a part of a composite. Consequently, fibres, seen as functional components, give an opened window in terms of material design (different fibre shapes and structural conformity and also the possibility to combine them with other materials by means of a composite). Therefore, fibres represent a promising approach to fabricate items with enhanced properties (higher specific strength, higher stiffness and strain to failure (19).

2.2.2.1 Poling of the fibres

When a ceramic forms, it does it with a randomised domain structure (left hand picture from Figure 7). The areas with different crystalline orientations are called Weiss domains. The process of aligning the domains is known as poling. A good definition would be that poling is the process that induces directional piezoelectric properties in a ceramic, the orientation of which is responsible of

the mechanical and electrical axis (20). The ceramic is exposed to a strong electric field is applied to do induce this orientation. It is very common to heat the ceramic to a certain temperature well below the Curie temperature, typically around 130ºC (21)(22). This increment enables the domains to be more mobile and they align preferentially with their axis of polarisation in the direction of the applied field. The ceramic is then cooled down with the external field still active. This leads to freeze the new domain structure in place and the ceramic ends up with directional piezoelectric properties or, in other words, remnant polarization or macroscopic polarization (see Figure 7). Theoretically speaking, during the poling process, the materials are switched between energetically equivalent states (metastable states) through which a net polarization is achieved in the whole material.

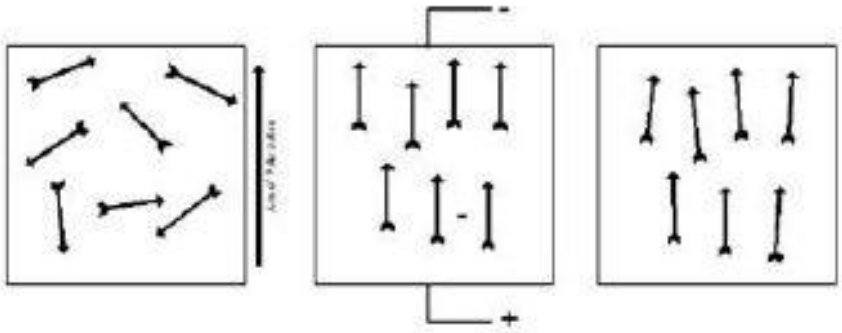

Figure 7: Alignment of different Weiss domain due to voltage applied

The polarization (P) of a piezoelectric material, after being poled, is referred to the potential difference originated by a stress applied. This polarization is directly proportional to the stress applied and the constant of proportionality (d) is called piezoelectric coefficient (see Equation 1, where σ is the stress applied).

$$\boldsymbol{P = d \cdot \sigma}$$

Equation 1: First polarization equation

Polarization is also referred as the charge created per unit of area (see Equation 2).

$$\boldsymbol{P = Q/A}$$

Equation 2: Second polarization equation

There are three general modes to cause a piezoelectric response of a piezoelectric material (23), applying a lateral force, a shear force or applying a force through the thickness, which can be seen in Figure 8.

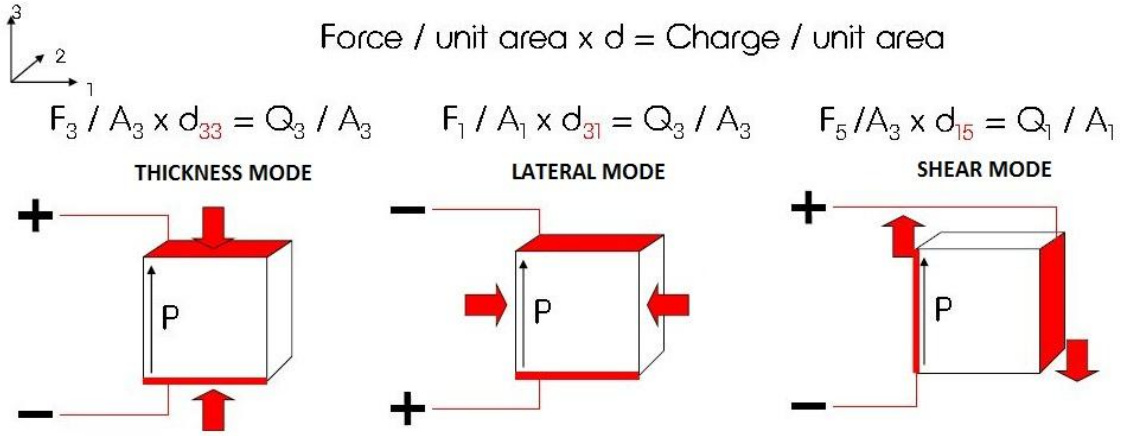

Figure 8: Different modes to cause piezoelectric response

Provided that the nature of the stress can be tridimensional, the piezoelectric coefficient d depends also upon the direction the stressing direction and the direction in which the electrical response is measured. This means it that can take the form of a matrix of coefficients.

At present, to check the capability of a piezoelectric material to transform mechanical energy to electrical energy is of special importance. It can be done looking at the two main parameters that will characterize the material: the piezoelectric charge coefficient d_{xy} and the permittivity of the material. Both of them are parameters related to the performance of the materials and its efficiency in converting stress to electricity.

The former indicates the polarization that the stress induces in the piezoelectric material or, on the other hand, the strain experienced by the material when it is submitted to an electrical field (24). The x subscript refers to the direction in

which the polarization is taking place when a stress is applied on the direction of the y subscript. Six directions are used in the normal notation, 1, 2 or 3 correspond to the classical Cartesian axes whilst 4, 5 and 6 correspond to the shear direction, rotations around the Cartesian axis. When two subscripts are used, it is to indicate relationships between electrical and mechanical parameters being the first the direction of the input and second the direction of the response.

The latter, the permittivity, so-called absolute dielectric constant (Ɛ) is the value of how much dielectric displacement occurs per unit of electric field. In fact, this value is also replaced by the relative dielectric constant (K) which represents the proportion between the amount of charge that the material is able to store and the absolute dielectric constant (Equation 3).

$$K = \frac{C_0 \cdot h}{\varepsilon_0 \cdot A}$$

Equation 3: Formula of the relative dielectric constant

C_o: measured capacitance at 1 kHz (F).
A: area of the electrodes (m^2)
ε_0: Relative permittivity of free space (8.854 x 10^{-12} F/m)
h: distance between electrodes (m)

Other parameters also of relevant importance to take into account are the coupling coefficients (k_{ij}) and the voltage coefficients (g_{ij}) (24). The coupling coefficient is a measure of its effectiveness and, in fact, is a percentage that gives an indication about how much electricity is transformed to mechanical energy per input of electrical energy (15). A comparison between different piezoelectric materials is given in Table 2, where some data was compiled by the California Institute of Technology. Note that for PZT, the properties can broadly change depending on the x factor from the PZT composition formula discussed in the PZT section (page 13).

Material	Piezoelectric Constant (d(pC/N))						Dielectric Constant			Curie Temperature (ºC)	Maximum k (Coupling coefficient)
	d11	d14	d15	d31	d32	d33	ε	ε1	ε3		
Quartz	2.31	0.73	-	-	-	-	-	4.52	4.63	550	0.1
PZT (depending on composition)	-	-	494-784	-94 to -274	-	80-593	-	-	425-1900	193-490	0.69-0.75
PVDF (Kynar)	-	-		23	4	-35	4	-	-	>Melting Point (150)	0.2
ZnO	-	-	-12	-4.7	-	12	-	-	8.2	-	-
Sol-gel PZT	-	-		-88.7	-	220	1300	-	-	-	0.49

Table 2: Chart comparing different properties from PZT materials (25)

In Figure 9, the output power generated by some of the most utilized and recent piezoelectric materials is given and compared by means of a bar chart and shows how PZT 5A fibres have superior normalized power output compared to PZT 5H fibres, polyvinylidene fluoride and barium titanate.

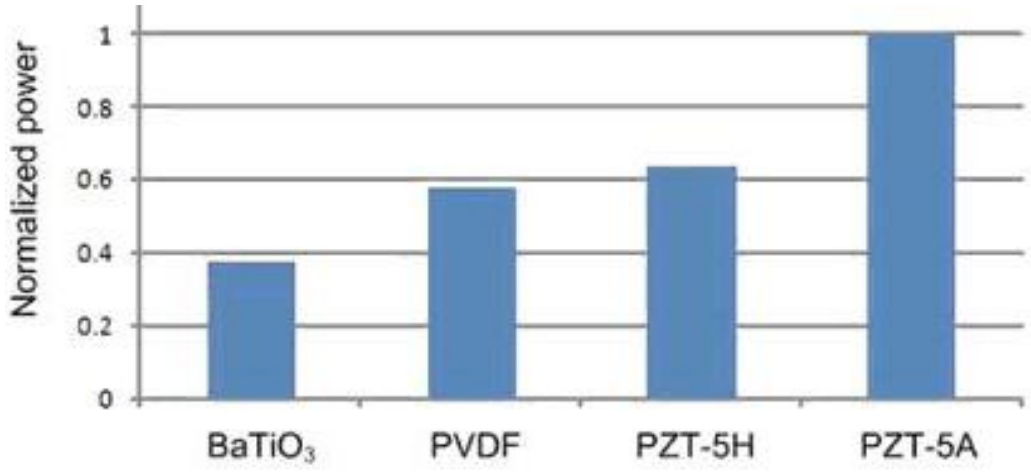

Figure 9: Comparison of the power generation from different piezoelectric materials (10 p. 14)

When selecting a piezoelectric material not only do the piezoelectric properties must be taken into account but properties like flexibility, elastic behavior, cost or ease of manufacturing are also of importance. De Rossi et al (26) made a good

summary (Figure 10) of the typical PZT materials used in transduction mechanisms.

Materials		
Organics	Inorganics	Hybrids
Polyvinylidene fluoride (PVDF)	Lead zirconate titanate	Inorganic piezoelectric particles
Polyvinylfluoride (PVF)	($Pb(Zr,Ti)O_3$) (PZT)	embedded in polymer matrices
Poly(vinylidene fluoride–trifluoroethylene)	Lead based lanthanum-doped zirconate titanate	e.g. PZT/PVDF–HFP
(P(VDF–TrFE))	((Pb,La)(Zr,Ti)O3) (PLZT)	e.g. PZT/polyuretnane (PU)
Poly (vinylidene fluoride–hexafluoropropylene)	Quartz (SiO_2)	
(P(VDF–HFP))	Zinc oxide (ZnO)	
Poly(vinylidene fluoride–tetraflouoroethylene	Barium titanate ($BaTiO_3$)	
(P(VDF–TFE))	Potassium niobate ($KNbO_3$)	
Polyamides	Lithium niobate ($LiNbO_3$)	
e.g. Nylon-11	Lithium tantalate ($LiTaO_3$)	
Liquid crystalline polymers	Bismuth ferrite ($BiFeO_3$)	
(flexoelectricity)	Triglycine sulfate (TGS)	
	$Ba_2NaNb_5O_5$	
	$Pb_2KNb_5O_{15}$	

Figure 10: Most used materials for some mechanical transducers (26)

2.3 Piezoelectric fibre composites

Fibre composites are of interest because their advantage over conventional monolithic materials given their low density and their high flexibility (27). They allow us to combine the best properties from different materials and, as a consequence, it has increased the interest of implementing ceramic materials into movable parts (piezocomposites). Not only did this augment the interest but their low cost and ease of conformation in addition to the anisotropic properties from the fibres compared to monolithic piezoelectric materials.

Lead, zirconate titanate (PZT) fibres are typical fibres used in recent works such as the 1-3 composites. However there is an extensive list of piezoelectric materials that have been used like modified $PbTiO_3$ and $PbNb_2O_6$.

Presently, different approaches are being taken to harvest energy form body movement, and fibber composites represent a good part from them. Priya and Inman give well summarized in the overview in their book (28 p. 17). Showing

the latest commercially available bulk transducers structures (Figure 11) which, from their point of view, are more promising. Note that not all of them are fibre composites but most of them.

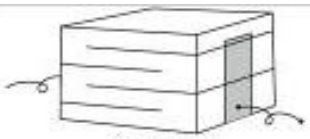 Multilayer	Supplier example: Morgan electroceramics, APC International, Tokin, PI. Characteristics: low frequency (~10 Hz), suitable under large uniaxial stress condition, easy mounting.
 Macro Fiber Composite (MFC)	Supplier example: Smart Material. Characteristics: flexible, both d_{33} and d_{31} mode possible, low strain high frequency application, large area coverage, can be used as a bimorph element.
 Thunder	Supplier example: Face International Characteristics: Various curvatures and heights possible providing wide range of stress amplification, suitable for very low frequencies (~1 Hz).
 Bimorphs	Supplier example: APC International. Characteristics: resonance frequency can be tuned in the range of 5–100 Hz, used in various configuration such as cantilever, end–end clamped, etc.
 Amplified Piezoelectric Actuator	Supplier example: Cedrat Characteristics: higher efficiency under large stress, resonance frequency can be tuned to lower ranges (~100 Hz).
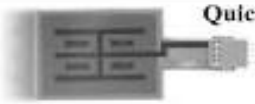 QuickPack	Supplier example: Mide Characteristics: similar to bimorphs but easier mounting, wide bandwidth, widely used in cantilever configuration
 Rainbow	Characteristics: curved surface resulting in higher charge under a given stress level, can be stacked to amplify charge.
 Moonie  Cymbal	Supplier: Micromechatronics Characteristics: metal caps protect ceramic allowing application under high stress levels, higher charge due to stress amplification, resonance frequency can be tuned by changing cap dimensions and material.

Figure 11: Different Energy harvesters (28)

On the other hand, there are drawbacks to deal with when choosing a piezoelectric fibre composite to be made, and are principally two: the high

voltage need and the difficulty of handling and processing these costly fibres (29).

2.3.1 Active Fibre Composites (AFC)

AFCs were discovered by Bent and Hagood (30 pp. 909-913). Characteristic from this type of composites is that the piezoelectric fibres are uniaxially aligned, allowing maximum volume fraction and causing high stiffness in this direction (29). An AFC is comprised basically by three parts: The active material, the matrix material and the electrical connections (31), which can be seen in Figure 12. The active materials are the piezoelectric fibres, which generate the electrical current and control the stiffness of the composite and are embedded into the matrix material. This matrix material tends to be a polymer, which is responsible of the shape and structural integrity of the composite as well as fracture resistance. The electrical connections (electrodes) between the fibres play a key role because depending on where they are placed, the charges generated could be balanced. They also help to align the electrical field generated.

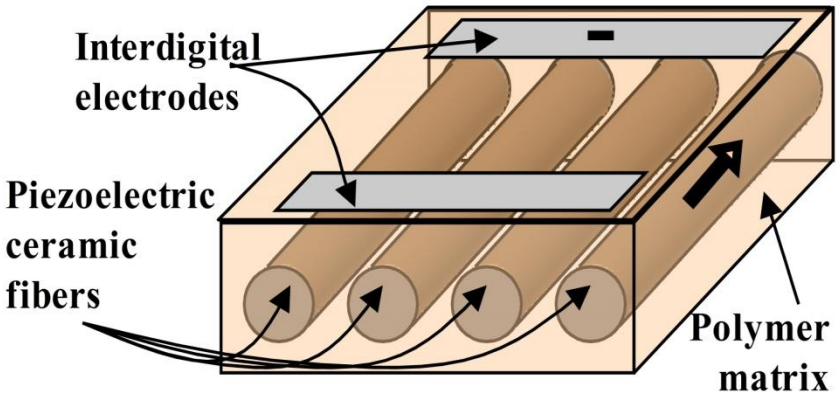

Figure 12: Schematic of an AFC (27)

AFCs hold 4 main advantages monolithic ceramics (32). First, they have directional sensitivity that allows making specific actuators or sensors seizing this property and with no need to think about special ways to transmit the actuation through any type of mechanism. Second, provided that they work in a

longitudinal manner they yield much more than normal monolithic piezoelectric materials. Third, and probably one of the most powerful advantages, provided the possibility to insert layers and films inside the AFC, their stiffness, toughness, resistance to damage can be very much enhanced. The latter advantage is that they are easy to be fabricated and can be fabricated in large areas leading to low cost production.

There are two types of AFC depending on their type of application, actuators and sensors (33), though the first group can be used as sensors as well in some cases. Actuators are defined by their ability to change their shape or strain when an external stimulus is applied whereas sensory AFCs respond with a change in a specific property such as the electrical conductivity. These two types of AFC, however, are not totally different.

Applications for actuators are often in the field of structural actuation (vibration suppression, contour and acoustic control) for instance, as noise reducers or in adaptable mirrors and lenses. They are capable to adapt their shape and this can be used to .On the other hand, sensors are often found in structural health monitoring systems, e.g. impact or damage detection or acoustic emission techniques to detect crack propagation.

2.3.2 Fibre volume Fraction

A priori, the idea of the more fibres in the composite the better in order to get the most electricity from it could seem potentially plausible. Nevertheless, Bowen et al (32) have a great debate in their paper about the relation between the amount of fibres in a composite and its mechanical properties and failure mechanisms. They specifically look at the case when the composite is stretched in the same direction of the fibres direction. They state the importance of the matrix and fibres having a similar Poisson's ratio (the relation between the longitudinal strain and transverse strain when submitted to a stretching force). Once selected the PZT fibres (in their case PZT-5A), and having a matrix that matches that requirement, they claim that two regimes that lead to failure might occur, shown in Figure 13, depending of the volume fraction of the fibres. First

of all, they describe two important thresholds, the minimum and the critical volume fractions (V_{min} and V_{crit}). The critical volume is associated with the minimum value of the volume to ensure that the strength from the composite is going to be greater than the matrix alone. On the other hand the minimum volume fraction it is just the transition between both regimes (formulae are given in their paper in order to do all the calculations of the commented factors). When above the minimum value we are in regime one, and then the failure mode is dominated by the fibres meaning that the whole composite fails provided that the matrix is unable to withstand the extra load transferred from the fibres, in case of any of them would break.. On the other hand, when the volume fraction is below this V_{min}, the matrix can support the load meaning that there is no failure of the whole composite.

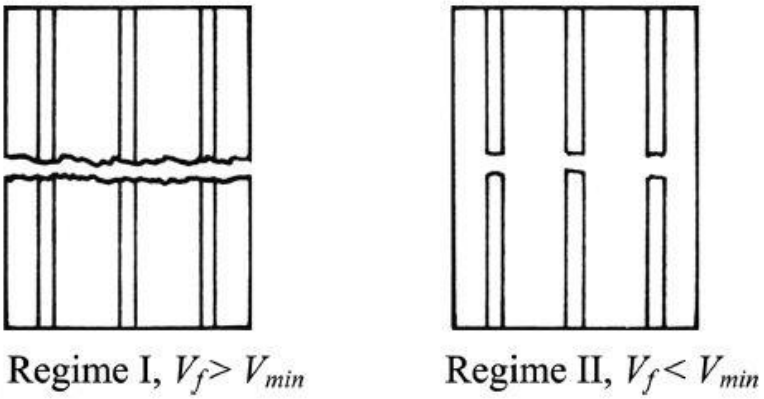

Figure 13: Diagram of possible failure modes depending on the volume fraction(32)

Their results show that there is a range of optimum values of volume fractions. The relation between the d_{33} and the fibre volume fraction is a curve. However, relation between the fibre volume fraction and the effective stiffness is linear. This means that there was a value from which the electric response of the fibres was only increased slightly and, alternatively, the stiffness increased in the same ratio. Hence, it is not worth to increase the fibre volume beyond this optimal point at it implies an important increase in the stiffness but not in the d_{33}.

2.3.3 Matrix Material

The matrix material is the material to be the bulk of the composite, typically an epoxy resin or belonging to the epoxy family (34), (35), (36), (37). Apart from epoxies, PDMS is also a known matrix material given its flexibility, non-toxicity and the possibility to use fillers to enhance specific properties of it (38)(39). Polydimethylsiloxane (PDMS) is a silicon-based polymer which means that its chemical repeating unit is formed by silicon and oxygen. PDMS is probably one of the most used silicon-based polymers. In addition to the properties already mentioned, it is optically clear and inert and viscoelastic.

The matrix material has the role to absorb some of the energy received by the composite to prevent the fibres, which are quite brittle. It is desired for the matrix to have low viscosity so that to ease the process of manufacturing helping to wet thoroughly the fibres and the electrodes in a compact piece. Provided that electrical current is flowing between the electrodes and the fibres, it would also be necessary and desirable a low dielectric constant so as not to lose energy or reduce the electric field (33). This is of importance especially if we take into account that this generated energy is usually relatively low, between 200 and few thousands of microwatts (40). Definitely the matrix could have an influence in the electrical field involved.

2.3.4 Interdigitated Electrodes (IDE)

In the case of AFCs there are specific types of electrode which represent a large advance to monolithic electrodes, the Interdigitated Electrodes (IDE).

“The interdigitated electrode configuration effectively aligns the electric field with the long axis of the piezoelectric filaments to enhance the directionality of the electromechanical response” (31)

They also could prevent to have cancelling of charges if fibres are bended in different directions along themselves. In Figure 14, it has been exaggerated the case of a fibre subjected to different stresses. Looking at the top surface of the fibre, it can be seen that the zone that the red arrow is pointing is submitted to

tension whereas the zone pointed by the blue arrow is submitted to compression. The different stresses could cause the generation of, respectively, different charges in these two areas of the piezoelectric material and, hypothetically, it could lead to the problem of balancing charges.

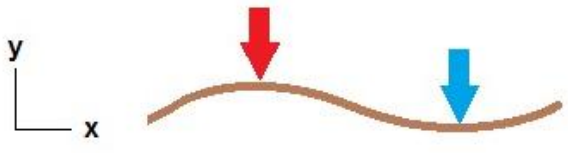

Figure 14: Illustration of a fibre submitted to different stresses

The best characteristic of IDEs is, definitely, that the electric field is applied in the direction of actuation and the fibre direction, which results in a larger piezoelectric coefficient (32). This could help to regulate the sensory or actuation responses. In the work of Bowen et al (32), it is suggested that using IDEs in combination with ceramic fibres could enhance toughness and damage tolerance of the composite. This is because the fracture of either individual fibres or part of a fibre would not lead to the failure of the whole composite.

In Figure 15, it can be observed how the electrical field goes between the different fingers of an IDE and along the PZT fibre. It important to mention that even a little amount of the resin between the fingers and the fibres can heavily affect this field. Hence, the efficiency of the AFC would be a great deal lower than, in theory, it could be (36). Besides the power required reaching certain grade poling of the fibres would be much higher. There is another issue regarding the interspacing of the IDE fingers, the possibility of having breakdowns. Probably, it could be possible to reduce the problem of having them by reducing the space between the fingers of the IDE. However, if they are too close “large electric field concentrations develop at the electrode edges, and when electrodes are too close to the brittle active elements the stress concentration set up in the fibres via the piezoelectric effect leads to a risk of brittle fracture.”(33). Nelson (33) also remarks in his paper that it exists a “dead zone” below the electrode fingers due to the field is smaller and perpendicular

to the actuation direction desired, producing little strains. He also proposes two ways to try to prevent it, the former is reducing the finger width, which would reduce the current carrying capabilities, and the latter is increasing the fingers interspacing, which would increase the voltage to pole the fibres. This problem is also referred by Rossetti et al (31) in the work of about recent advances in AFCs technology. They mention a parameter defining the overall composite architecture: the ratio between the electrode pitch and the fibre diameter. Though there is no proper explanation of the pitch in the paper, a normal definition of it is the thickness of the electrode plus the spacing or what is the same the distance from the center of one electrode to the center from the subsequent one. Their discussion goes through the relation between this parameter and the voltage obtained and the efficiency. For their composite they tried different ratios between the pitch and the thickness of the fibres in the quest of an optimum value. For lower ratios, the whole composite can act at lower voltages compromising a lower efficiency due to the curvature taken by the electric field in between the fingers of the IDE. On the contrary, larger ratios give better efficiencies with the requirement of higher voltages of actuation (see Table 3).

p/h Ratio	p:h (µm:µm)	Voltage (V)	Strain (ppm)
2.7	635:239	±850	960
4.6	635:137	±850	1131
8.3	1143:137	±1500	1350
16.7	2286:137	±3000	1580

Table 3: Relation between the p/h ratio and the voltage obtained to attain an electrical field of 1.3 KV/mm(31)

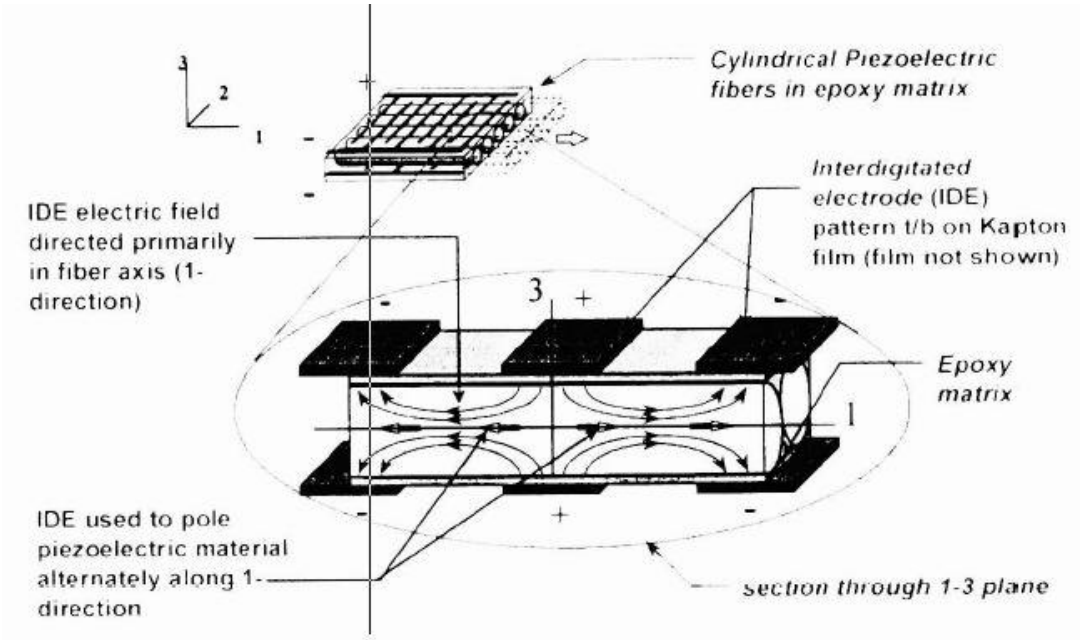

Figure 15: Electrical field generated when poling fibres throughout an IDE setup (36)

It is important to say that the efficiency of the active composite not only depends upon the parameters above discussed but also upon which mode is it working (3-3 or 3-1). So often, d_{33} is twice the value of d_{31}. That is the case of PZT5A fibres (41). Although it could seem that a composite would produce more electricity working in 3-3 mode. In fact, it is just the opposite when using IDEs. A work demonstrating this claim was made by Mo et al (42) who stated that, in theory, mode 3-3 was less efficient than mode 3-1. In practice, Sodano et al (43) showed that this basis was right and that the electrical power produced by mode 3-1 was about triple the produced by the mode 3-3, in terms of power output.

As a conclusion, although IDEs enhance the performance of harvesting composites, some parameters have to be taken into account in order to have a proper design of them and so having an optimum efficiency such as the finger interspacing or the fingers width always bearing in mind that there are external parameters that may influence the IDE design like the fibres thickness.

2.3.5 Devices and applications devoted to harvest energy from bodily movement.

Different approaches have been taken to harvest energy from the body. There have been previous works demonstrating that it is something feasible to scavenge energy from a broad range of sources. A good review is done by Romero et al (44). One of the most common is placing a transducer inside the sole of a shoe. Different attempts to try to harness this energy have been accomplished (45), (46), (47). However, even though the most energy can be harnessed, there is still the problem of the circuitry and batteries which very often are attached to the shoe with the added consequence of increased weight and visual impact giving rise to problems of comfort. As shown in Figure 4, stepping is one of the body actions where most energy is involved. Therefore, it is understandable that most efforts have been devoted to this purpose.

That is the case of the work from Shenck and Paradiso (48), where they investigated the use of a PZT bimorph as well as the use of a flat PVDF stave multilaminate of 16 layers so as to harvest the energy from heel striking. The bimorph consists in three layers: two piezoelectric (the active layers) on the top and bottom and one made of metal in the middle as an electrode, as shown in Figure 16. They placed this device in the shoe-sole so that it least interfered with the individual in terms of comfort. The device worked in 31-mode which means that whilst the PZT was flexed, the electricity was generated through the thickness. In their work they remark that, although it seems very attractive to use 33-modes where the electricity and stress are equally directional, the actual inelastic properties of ceramics make impossible such a thing in this type of applications were the human weight is involved. Peak voltages as high as 200 mV were achieved with the PZT device compared to the 60 mV of the PVDF at a frequency as low as 0.9 Hz with average intensities of 8.4 mW and 1.3 mW respectively. In terms of efficiency, the PZT bimorph could reach values around of 20% whilst the PVDF only achieved 0.5% (to get these values of efficiency they computed the ratio of the open-circuit voltage of each device over the

capacitance of each device under a constant test force). This is proof of the current advantage of the PZT devices over piezoelectric polymers.

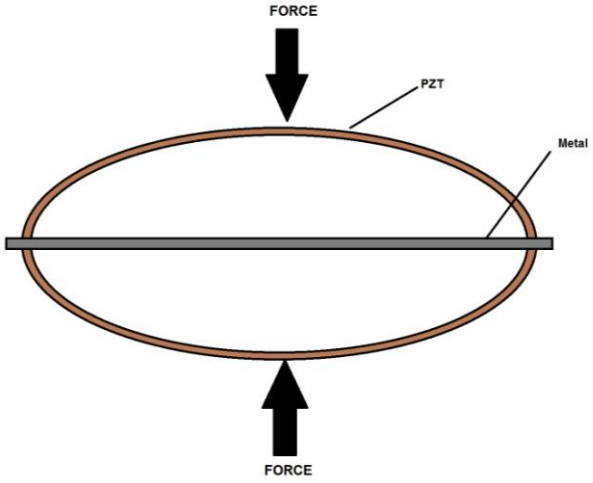

Figure 16: Schematic of a bimorph

There is even more impressive works in relation to take advantage of the weight of individuals to generate electricity accomplished by Rome, et al (49) in which using an electromagnetic transducer, mounted in a shoe. They managed to get 7.4 W from their device for a person carrying a heavy weight (around 38 kg).

Complex ways to harvest energy have also been explored. Single Wire Generators (SWGs), usually a flexible substrate with a nanowire, are part of the latest nanotechnology which is drawing much of the scientific interest provided that it is very suitable for low frequency applications, are robust and adaptable and the wide range of places where it could be embedded like in clothes, surface layers, shoe pads, etc (50).

An example of an astonishing work with SWGs is the made by Li et al (51) in which they used ZnO nanowires. This SWG was placed inside the diaphragm of a rat so that to take advantage of the movement when the rat was breathing (biomechanical energy). An AC output was produced with values for the voltage around oscillating from 1 to -1 mV and intensities from 2 to -2 pA were obtained.

The rat was breathing round about 90 times per minute. In conclusion, it has been demonstrated that in vivo devices to generate electricity are a real application, yet needed to be improved because of the output is still low if we compare it to the risk entailed. This type of work has significant potential benefits if we think that in a future application it could be applied to humans so, for instance, people with heart disease who need pacemakers could have longer periods of time if the battery of the pacemaker could be partially supplied by energy from the heart itself.

Another work in SWG to harness biomechanical energy, in this case, finger tapping or typical movements from a rat, is made by Yang et al (50). Their device was composed by a polyimide film (substrate) with a ZnO nanowire (100-800nm of diameter and 100-500 µm long) fixed at both ends. Moreover, they used a special diode (Schottky contact), capable of rapidly switching between direct and inverse current so as to output the electricity. The dummies never exceeded a 0.2% of strain. For finger tapping action, their results obtained were around 25 mV and 150 pA for a single SWG.. Although the seemed a very low energy action, we can see that electrical current is fair enough as a beginning for only one nanowire. For the rat test, a SWG was implanted in a jacket that the rat wore. Frequencies were around 10-11 Hz giving voltages of 50-100 mV and currents of 0.5 nA. Besides, they went further and tried a device with a couple of SWGs (in parallel and in series), with the additional issue of synchronization, finding that, once they synchronized the different SWGs, the behavior from the device was enhanced (output voltage about 100mV when in series). The most astonishing result was achieved when 4 nanogenerators were in series, the output voltage rose to until around 0.1-0.15 V which is near to the primary cell voltages.

ZnO is a material which is being currently investigated. Papers can be found about applications were voltages as high as 3.2V can be attained (52), which represent a very good approach, for example, to become electronic textiles (devices attached into wearable fabrics). Effort and investigations are being oriented into this way. A very flexible material is a specific requirement for such

purpose given that it would have to adapt to body movements. There are lots of movements involved in a piece of fabric when worn. A good proposal could be, piezoelectric ribbons printed on PDMS as Qi et al (53) suggest, the use of flexible rubbers with highly efficient materials like PZT.

2.4 E-textiles and wearable electronics

Electronic textiles are computational fabrics made as its name indicates of fabrics which are the support/platform and electronics. This setting allows fibres and thin films to be embedded into the fabrics without losing the comfort of the individual. This topic is cutting edge technology (now it has been around 13 years of since first it was introduced) still waiting for further development. In the literature, thesis can be found doing a deep overview on the subject (54) (55) (56), most of it done in the Virginia Polytechnic Institute in the USA. For instance, in the thesis of Nakad (57) there are given some reasons and motivations for making the e-textiles, summarized in:

1. Cheap and large areas are possible.
2. Ease of deployment (possibility to be rolled up into a bundle).
3. Concealment and comfort.
4. Fault-tolerance. (A fabric is a less fragile environment than spread wires and the break of a node does not imply the failure of the e-textile)
5. Power consumption (they represent a saving times less than a wireless device (58))

Although it is a modern advance, some applications are taking shape by now. A very interesting example could be the screen scrollable (59). Researchers of the company Philips Electronics in the Netherlands found a way to print liquid crystal displays (LCDs) onto different materials like clothes. Flexible and light screens, called flexible organic light-emitting devices (FOLEDs, see Figure 17),

have opened the door for ambitious goals such laminated screens onto military sleeves, the face guard of a helmet or even in the windshield of a car.

Figure 17: Flexible screen

Other ambitious projects (60) (61) (62) arising are antennas embedded into military clothes or gloves that can determine if water is potable by just touching it with the tip of the finger. The aim is to make military clothes become electronic networks by placing devices capable of interact with each other embedded in the fabrics. Some real applications are well described and analyzed by Post et al (63) such as a musical jacket with an embroidered keypad that permits to play music, a firefly dress which changes light thanks to the LEDs embedded into the fabric, an electronic tablecloth that allow users to interact with each other and with a computer, etc .

If we narrow down the focus of the review to harvesting energy with electronic textiles, then things get more complicated as it is really a cutting-edge technology so research is done under strict confidentiality.

From the literature available at the moment there is a interesting research paper done by Post et al (64) which going further in the topic of e-textiles, investigated the possibility of seizing the charges generated by material rubbing (electrostatic energy), for example PTFE and nylon, and transferring them through a harvesting circuitry. First, they tested two active triboelectric materials: PTFE (A) and Nylon (B) (see Figure 18).

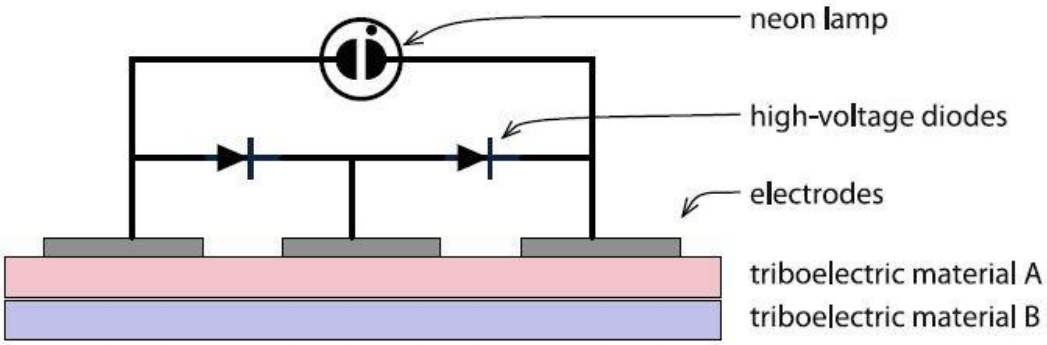

Figure 18: Trial to assess how much energy would be available ideally (64)

One of them was connected to a neon lamp with a breakdown of 100V. Then both materials were rubbed against each other at a frequency of 4 Hz. They managed to turn on the lamp and get an instantaneous 22.5 μW and charging voltages up to 120 V. In the light of such results a prototype (see Figure 19) was made with diodes to ensure the unidirectionality of the electricity, everything embedded to the fabric of a skirt. At 2 Hz of frequency, an average current intensity of 162.2 μW was obtained in an interval of 1 second with a maximum peak of 1.2mW. Their journal demonstrates the scope and energy that this sort of application could have. However, there is a lack of comfort in their device in addition to probably, the extra-weight of carrying all the circuitry and materials.

Figure 19: Skirt prototype (64)

A different work is the one taken by Guilot, et al (65) who proposed an approach to incorporate piezoelectric fibres in clothes. They intended to give the needed flexibility to the piezofibres by coating them with a polymer, in order to be in garments. This allowed the fibres to be woven them into the fabric.

A latest garment is starting to be used by the Australian army (66) in order to get electricity from the soldier's motion and storing it in a super-capacitor. It is said that 87 mW can be achieved per Kg of the individual.

2.5 Mechanical testing: The three point bending test

The three point bending test, so-called flexural test, is used to measure the performance of materials under simple-beam loading (67). Whereas the tensile test is used to measure the mechanical properties of ductile materials, such as metals, the low ductility of ceramics and other brittle materials makes difficult to utilize this test and gives sense to the utilization of the flexural test (68). Callister (11 p. 447) gives in his book three reasons why the flexural test is a preferable method for brittle materials instead of the tensile test:

1. The difficulty to prepare the required geometry of the specimen to be tested for a tensile test.

2. The difficulty to clamp the material so as to stretch it without breaking it.

3. The necessity of having perfectly aligned materials in the tensile test. Ceramics usually fail after a 0.1% of strain. Then, it is very easy to get distorted measurement in such a small range of length to test. A material misalignment would generate an extra bending stress in the material that would affect considerably in the results.

Two types of bending tests can be identified: the 3 point bending test and the 4-point bending test which are shown in Figure 20. In the former, there is no friction between the sample and the holders (68).

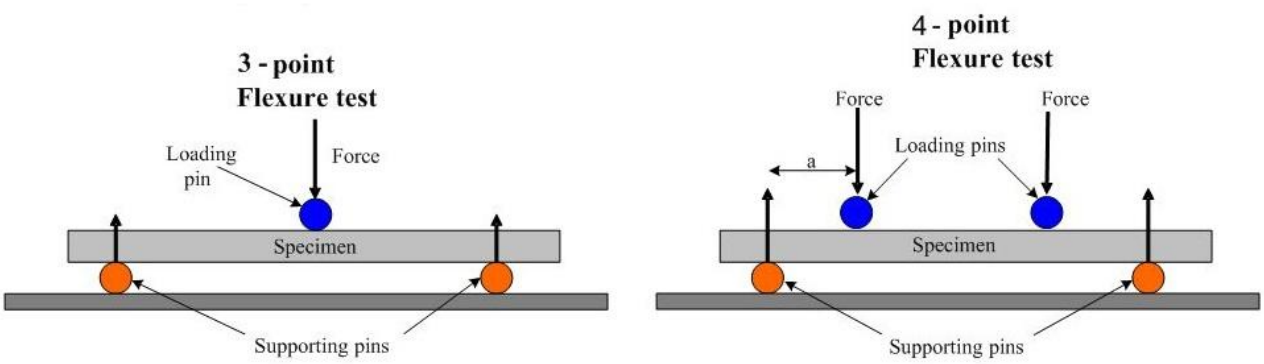

Figure 20: Representation of the different bending tests (68)

Both of the bending tests can measure the maximum stress and strain of fibres. All the specimens to be tested by this method will suffer two states of stress, compression in the concave side, in which the force is applied (blue zone of Figure 21), and tension in the convex side (red zone of Figure 21), the opposite side to where the force is applied. This system generates a plane of shear stress just in the middle of the specimen which has to be minimized in order to ensure good results (67). What it is done so as to avoid or reduce to the minimum possible these shear stresses is to calculate the ratio of the span length over the thickness of the sample. This ratio, which is depending on the materials, has always to be greater than 16 (67) because it will ensure that the shear stress will be reduced to minimum values.

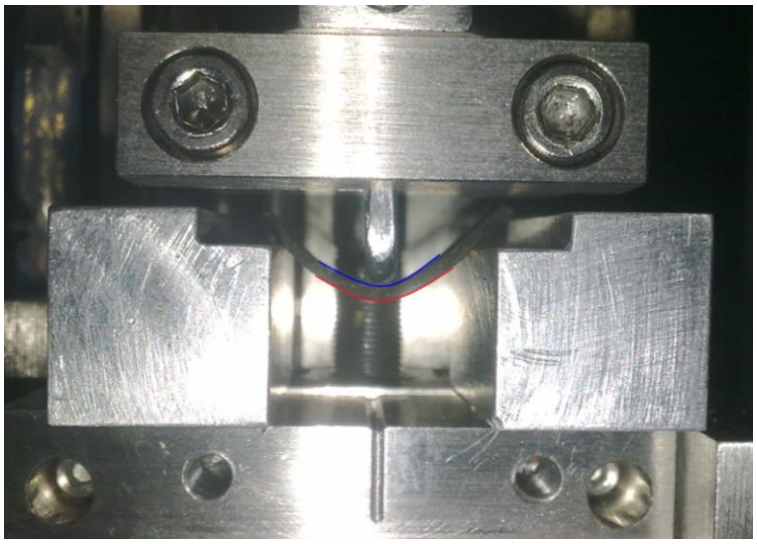

Figure 21: Bending test in the microtester

If a stress-strain plot is drawn from the test, the slope of the curve is to be the flexural modulus (equivalent to the Young Modulus of a tensile test). When fibres are tested then the modulus is called the Rupture modulus. In cases where there is non-linearity, a secant line is used (67). The stress depends upon factors like the thickness, the cross-section which affects the moment of inertia and the bending moment (11). The maximum stress always occurs in the surface submitted to tension. Equation 4 and Equation 6 show the maximum stress for rectangular and circular cross-section fibres whilst Equation 5 and Equation 7 give the Young modulus respectively.

Regarding the stress, Callister (11) makes a special point. He claims the dependence of this parameter to the volume of the specimen. It is made a special effort in remarking that the larger the specimen is, the larger the possibilities of having flaws in it are. As a consequence, a lower flexural strength is measured. He also states that the Modulus computed in bending mode will always be greater than the fracture strength measured in a tensile test provided the difference in nature of both methods.

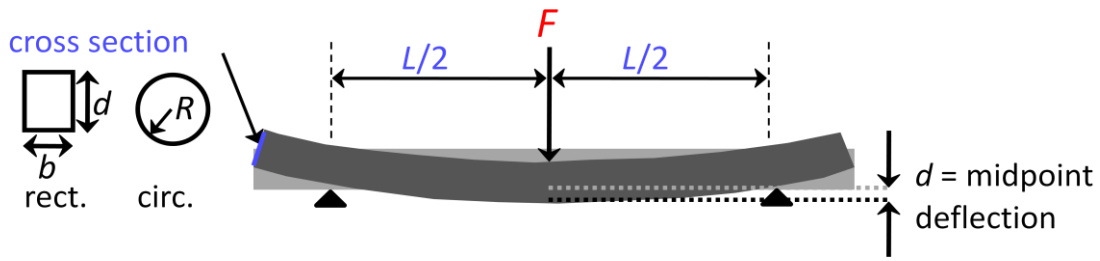

Figure 22: Bending test scheme to aid understanding of parameters of subsequent equations (3, 4, 5 and 6) (11 p. 448) .

Equation 4: Flexural strength for a rectangular cross-section sample, where F_f is the load at fracture

$$\sigma_{fs} = \frac{3 \cdot F_f \cdot L}{2 \cdot b \cdot d^2}$$

Equation 5: Elastic modulus of a rectangular cross-section sample

$$E = \frac{F \cdot L^3}{\delta \cdot 4 \cdot b \cdot d^3}$$

Equation 6: Flexural strength for a circular cross-section sample

$$\sigma_{fs} = \frac{F_f \cdot L}{\pi \cdot R^3}$$

Equation 7: Elastic modulus of a circular cross-section sample

$$E = \frac{F \cdot L^3}{\delta \cdot 12 \cdot \pi \cdot R^4}$$

2.6 Future potential electronics

Some advantages have been explained from active fibre composites such as the flexibility they give in order to produce relatively complex shapes or the anisotropic actuation. These advantages offered by AFCs are expected to be exploited in applications including contour control, vibration suppression, acoustic control, and structural health monitoring. Presently, few real commercial devices are known yet but there are a lot under investigation. According to Nelson (33), reducing the diameters of the fibres whilst keeping the piezoelectric activity is of special interest in order to achieve the performance values of monolithic materials and represents the actual challenge.

The field with most potential to be developed is wireless applications. There is much of interest for the army to have wireless harvesters from bodily movements as it would suppose more autonomy of their electronics (66). For instance, a piezoelectric composite could be placed near the chest of a solider emitting a signal each time the individual breathes. In the hypothetic case of an injured soldier in a minefield, it would be very useful to know in the distance if he stills alive or if, on the other hand, he is dead. Then it would be really worth sending somebody to aid him, otherwise, it could be risked other soldiers' lives sending them to rescue a dead man.

3 EXPERIMENTAL WORK

As mentioned in the introduction, it was decided to recreate the fibre arrangement of Figure 3. The cross-section of an ideal fibre arrangement is shown in Figure 23. In this cross-section, the polymer matrix is green portion, the carbon fibres are in black, the PZT fibres are in yellow and the IDE is in red. From bottom to top the layers of this composite would be: carbon fibre array/IDE/PZT fibres array/IDE/carbon fibre arrangement. Everything is enclosed in a polymer matrix. The flow of an ideal process is:

1. Align the PZT fibres.
2. Hold this alignment by means of a polymer matrix substrate.
3. Make the IDE and put it in good contact with the fibres.
4. Align the carbon fibres arrays in accordance to the alignments of the IDEs and the PZT fibres.
5. Fill the composite with polymer matrix.

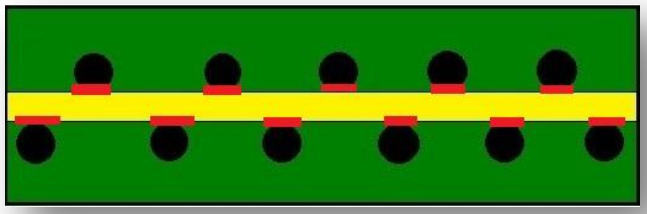

Figure 23: Schematic of composite parts

The PZT fibres used during the whole project were PZT5A supplied by CeraNova Corporation, with a thickness of 260 µm. One fibre was checked with the micrometer just to ensure that the thickness was right. 253 µm was the thickness of the fibre measure which is close to 260 µm.

3.1 Polymer matrix

In the literature review it has been shown that the most utilized polymers in previous investigations are epoxy resins. However, in some of the latest researches the polymer matrix PDMS has shown good results.

In this project, two polymers have been used: PDMS and a polymer belonging to the family of epoxies, - SBX Liquid Resist Emulsion. SBX is sandblasting photo-resist supplied by *IKONICS Corporation.* It is primarily composed of volatile compounds (75% of the weight).

The idea of using SBX was to utilize its particular response to light. SBX is a negative photoresist. This emulsion is a two-part system comprised of a clear or dyed emulsion and a dry photo-sensitizer powder. This sensitizer is a green powder called Diazonium salt. Once the two parts have been mixed, the SBX is ready to be cured under UV light. SBX which has not been cured may be removed using pressurised water (developer) in what is called a development process.

During the project two SBX batches were utilized. In the beginning there was SBX already sensitized on the laboratory shelf and all the initial work was made using it. This SBX is referred to as old SBX and looked very viscous. Three first trials were first made pouring old SBX. The former was prepared stirring the SBX thoroughly and pouring it directly onto a glass slide, the second was prepared mixing SBX with water and then pouring it on a glass slide and the latter was prepared stirring SBX and sonicating it in an ultrasound bath for 7 minutes to ease the SBX flow. In the light of the results, it was decided to apply sonication to every sample from that moment onwards because it gave fluidity to the SBX which is important to be spun. Results obtained later denoted that this SBX could have been spoiled or just be already partially cured so an order was done in order to have another SBX. This SBX is referred to as New SBX. The new SBX was prepared mixing following the liquid emulsion and the sensitizer in the proportions said in the instructions. Although it was enough

allowing 2 hours after drying, it was left the SBX one day to make totally sure it was ready.

3.2 Fibre alignments

As mentioned in the previous section, SBX may be removed (developed), after a selective curing using a pattern, in order to transfer this pattern to the SBX. Therefore, a suitable mask could be designed to be utilized when curing the SBX so that put grooves onto the SBX, which would give the orientation to the PZT fibres. A good resolution, though, would be needed when developing as the grooves should have widths close, and always larger, than the thickness of the PZT5A fibres for these to fit in. Regarding this, the company that produces SBX states:

“SBX is a photoresist which gives extremely high quality resolution when developed” (69)

So, in principle, it should give good results as they claim that the resolution is between 177.8 and 254 µm, precisely in the range of the PZT5A thickness.

A mask (Figure 24) was designed with AutoCAD and ordered to be printed with high quality in an acetate sheet. Two different sets of grooves were drawn taking into account that the development process may affect the width of the grooves. The widths are 300µm for the two sets on the right and 200µm the two sets on the left. The separation between the centres of consecutive grooves was established at 0.7mm. Alignment marks for subsequent masks. Designed for the IDEs, to be well aligned on top of the fibres were included in the design. The shape of these features is a symmetric cross which fits perfectly on a square of 15 µm. The line features between each set of grooves were meant to be an indication to lay, in a later stage, carbon fibres in the right position. Eventually, a clearfield as well as a darkfield were drawn so that they could be used for positive as well as for negative photoresists if wanted.

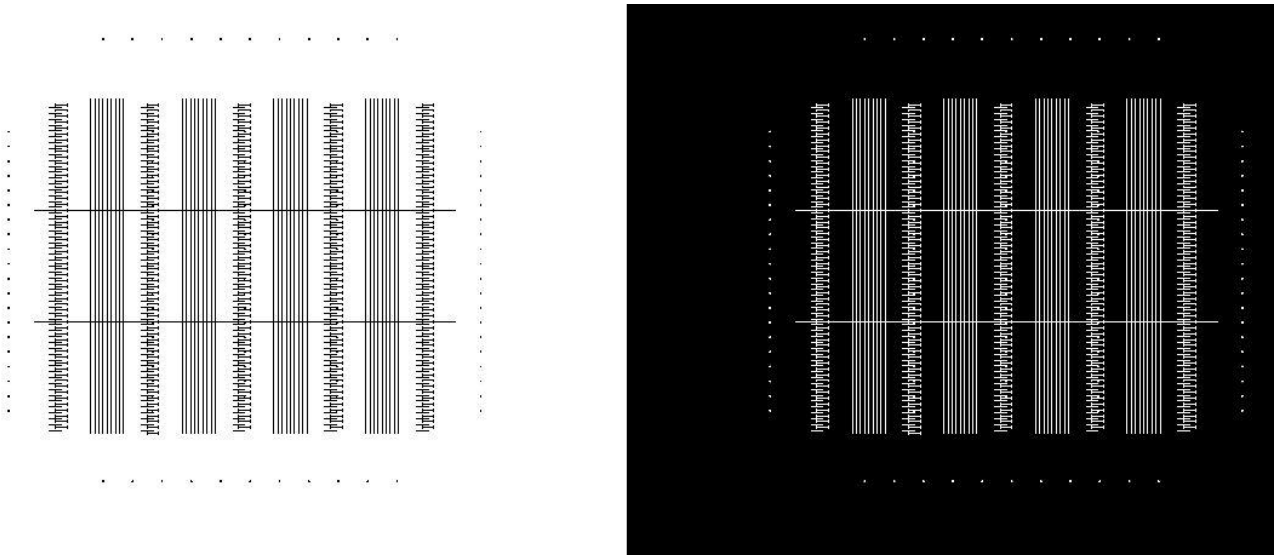

Figure 24: Grooves mask for the SBX

On the other hand, PDMS needed another way of fibre alignment. In this case, an alignment frame was designed with Solidworks, the drawings of which are shown in Figure 25.

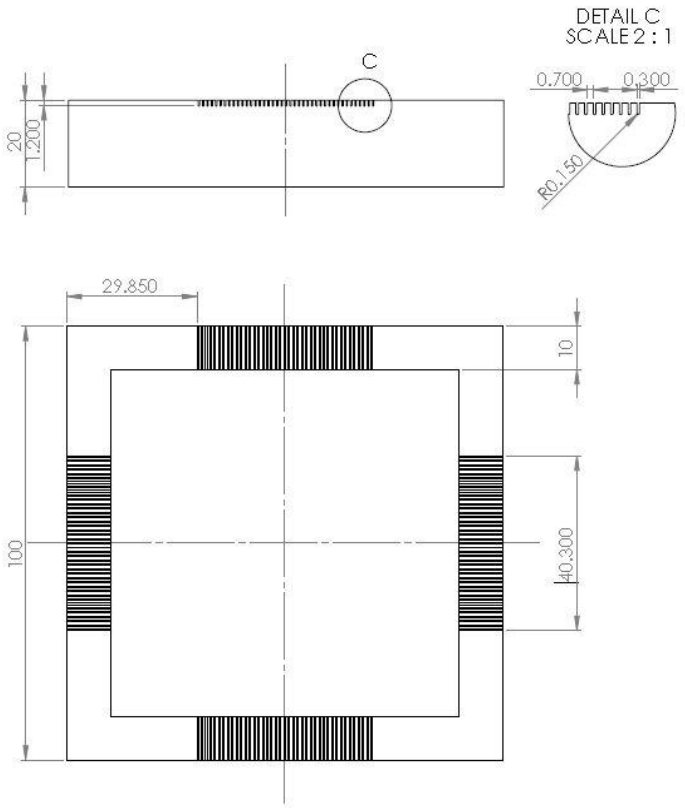

Figure 25: Fibre alignment frame (units in mm)

A 3D view has also been included next to a photograph of the real frame in Figure 26.

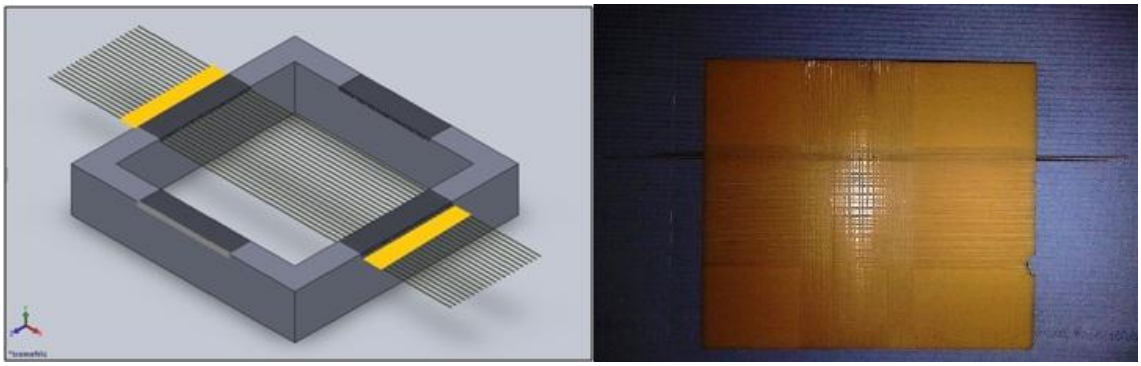

Figure 26: 3D view of the frame (left) and real frame (right)

Fibres could be aligned by means of this frame, and subsequently, with the help of some type of tape (shown with yellow lines in the left image of Figure 26) they could be taken out keeping the alignment of the PZT fibre array.

To start with, a simpler frame was made on a Tufnol piece. Tufnol is a material made from phenolic resin and a linen fabric or cotton. The grooves were machined using a *Logitech 1MOD1* dicing saw with a 0.3mm thick silicon carbide wheel. The Tufnol was marked out and then placed on a vacuum chuck. Subsequently, the depth was set and the wheel started to pass across the Tufnol. The wheel was lifted at the end and run back to the start, where it was index across the 0.7mm. Finally this process was repeated a number of times.

This frame was finally the used for all the alignments that were done in this project.

3.3 Releasing approach

First of all, a substrate was needed to support either PDMS or SBX deposited layers. Some of the layers prepared needed to be easily removable once cured, so as to test them as samples. In addition to this, it is necessary to put two IDEs in the composite, one at the top part of the fibres and the other at the bottom

part. Accordingly, at some point the composite should to be turned upside down to put in contact the second IDE.

After ensuring that both PDMS and SBX were stuck to the glass slides, it was decided that a releasing approach was needed. Two approaches were considered:

i) PTFE film

The PTFE would be spread on top and allowed to dry. A priori, it should be easily removed with the help of a spatula. This method was the first tried and as it worked it was decided to keep using it.

ii) Polyimide film

Polyimide film was used as a support substrate but not released from the polymer afterwards. The drawback of this method would be that only one IDE could be placed in position instead of two (one in each side of the fibres). On the other hand, the advantage is that, the polyimide would be an insulating film between the piezoelectric fibres and the carbon fibres that will enhance the stress along the piezoelectric fibres.

3.4 Coating / sample preparation

One of the critical objectives for this project was to reach a coating thickness equal or less to the PZT5A thickness in order to ensure that the top side of them would be free of polymer when placing the IDE.

The following approaches detail the experimental method used to prepare samples made from layers of the matrix materials.

3.4.1 PDMS

A strict methodology was followed to prepare the PDMS. Firstly, a petri dish was covered with PTFE film. A 10:1 in weight mixture of Silgard silicone elastomer and Silgard curing agent 184 (initiator) were poured in small pot and

stirred. Subsequently, the pot was placed in a vacuum chamber at around 50 mbar to help the bubbles formed to leave the PDMS prepolymer. After half an hour, it was taken out of the vacuum chamber and poured on the petri glass. When fibres were wanted to be put, they were first aligned in the alignment frame and then transferred and attached to the PTFE film. Then another petri glass with PTFE film was placed on top of the previous one and a weight of 90.72g was put on top in order to keep the thickness in the range of the fibres. Eventually, the samples were left overnight at room temperature so as to let them time to fully cure before releasing them.

3.4.2 SBX

Two approaches were taken in order to produce controlled targeted SBX layers which were casting and spinning.

3.4.2.1 Spinning

No PTFE film was used to prepare SBX layers due to the most probable substrate for the SBX in the final process would be a polyimide film, which imply no need of releasing the SBX from the substrate.

75 by 50mm glass slides were utilized in order to spin the SBX and were prepared as follows:

1. The glass slide was cleaned with deionised water.
2. Then they were rinsed with isopropanol (IPA)
3. Finally they were left to dry in a fume hood. When a quicken process was needed, samples were left in a hot plate at 150ºC for 4 minutes.

The spinning machine was an *EMS (Model 4000) Photoresist Spinner*. All the samples were spun for 30 seconds.

3.4.2.1.1 Drying

All samples were left overnight to ensure that the films were thoroughly dried. They were left on a flat surface that was in a fume hood with a laminar flow of air over the surface to enhance drying.

Part of the SBX film was removed from the samples after drying using a scalpel so as to check the thickness afterwards by means of the Dektak machine.

3.4.2.1.2 Curing

The samples made in the spinner were UV cured by means of Karl SUSS MA56 Mask aligner. Due to time constraints, the exposure time needed in relation to the thickness of the specimen was not researched.

First of all, a sample was exposed 10 min, but the sample was totally black and looked overcured. Then a sample was exposed 2 minutes and seemed fine so this exposure time was determined for subsequent samples.

For the new SBX section, a black paper was placed underneath the sample in the UV light Mask aligner in order to try to minimize the light reflected by absorbing some of the reflected UV light.

3.4.2.1.3 Developing

Before designing the mask in Figure 24, the basic mask based on Figure 27 was made on an acetate sheet using a normal printer. The intention was to compare the widths in the SBX after development against the widths in the mask. From left (first set of grooves) to right (last set of grooves) of Figure 27 the widths were: 300, 250, 200, 150, 350 and 300 µm. It was checked under the microscope that the grooves widths on paper were the same as designed.

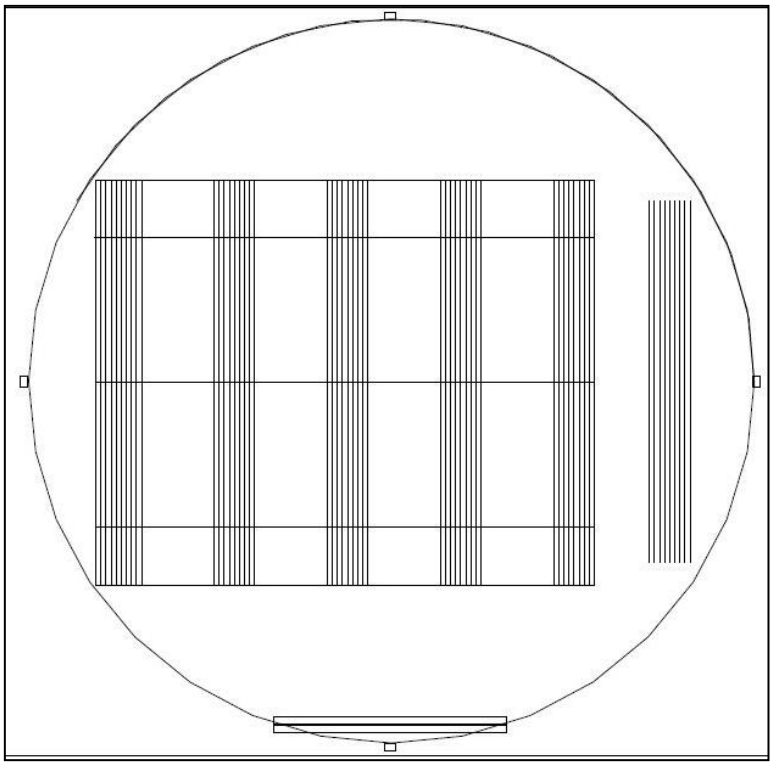

Figure 27: Mask trial with different sets of grooves

Reproducibility study

The full development through the new SBX thickness seemed very difficult. Because of this, a batch of samples was prepared at the same speed. The data obtained was used to assess the thickness reproducibility of the samples and is shown in Table 11. These samples were also afterwards utilized to study the development depth whilst the designed mask (Figure 24) was being made. They were cured under a good quality mask with rectangular features from a previous project

In terms of exposure time, it was thought that it would be good to find a minimum time for curing because 2 minutes or more were probably too many. Less UV exposure could ease the development process as well as reducing the probability to partially cure the grooves with reflected light. Different exposure times were tested and are shown in Table 16. Additionally, some additional samples were also made at different speeds and exposure times.

Multi-layer sample

Three layers were spun on a glass slide, one on top each other. The first one was spun at 2000rpm and the other two at 1000rpm. Each layer was left to dry 5 minutes and it was checked that the film became transparent (a proof that it is totally dried) before spinning the next one. After that the sample was placed 1 minute in the UV system to be cured under the designed grooves mask (Figure 24) at a light intensity of 5.5mW/cm^2.

3.4.2.2 Casting

Manual casting is another way to deposit SBX films. There is less control over the thickness provided that the individual has more influence on the process thus a higher probability to induce an error.

Casting was the method used to fabricate the samples that later on would be mechanically tested. Samples are easily made with specific sizes with this method. Given the own limitations of the microtester, explained in the later section of mechanical tests, the samples could only be as long as 20 millimetres.

The methodology used to cast the SBX was strict. First, a glass slide was lined with PTFE film in order to help the sample removal later on. Subsequently, a couple of tape strips where placed on the sides, leaving in between the zone where the SBX was poured. The thickness of the tape was measured with the micrometer and was equal to 130 micrometers. In this way, the SBX wet thickness may be controlled. Once the tape strips were placed on the sides, the SBX was poured down. Eventually, the SBX was drawn smoothly across the whole surface, with the help of the edge of a glass slide, as shown in Figure 28.

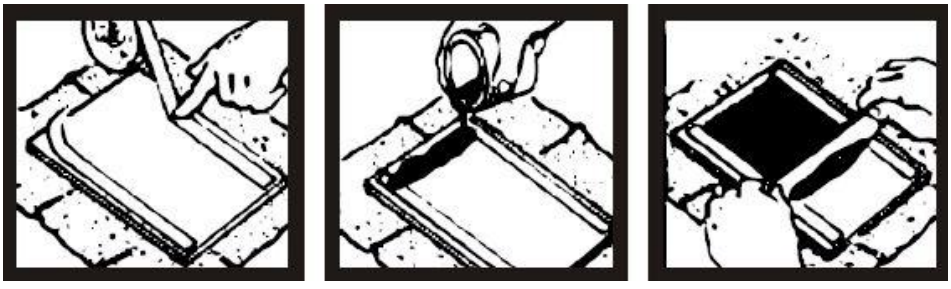

Figure 28: Casting process followed

3.4.2.2.1 Drying

The samples were left overnight to make sure they were totally dried.

3.4.2.2.2 Curing

All manually cast samples were UV cured by exposure to sunlight for 2 minutes.

3.5 Sample thickness measurements

All the thicknesses under 130 µm were checked utilising a *Veeco Dektak 150 Profiler*. Thicknesses over this value were out of the range of the Dektak machine and hence a micrometer was utilised (*Mitutoyo Digital Display Micrometer 810-475)*. Both of them are shown in Figure 29.

Figure 29: Image of a Dektak machine (left) and a profilometre (right)

3.6 Optical microscope

A Confocal microscope was used to observe the film surface or the samples grooves and sometimes pictures were taken. The microscope used was a *Confocal Laser Scanning Microscope LEXT*, model *OLS3100*, made by *Olympus*.

3.7 IDEs and its implementation in the composite

3.7.1 Design

Part of the mask designing carried out in this project incorporated different IDE patterns for the composite. It was discussed in section 2.3.4 that the p/h ratio

plays an important role in the efficiency of the composite as well as in the poling voltage needed. It was tried to keep this ratio low so that the poling voltage would be low as well provided that there is a probability of not getting a compact composite, at least for the first dummies (it may be left some bubbles, SBX or adhesive between the fingers and the fibres). The IDE designs are shown in Figure 30 and the design details in Table 4. All of them are 18 millimetres long by 8 millimetres wide.

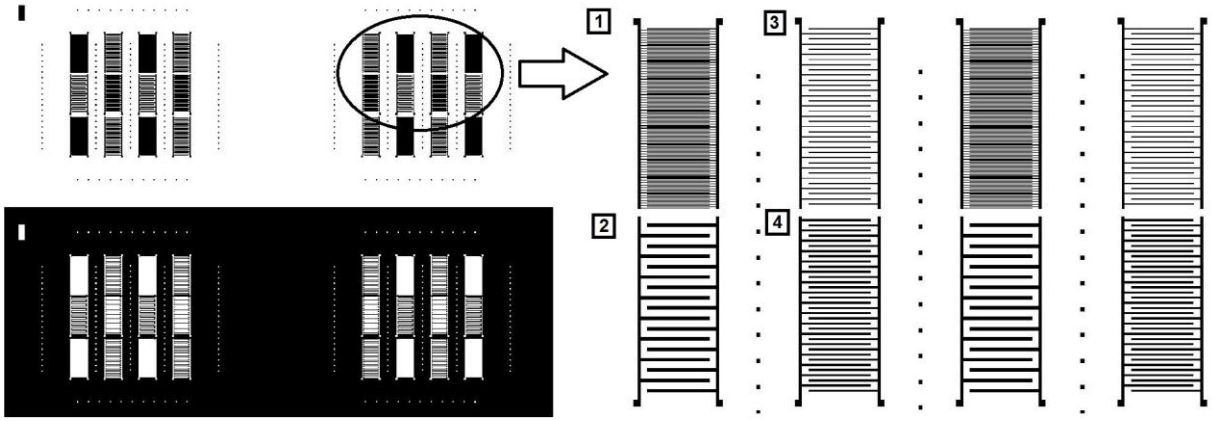

Figure 30: Clear and darkfield IDE masks (left) and zoom of the four types of IDE masks designed (right)

Alignment marks were incorporated within the design so as to facilitate alignment with the grooves mask previously described in section 3.2.

Sample	Finger width (µm)	Interspacing (µm)	Pitch (µm)	p/h ratio
IDE 1	13.8	111	124.8	0.48
IDE 2	300	700	1000	3.85
IDE 3	55	443.2	498.2	1.92
IDE 4	150	350	500	1.92

Table 4: IDEs design data (IDE numbers in accordance with Figure 30)

A second criterion was taking into account in order to design the IDE: the number of fingers in contact with the PZT fibres between the interspacing of subsequent carbon fibres. It was discussed in the literature review the hypothesis that the s-stress at which the PZT fibres would be submitted by the carbon fibres in the fibre arrangement planned (Figure 3) could generate

alternating plus and minus charges along the surface of the PZT fibres. The IDE electrodes should be coincidental with the plus and minus points in order to solve this hypothetical problem. IDEs 1 and 3 from Table 4 were designed with AutoCAD bearing in mind this. It was noticed that the fingers were very thin that it could represent a problem so as to deposit the IDE and also for the IDE conductivity. Because of this, IDEs 2 and 4 were designed with thicker fingers, in the order of the fibre diameters.

Calculation of IDEs 1 and 3

The spacing between the centres of subsequent carbon fibres on the same side of the PZT fibres is 1 mm; both for the grooves mask approach (Figure 24) or the alignment frame approach (Figure 25). The carbon fibre diameter was meant to be 0.3mm. Therefore, the distance between subsequent carbon fibres centres from different sides of the PZT fibres is 0.5mm as shown in Figure 31.

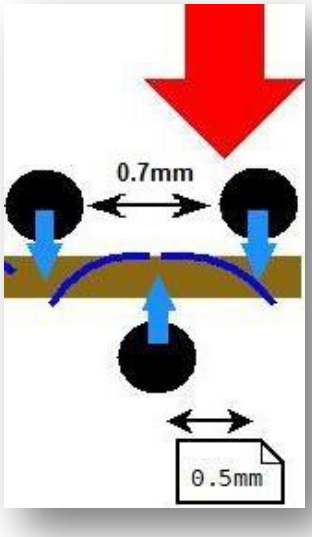

Figure 31: Zoom of fibre arrangement

Provided that the position of the plus and minus points was not known, around five IDE fingers between subsequent carbon fibres of different sides was thought to be a good value. Therefore, the design was based on the fact that five IDE fingers had to be placed in 0.5 millimetres, , represented in the

Equation 8, where x is the finger width and y is the finger interspacing. In the work of Rossetti et al (31), a ratio factor of round about 8 between the finger interspacing and the finger width is used. This relationship was taken as the second equation (**¡Error! No se encuentra el origen de la referencia.**) in rder to complete the equations system.

Equation 8: IDE first design equation

$$0.5 = 4x + 4y$$

Equation 9: IDE second design equation

$$y = 8x$$

Solving the equations systems, a finger width of 0.0138mm and an interspacing of 0.111mm were obtained as shown in IDE 1 on Table 4. For the IDE 3 the calculations were done doubling the space between the carbon fibres (leaving one space vacant between them).

3.7.2 IDEs deposition

Three attempts were considered in order to lay down the IDE: Screen-printing, Evaporation and Sputtering. The IDEs had to be thin enough so that no to affect the composite performance, but thick enough to withstand the stresses at which they might be submitted.

3.7.2.1 Evaporation

This method was one of the two thought for the IDE to be deposited directly on the PZT fibres. Depositions done by evaporation are more directional than for sputtering though more energy is required. The temperatures reached in the evaporation imply a risk. They could affect and degrade the SBX.

A shadow mask (Figure 48) was prepared by a method called lithography and then wet chemical etching in order to deposit the IDE on the PZT fibres

afterwards in the evaporator. The steps followed to make the shadow mask were:

1. A 35µm thick sheet of copper was cleaned in an ultrasound bath of acetone and a Nitton^{TM} sheet was attached to one of sides of the copper sheet so as to protect it against the etching.

2. The whole thing was attached to a glass slide and S1818 resist, supplied by Rohms Haas, was spun at 1500rpm for 30 seconds.

3. Then it was baked at 100ºC for 5 minutes.

4. The resist film was exposed in the MA56 Karl Suss aligner for 50 seconds, at an intensity of UV light of 5.2 mW/cm^2, using the darkfield IDE mask.

5. Subsequently it was developed for 50 seconds soaking it in a MF319 developer container.

6. Afterwards it was rinsed, dried and post baked for 2 minutes at 100ºC.

7. The etching was performed using 42º Be Ferric Chloride solution at a temperature of 45ºC by 30 seconds of dips/agitation followed by water rinsing. The total etch time spent was 5-6 dips.

8. Eventually, the sample was removed from the glass substrate and rinsed in acetone to remove the S1818 and to release from the Nitton^{TM} tape.

First approach (the evaporated IDE)

In this approach, tow IDEs were meant to be placed, one on each side of the composite.

The process steps were as follows:

1. 9 PZT fibres were aligned in the frame rig and the ends taped.

2. A glass slide was lined with PTFE film.

3. SBX was spun at 190 rpm on it.

This speed ensured that the wet thickness of the SBX would be 255 micrometers and, therefore, below the fibre thickness (260 micrometres). First the dry thickness for 190 rpm was computed using the model in Figure 39. The result was around 68 micrometers. Then the wet thickness was estimated using the theoretic shrinkage factor given in the SBX instructions (3.75) because it was the largest among all the shrinkage factors found in the casting method in section 3.4.2.2. The estimated wet thickness was 255 micrometers.

4. The aligned PZT fibres were laid down on the SBX layer pressing until the fibres reached the bottom.

5. Once the SBX was dried, it was cured for 2 minutes in the MA56 Karl Suss aligner for 2 minutes at a UV light intensity of 5.3mW/cm^2.

6. The SBX plus the 9 aligned fibres was released carefully from the PTFE.

7. The sample was placed in an Edwards E480 evaporator at a base pressure of 2x10^{-6} Torr and 5-15 nm of chromium (Cr) were first deposited to enhance the adhesion of gold. Finally, 20 centimetres of gold (Au) where evaporated at a distance of 11 centimetres from a 35A molybdenum boat.

3.7.2.2 Sputtering

Aluminium cannot be deposited using resistive heating in an evaporation chamber (70). Therefore, an aluminium layer was deposited on a polyimide film in the sputtering machine. The idea was to etch the aluminium layer afterwards to give it the IDE pattern. The method used was again lithography and then wet chemical etching. The steps followed to make the IDEs (Figure 50) were:

1. A polyimide film was cleaned by rinsing it first with acetone and afterwards with isopropanol (IPA).

2. The polyimide film was placed in a Nordiko^{TM} NS-2500 R-M magnetron sputtering system at a power of 300W and a sputtering pressure of 5 mT for 4 minutes. The sputtering inert gas was Argon at $3.5x10^{-4}$ mT.

3. Then the aluminium sample was prepared to be etched. The sample was attached to a glass slide and acetone was spun over its surface. Then, it was plasma etched with O_2 at 12 Watts for 2 minutes.

4. S1818 positive resist was spun at 3000rpm over the surface in the spinner for 30 seconds and once done, it was left on a hot plate to prebake it at 115ºC for 2 minutes.

5. Subsequently the S1818 was exposed in the MA56 Karl Suss aligner for 40 seconds at a UV light intensity of 5.6mW/cm^2 under the darkfield IDE mask.

6. The development was effectuated with MF319 developer.

7. Finally, the Aluminium was wet chemical etched using Laporte Aluminium etchant at 35ºC for 30 seconds.

Second approach (sputtered IDE)

The process steps were as follows:

1. 9 PZT fibres were aligned using the alignment frame (Figure 25) and the ends were taped.

2. A polyimide film was rinsed first with acetone and second with isopropanol and then left to dry.

3. SBX was spun on top of the polyimide film at 190 rpm to ensure that the SBX wet layer was thinner than the thickness of the PZT fibres as in the section before (0).

4. The fibres were pressed against the SBX layer until they made contact with the polyimide film. The sample was left to dry.

5. The sample was cured in the MA56 Karl Suss aligner for 2 minutes.

The next stage was to put in contact this polyimide film just made (with the SBX and the PZT fibres) with one of the Aluminium IDEs sputtered onto polyimide film. During the PDMS testing, one of the more obvious properties was that it was its tackiness. Because of this, PDMS was decided to be used as an adhesive between both polyimide films.

The same procedure as in section 3.4.1 was followed to prepare the PDMS. Unlike the PDMS procedure explained in section 4.1, the way of mixing the elastomer and the initiator was changed slightly in order to avoid bubble formation. They were mixed in a small inclined pot and then this small pot was placed inside a big pot and left in a roller for 10 minutes. After these 10 minutes the PDMS was totally mixed and bubble-free.

At this point there was: a polyimide film plus the SBX and the aligned fibres, the PDMS prepared and two IDEs trimmed from the IDEs film. The IDEs were rinsed with IPA and sprayed with a nitrogen gun for dust removal. The IDEs were attached to a glass slide where two 300 micrometers thick wires were situated on the sides. After that, some silver epoxy was prepared connect the electrical pads with the outside, as shown in Figure 32.

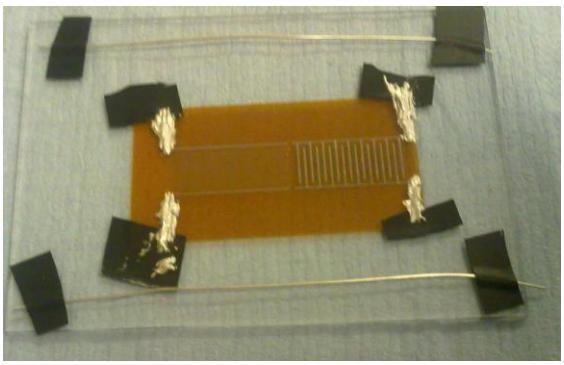

Figure 32: IDE ready for the PDMS to be poured (left) and final sample with fibres (right)

Once the wires were in position, the PDMS was poured onto the two IDEs and a blade was passed across the wires to ensure that no more than 300

micrometres of PDMS stayed on the film. Eventually, the polyimide film with the SBX plus the PZT fibres was pressed against the PDMS. A glass slide with two weights of 0.2 pounds each were left on top in order to apply a force whilst the PDMS was curing. The sample was put in the vacuum chamber at 50 mbar for 30 minutes and ultimately left overnight for the PDMS to polymerise.

3.7.2.3 Screen-printing

This idea came from the literature review, where this approach was taken as an alternative using a conductive epoxy resin. The conductive epoxy is pressed against a mask with the IDE pattern. A blade or roller forced the resin to pass through the mask. In this approach the shadow mask made out of copper (Figure 48) was used and the conductive epoxy resin was a silver epoxy CW2400 from TW Chemotronics.

The steps followed to screen-print the IDE were:

1. Preparation of the silver epoxy resin by mixing the two components in the same proportions.
2. Some acetone was dropped to thin the epoxy as it was too thick to make it pass through the mask.
3. The epoxy was put on the mask and with the help of a blade it was forced to pass through.

Third approach (Screen printed IDE)

The process was as follows:

1. A glass slide was cleaned with deionised water, rinsed with IPA and baked in a hot plate at 150ºC for 4 minutes.
2. SBX was spun at 70rpm and left drying. Then it was cured in the MA56 Karl Suss aligner for 1 minute at a UV light intensity of 5.3mW/cm^2 under the designed mask with the grooves.

3. It was developed under water tap jet for about 3 minutes. The depth of the grooves was checked with the Dektak to be around 25 micrometers.

4. SBX was spun at 2000rpm so as to have the thinnest possible layer to place the fibres in position whilst it was still wet and so it could enhance the adhesion.

5. The fibres were placed into the grooves and the sample was cured 2 more minutes in the MA56 Karl Suss aligner.

6. Silver Epoxy resin was prepared and thinned with acetone.

7. The shadow mask was put on top of the sample and with the help of a blade the silver epoxy resin was forced to pass through the shadow mask.

3.8 Mechanical testing

A Deben Microtester 200N tensile stage was utilized to run the mechanical measurements. Not only the possibility to test to small assemblies but the capacity of sensing loads from 0 to 2 N gives interest to the utilization of this microtester (Figure 34). This feature results in special importance as well as its precision, especially taking into account that bodily forces would never be very high in most of the cases. In addition, loads up to 200N can be applied if necessary using its hydraulic system. The model used had a load cell of 2N, an 1119:1 gearbox and an extensometer fitted of 10mm.

The machine was designed to run tensile tests so it had to be adapted. The idea was to put the machine vertically and bend the samples with the help holders specially designed. In Figure 33, the two holders and the bending tip designed are shown.

Figure 33: Pieces designed for the bending test

The holders allowed testing samples up to 20 millimetres wide and 20 millimetres long. In section 2.5, it was explained that the ratio of the span over the sample thickness had to be always greater than 16 in order to avoid shear stresses in a mid-plane of the sample. The thickest sample made in this section was 0.764 mm. The computed ratio was around 26 which is a much larger value than the minimum specified. As a result there were no shear stresses in a mid plane.

Before start testing, it was checked whether the machine could work in vertical as well as in horizontal provided that the bending test would require the microtensile tester to work vertically.

Two vertical tests and one horizontal test were done for an elastic band piece of 2mm which its rectangular cross-section measured 1.2 mm by side. The stress-strain curves were compared afterwards. For the vertical tests the machine was in a 13.3º angle.

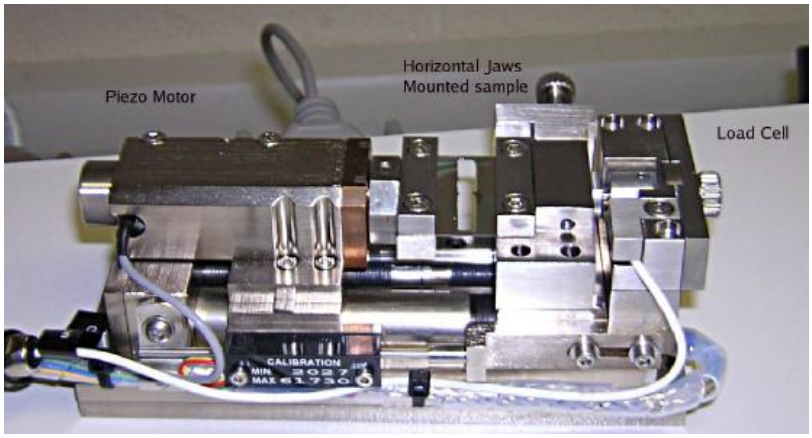

Figure 34: Deben microtester

Different tests were run for PZT fibres alone and for SBX either alone or with one or two fibres inside. Some other tests were run in order to check the mechanical properties of the SBX.

Some samples were made and left one week under the sun and others left in darkness for the same period of time and finally compared against a sample just cured and tested (control sample) in order to check the possible change of the SBX properties with time under certain conditions.

Eventually, multi-fibre samples were prepared for the new SBX. Three different PZT fibres-carbon fibres combinations were tested.

The samples were casted as described in section 3.4.2.2 and cured under the sun for 2 minutes. The size of all samples was 19 mm long by 5 mm wide except for the samples with carbon fibres that were 19mm long by 15mm wide. The testing speed was set to 1.5mm/min.

4 RESULTS AND DISCUSSION

4.1 PDMS

PDMS samples with fibres aligned inside like the one shown in Figure 35 were prepared. Once the samples were cured, the composite tried to be taken off the PTFE film. However, it was impossible for all of them to do it without breaking

the fibres. The samples made without fibres (only PDMS) were not stiff enough to be tested. The PDMS was not able to retain its own shape. PDMS was discarded for this reason, it would not be able to share any load applied to the fibres. Furthermore, bubbles were trapped within the PDMS and between fibres. They would act as stress concentrators and would represent a problem for the poling process.

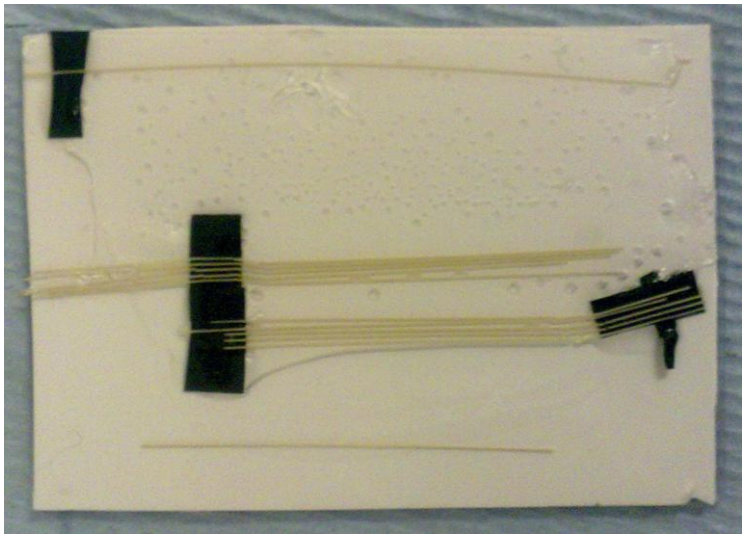

Figure 35: PDMS sample with fibres

4.2 SBX

The two main reasons to try the spinning machine were flatness and thickness control. An even surface would enhance the contact between the IDE and the fibres and would allow the IDE to have fewer strains in it. Samples as flat as possible were therefore desired as it is vital for the IDE performance. Likewise, reaching a layer thickness equal or less than the one of the fibres is crucial in order to be able to predict the thickness and in order to have reproducible method. Spinning is an automatic process so few human error is involved and more accurate data should be obtained than for the manual casting.

Most of the relatively thin samples (under a certain thickness value which was not determined) became clearly translucent after drying whereas thicker samples were totally dark brown. For these thick samples there was no way to know whether they were dried or not just looking at the colour.

As mentioned in the experimental section, part of the SBX film was removed from the samples in order to have an area on the sample where to measure the film thickness. Nevertheless there was an error involved: when SBX was removed, the rubber nature of the SBX meant distortion occurred increasing the thickness of the surrounding SBX specifically in the step measuring region. Long traces were tried to be run in order to overcome this problem and to try the stylus to end up as far as possible from the distorted area, where the SBX was still attached to the substrate and the film thickness measurement is more reliable. Anyhow an error was involved.

4.3 Old SBX

4.3.1 Spinning

All the initial work was carried out on the old sample of SBX referred to in section 3.1. Comets were present in almost all the samples. Although Figure 36 is not of high enough magnification to see the classical comets shape, it shows how the air trapped in the SBX due to its high viscosity formed some blisters.

Figure 36: Comets in a sample

A correlation between the rotational speed and the SBX dried thickness on glass slide was researched. This correlation would help to predict future samples thicknesses. The data obtained is given in Table 5 and plotted in Figure 37.

Rotational speed (rpm)	Thickness (µm)
170	670
290	112
390	103
400	85.8
600	79.03
800	41.6
1000	25

Table 5: Data obtained for the relation between rotational speed and SBX film thickness

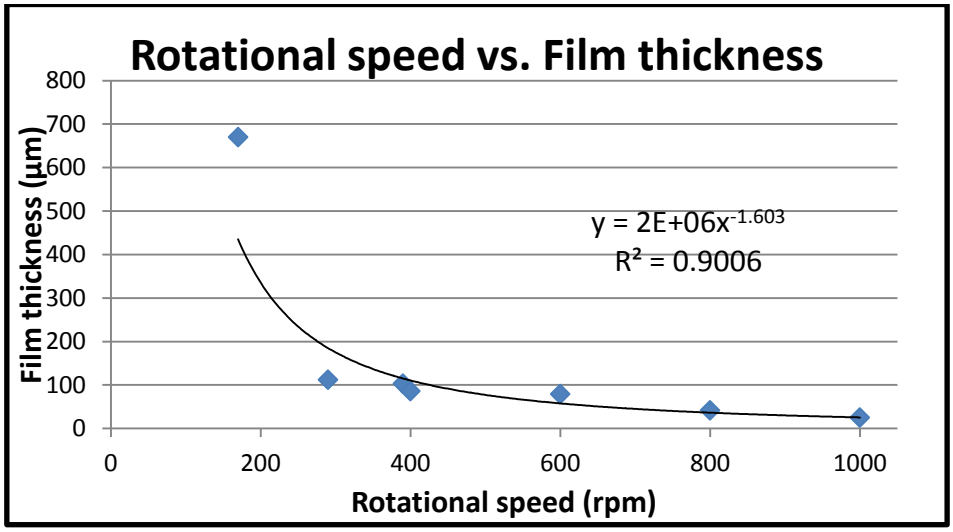

Figure 37: Correlation between rotational speed and film thickness

The regression factor is not very good and the reproducibility of each thickness was not checked. However, a power regression trend seems to be followed. Reasons why the trend is not perfect could be:

- The amount of SBX put onto the glass slides had an influence on the final thickness although it was always aimed to cover ¾ of the glass slide.
- Due to the SBX viscosity, it could have been possible that the spinning time was not enough to reach the equilibrium of forces in the spinner, especially for low speeds. This equilibrium of forces is a balance between centrifugal forces and the viscous forces (71).

4.3.2 Developing

Many samples made out of old SBX during the project showed comets. These non-desired comets may act as stress-concentrators in the composite and hindered the task of getting well-defined grooves as it could be seen in Figure 38. Comets were in this example as wide as the grooves were.

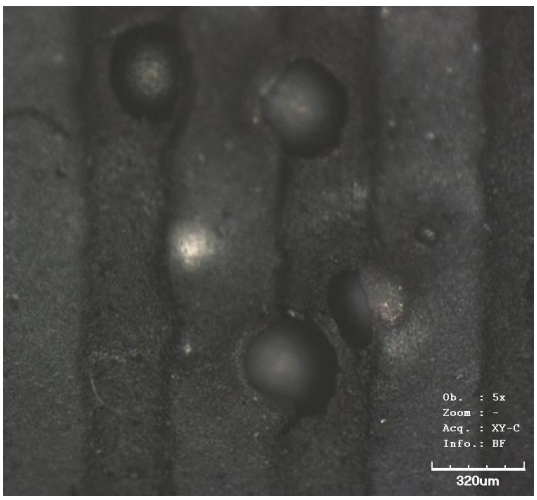

Figure 38: Confocal microscope image of blisters on a sample

The SBX was old and might be not profitable. In addition to this, developing the samples by just dipping them into water turned out to be useless. Because of this, three samples were prepared (Table 6) in order to try different manners to develop them and to check the grooves depths.

Sample	Rotational speed (rpm)	Exposure time	Intensity of UV light (mW/cm^2)	Thickness (µm)	Comments
S41	400	1’	5.3	85.8	Water bottle jet plus 5 min sonication in water. The layer was coming off.
S42	800	1’	5.3	41.6	2 min of sonication in water. No grooves beyond 2 microns deep
S43	600	1’	5.3	79.03	Only water bottle jet used. No grooves beyond 2 microns deep

Table 6: Data from different ways of developing

Different conclusions were obtained from these samples:

- The water jet was not enough to develop, more pressure was needed.
- The ultrasound bath removed partially the SBX and gave bad definition of the grooves sides which were distorted probably by the vibrations produced.

In the light of these results finger rubbing was determined as the development method to be used. Two samples were prepared (Table 7) to check the grooves widths transfer from the mask pattern to the SBX.

Sample	Thickness (µm)	Exposure time (s)	Intensity of UV light (mW/cm^2)
X	79.03	60	5.3
R	377	60	5.3

Table 7: Samples made to check width of the grooves onto SBX

The grooves depths and widths measurements obtained in the SBX have been written in the first columns of Table 8 and Table 9. In the last column, the mask width of the grooves is shown (the targeted width that the SBX grooves should be).

Dipping samples on a water recipient, as it would be done in a normal development, was noticed to be ineffective. Water was also thrown from a bottle through a nozzle with no effect. Because of this, it was decided to help developing by finger rubbing. The grooves width was extremely affected by finger rubbing and the grooves were much wider that they were meant to be after developing. With regard to the depth of the grooves, not even a 50% of the SBX thickness was developed in the best case (2nd set of grooves).

SAMPLE X					
1st set of grooves					
SBX grooves depths	Mean	SBX grooves widths	Mean	Mask width	OBSERVATIONS
1.27	2.69	211	277.8	150	Developed by finger rubbing. Lower force applied than for second set
4.11		270			
		271			
		309			
		328			
2nd set of grooves					
SBX grooves depths	Mean	SBX grooves widths	Mean	Mask width	OBSERVATIONS
36.9	37.96	560	664	350	Developed by finger rubbing
37.6		733			
36.7		695			
30		695			
48.6		637			

Table 8: Sample R developing data

For Table 9, the data missing is because the values obtained were very close one to each other that no more data was taken.

SAMPLE R				
1st set of grooves				
SBX Groove depth	Mean	SBX grooves widths	Mean	Mask width
75	87.5	190	226	150
100		176		
--		312		
2nd set of grooves				
SBX Groove depth	Mean	SBX grooves widths	Mean	Mask width
--	20	405	405	350
--		424		
--		386		
3rd set of grooves				
SBX Groove depth	Mean	SBX grooves widths	Mean	Mask width
15.3	21.98	232	289.75	300
15.4		309		
17		309		
40.2		309		
4th set of grooves				
SBX Groove depth	Mean	SBX grooves widths	Mean	Mask width
--	20	256	279	200
--		270		
--		311		

Table 9: Sample R developing data

Although the grooves depths were very low, the widths were quite good and even though they were not the desired values, at least they were close to them.

Development through-the-thickness was difficult whilst, in theory, it should be an easy and fast process. A sample was spun and dried overnight in order to test the solubility of an uncured film. The SBX layer was tried to be washed off using warm water (28ºC). It proved to be as difficult as when it was tried to develop the grooves. From this last experiment and taking into account all the previous experiments the SBX was determined to be probably either partially cured or spoiled after the time spent on the shelf before use.

Reasons why the exact width desired for the grooves was not obtained could be:

1. The quality and resolution of the printed mask from the photocopier was low. This masked was observed under the optical microscope. The ink spots in the lines were able to be seen and due to these ink spots, the line edges were irregular. Therefore, light could go through the space between the ink spots, strongly affecting the definition of the SBX grooves as they were partially cured.

2. The samples substrate was a glass slide. Therefore some of the light could have been reflected off the metal chuck of the UV system, curing the grooves from the bottom. Furthermore, the thicker the sample the higher the possibility that some of the light was deflected by the SBX layer and cured part of the grooves.

3. Developing should be an even process. However, water pressure seemed a key thing to develop SBX. Besides the pressure was applied in small regions instead of on the whole surface by means of a jet which promoted an uneven development. This could have lead to the differences between the grooves depths and widths.

4.4 New SBX

4.4.1 Spinning

The new SBX was much more fluid than the old SBX so ultrasound bathing was no longer required. Besides, the samples made with new SBX had no comets after spinning.

An SBX film was spun at 400 rpm on a glass slide and after drying the SBX layer was tried to be washed off. It took 4 minutes under the tap to remove the film. Yet unlike what happened with the old SBX, this time it was possible to wash the SBX off.

As for the old SBX, the relation between the rotational speed and the SBX film thickness was researched. The data obtained is shown in Table 9.

Rotational speed (rpm)	Film thickness (µm)
150	88.46
180	64.5
190	72
200	65.1
210	62.2
270	45.2
340	39.4
390	33.5
2000	6.4

Table 10: Data obtained for the relation between the rotational speed and film thickness from the New SBX

This data has been plotted in Figure 39. A power regression trend seems much more obvious with respect to the old SBX. The regression factor is very acceptable (0.995). The old SBX data has been plotted in blue points for reference.

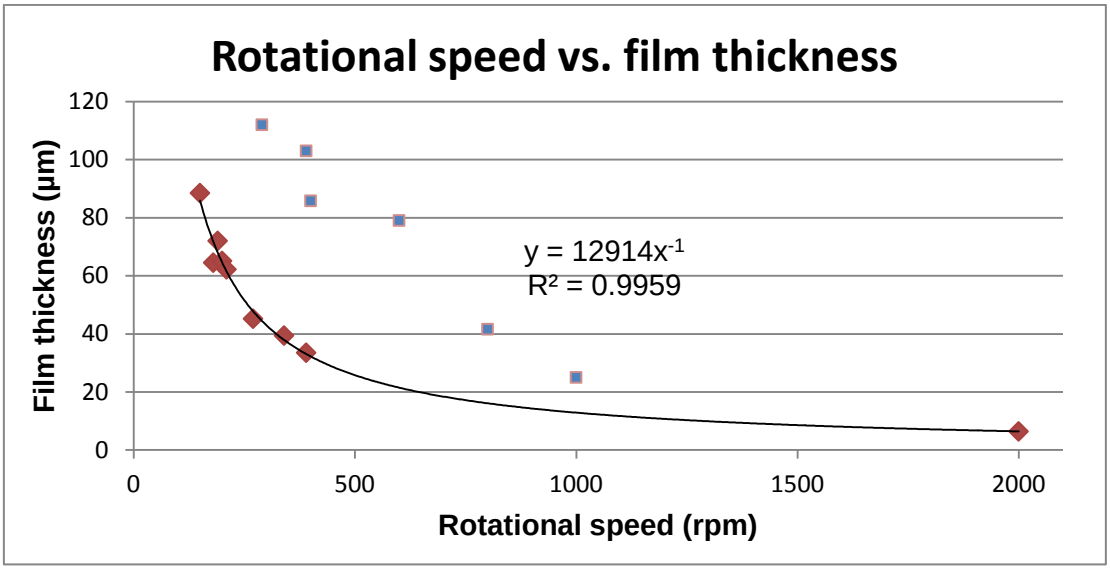

Figure 39: Plot of the correlation between rotation speed and film thickness from the new SBX. The blue points correspond to the data from the old SBX

Thinner films were obtained for the new SBX, demonstrating much better fluidity in addition to a clearer and more accurate trend which assures more reliability in future thickness predictions using this model. This trend is completely in accordance with the first model proposed by Society of Components, Packaging and Manufacturing Technology (71) where it is stated that for cases with no evaporation during the spinning process, the film thickness varies with the spin speed and time. Provided that the time was set constant and equal to 30 seconds their equation shows that the film thickness is directly proportional to the inverse of the rotational speed just.

The reproducibility of the thicknesses was studied by means of some samples prepared at low speeds with the new SBX (Table 11). Low speeds had to be used in an attempt to reach the desired film thickness of 260 µm (fibre thickness). After some trials at low speed watching the SBX behaviour, 70 rpm was decided to be the minimum speed to spin SBX. Different samples were spun at 70 and 80 rpm. For the former speed, thicknesses varied around 13 µm whereas for the latter speed varied round about 40 µm. These variations may be attributed to:

- The difference in the amount of SBX poured on the glass slide for each sample.
- The spinner time was not enough to reach the equilibrium of forces in the film.
- The low speeds at which the samples were spun may have been too slow for the spinning to have enough effect.

It was concluded that thicknesses were not reproducible at low speeds.

Rotational speed (rpm)	Film thickness (µm)	Mean (µm)	Standard deviation
70	99.76	105.16	5.87
70	102.4		
70	113.33		
80	128	108.33	11.87
80	111		
80	104.56		
80	88.9		
80	102.4		
80	113.33		

Table 11: Reproducibility tests

One of the batches of samples prepared was dried on a slightly tilted surface. As a consequence, all samples end up with uneven surfaces and the batch had to be discarded. The conclusion is that in order to ensure the SBX film flatness a flat surface is required.

4.4.2 Development study

To start with, three samples were prepared, cured using the low quality mask shown in Figure 27 and finally developed. They main objective was check the width of the grooves. The data regarding these samples is given in Table 12, Table 13, Table 14 and Table 15.

Sample	Film thickness (µm)	Exposure time	Intensity of UV light (mW/cm^2)	Observations
46	39.15	2'	5.3	Developed under tap nozzle
47	45.2	3'	5.3	Developed with water bottle jet
48	33.5	4'	5.3	Developed with water bottle jet

Table 12: Data from samples 46, 47 and 48

SAMPLE 46			
1st set of grooves			
Mean grooves depth (µm)	Widths (µm)	Mean	Mask width (µm)
0.4866	260.21	318.4	300
	312.75		
	382.24		
2nd set of grooves			
Mean grooves depth (µm)	Widths (µm)	Mean	Mask width (µm)
3	364.86	370.66	350
	364.87		
	382.24		
3rd set of grooves			
Mean grooves depth (µm)	Widths (µm)	Mean	Mask width (µm)
3	208.50	217.45	150
	243.24		
	200.62		

Table 13: Sample 46 developing data

SAMPLE 47				
1st set of grooves				
Mean groove depth (µm)	Widths (µm)	Mean	Mask lines width (µm)	Comments
20	173.74	208.49	300	This set of grooves seemed well developed
	225.87			
	225.87			
2nd set of grooves				
Mean groove depth (µm)	Widths (µm)	Mean	Mask lines width (µm)	
2	278.80	301.1	350	
	329.15			
	295.36			
3rd set of grooves				
Mean groove depth (µm)	Widths (µm)	Mean	Mask lines width (µm)	
2	277.99	289.57	150	
	295.37			
	295.37			

Table 14: Sample 47 developing data

SAMPLE 48			
1st set of grooves			
Mean groove depth (µm)	Widths (µm)	Mean	Mask lines width (µm)
2.1	295.37	249.03	300
	225.87		
	225.87		
2nd set of grooves			
Mean groove depth (µm)	Widths (µm)	Mean	Mask lines width (µm)
2.6	399.62	330.12	350
	312.74		
	278		
3rd set of grooves			
Mean groove depth (µm)	Widths (µm)	Mean	Mask lines width (µm)
3	225.87	231.66	150
	208.5		
	260.62		

Table 15: Sample 48 developing data

The conclusion from these three developed samples is that the grooves widths are in the range of 50 µm compared to the original width in the mask except for the narrow grooves. In particular, for thick grooves (300 µm and 350 µm) the developed widths were always below these values except in one case. On the other hand, for the thin grooves (150 micrometers), the values obtained were above the mask width. This means that if 260 microns wide grooves are desired, it should be used the 300 micrometers mask lines in order to have a safety margin. Besides, the low development efficiency of both the water bottle jet and the development close to the nozzle of the tap denoted that more pressure was r.

Reproducibility study

The reproducibility data at a certain speed from the samples mentioned in section 3.4.2.1.3 is shown in Table 16 and Table 17. The development depth was also investigated. These samples were prepared in the meantime whilst the designed grooves mask was being made. Because of this, the development was done under a special mask with rectangular features from another project.

Sample	Rotational speed (rpm)	Exposure time	Development time	Intensity (mW/cm^2)	Thickness (µm)	Depth of best feature (µm)
53	80	35"		5.2	128	62.3
54	80	45"	1'34"	5.2	111.00	57.2
55	80	55"	3'30"	5.2	104.57	70.3
58	80	60"	8'	5.2	113.33	60.5
56	80	1'05"	4'14"	5.2	88.90	45.3
57	80	1'15"	4'	5.2	102.40	69.1
Extra samples						
A1	70	2'	2'42"	5.3	30.77	11.7
A2	150	1'	2”35”		88.47	89.3
A3	210	40"	2”15”		55.90	62.2
A4	190	1'	2'30"		72.00	72

Table 16: Reproducibility data obtained

Furthermore, notes were taken during the experiments and are attached in Table 17.

Sample	Observations
53	Only finger rubbing seems effective but not much. SBX film dissolves when placed in ultrasound bath with water.
54	Only finger rubbing seem effective but not much. When put in ultrasound bath, SBX dissolves and features seem to be removed in particles (pits). Low quality of the features.
55	SBX seem cured but it is soft. First was developed under certain distance from the tap and then it was placed in an ultrasound bath and after 3 minutes some of the features was totally developed but with low quality.
58	Developing is hard. Finger rubbing seems to help. Apparently, the layer is too thick to be well developed with the tap pressure. Confirmed that the SBX develop by layers. Water comes underneath the film. Curing seems complete.
56	Feature developed. Left 3 min in ultrasound bathing. Features are developed with low quality and water comes underneath the film.
57	SBX seems clearly cured. Left 6 minutes in ultrasound bathing. The features are developed in a pitting-like way.
Extra samples	
A1	Developed using water bottle jet plus 1 min under the tap. SBX only comes off when rubbing with finger and very difficulty
A2	Almost impossible to develop, only a big feature developed. Warm water (32ºC) was used after with no better effect though supposedly should have dissolve totally SBX.
A3	Features difficult to develop. The SBX does not seem cured at all. Water gets underneath SBX film.
A4	Easy development under tap. Good sample with some features fully and well developed features.

Table 17: Observations and notes taken for samples developed with the features mask.

Development through the thickness was not viable provided the low quality of the fully developed features. Examples of this low quality are shown in Figure 41, where it can be observed that the features edges were poorly defined even for the best developed sample (sample A4). On the contrary, features not fully developed had good definition as shown in Figure 42. An ultrasound bath was given to some samples in order to promote the development; however, the features edges were extremely distorted as shown in Figure 40.

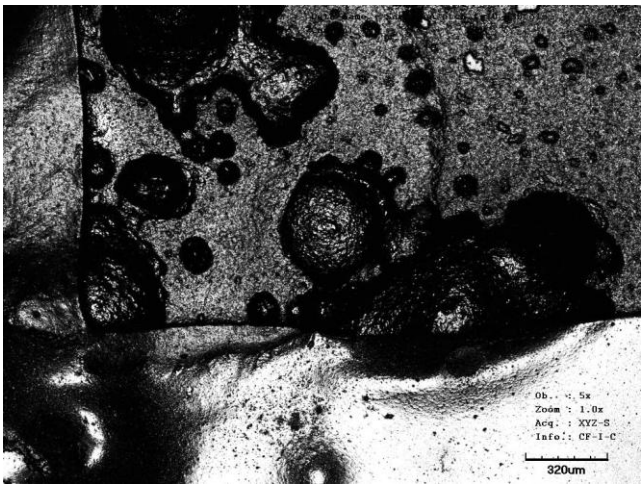

Figure 40: Effect of ultrasound bath on a feature

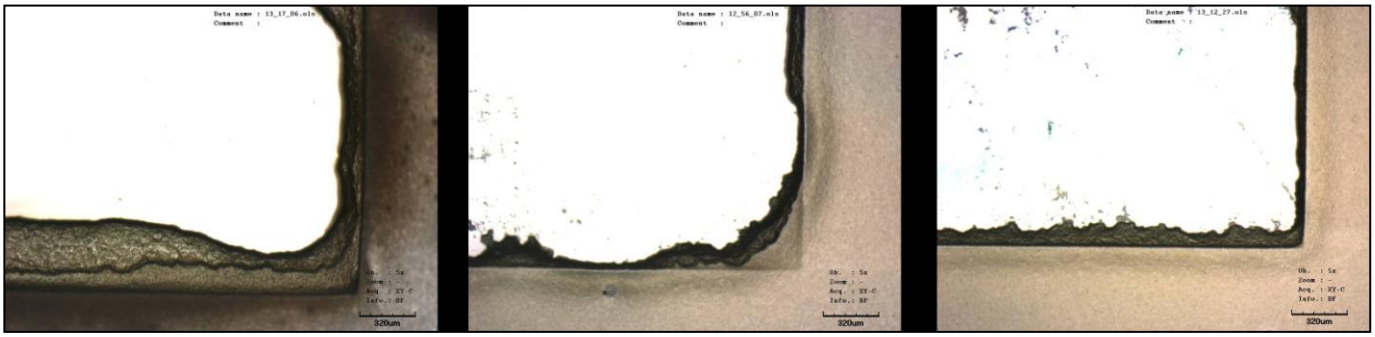

Figure 41: from left to right, samples A1, A2 and A4. Features developed through the thickness. The scale shown in the bottom right corner is 320µm

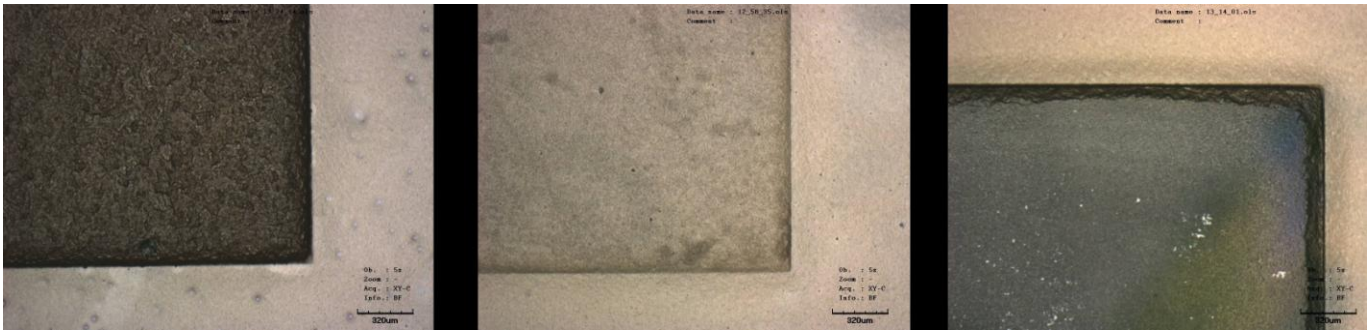

Figure 42: from left t right, samples A1, A2 and A4. Features not totally developed. The scale shown in the bottom right corner is 320µm

Designed mask samples

A single test was performed to check the development of an overcured sample and the effect of water on cured SBX. Sample 62 was prepared for this purpose. The data is shown below in Table 18. The sample was impossible to be developed and after leaving the sample an entire night soaking in water, the film was not affected and did not come off the substrate.

Once the designed mask was received, two samples were prepared so as to research the development depths and widths. The samples data is shown in Table 18. This time, a small tube with a change in section between the inlet and the outlet (smaller) was attached to the tap nozzle in order to increase the pressure of the water jet.

Sample	Rotational speed (rpm)	Exposure time	Development time	Intensity (mW/cm^2)	Thickness (µm)
59	180	1'	2'30"	5.5	64.50
60	200	1'	2'30"	5.5	65.05
62	150	10’	5’	5.7	Not checked

Table 18: Data regarding how the samples 59 and 60 were prepared for development

For sample 59, SBX seemed developed and the pressure effect peeled off part of the SBX from the substrate. Only the first set of grooves fully survived the water pressure applied. Some of the grooves were distorted as shown in Figure

43 because of pressure effect. The SBX remaining between the grooves may not withstand the water pressure if this is too high. In the same way, pressure affected sample 60. The development seemed successful though and the grooves were fully developed. The profile shown by the Dektak machine of the grooves bottom was flat indicating that the glass surface was reached.

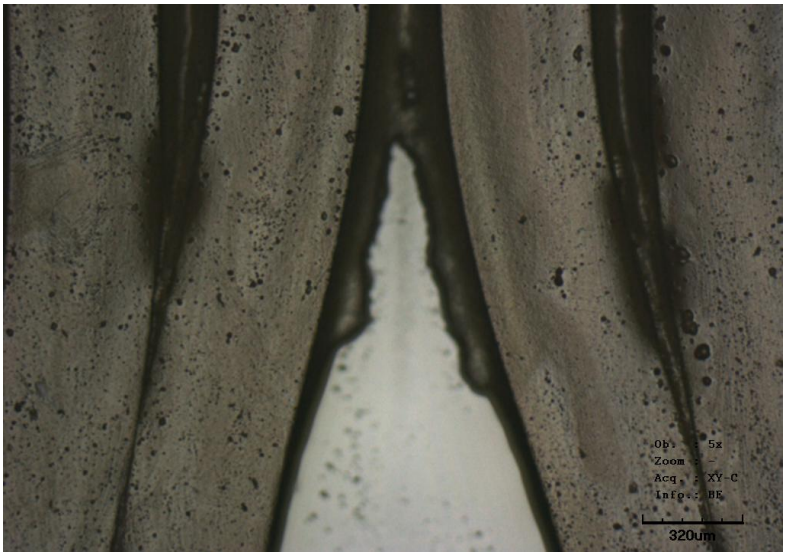

Figure 43: Distorted grooves by the pressure effect in sample 59

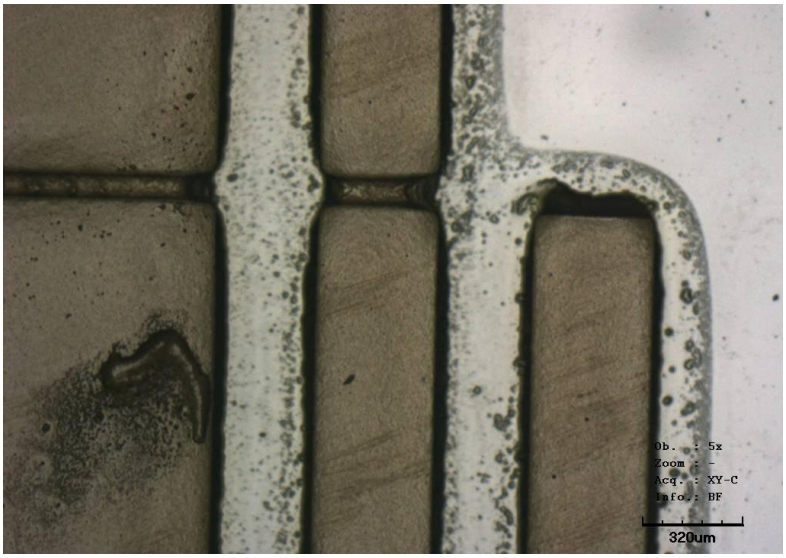

Figure 44: Grooves well developed in sample 60

The alignment marks were meant to serve as guidance for subsequent fibre arrangements and IDE alignments on the PZT5A fibres. However, they were not

fully developed partly because it was not spent as much time developing them as for the grooves. They seemed well defined as it can be observed in Figure 45 though. The sides of the squared alignment marks were measured on the SBX to be around 50 micrometers which was what they were meant to be.

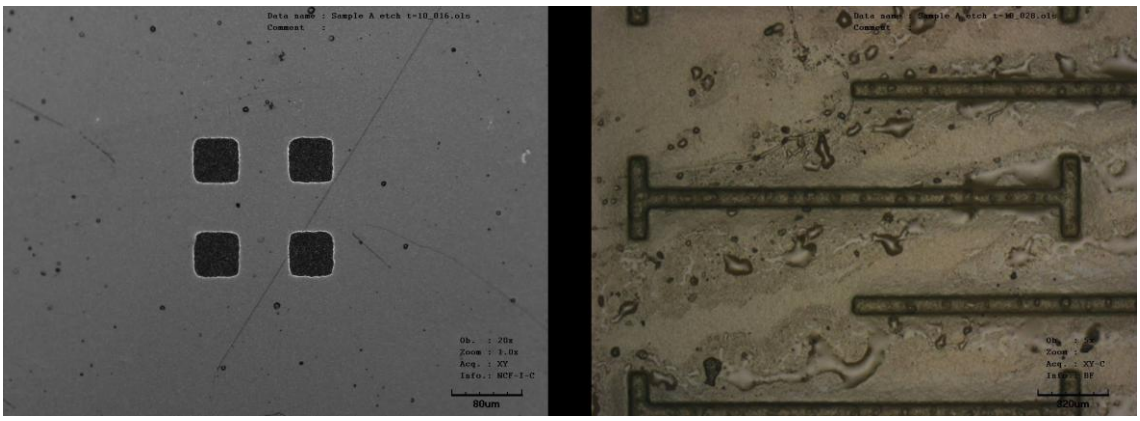

Figure 45: IDE mask alignment (left) and carbon fibres mask alignments (right)

As commented before during this section tests, it was noticed that at some stage of development of some samples, the SBX was being removed in layers when developed. Then, it was thought that it could be enhanced the development process if a sample composed of different thin layers would be prepared. Then, a multi-layer sample was prepares as described in section 3.4.2.1.3, the development results of which are shown in Table 19.

Multilayer sample	Thickness (µm)		Developing time		
	62.67		4 ‘		
1st grooves set	Grooves depth (µm)	Mean	Groove widths (µm)	Mean	Mask lines width
	15.4	**11.68**	222	**254.18**	**300**
	12.3		260.62		
	7.35		279.92		
2nd grooves set	Grooves depth (µm)	Mean	Groove widths (µm)	Mean	Mask lines width
	43.5	**38.67**	318.53	**305.56**	**300**
	38.3		289.58		
	34.2		308.58		
3rd grooves set	Grooves depth (µm)	Mean	Groove widths (µm)	Mean	Mask lines width
	56.8	**58.13**	220.08	**212.36**	**200**
	58.8		220.08		
	58.8		196.91		

4th grooves set	Grooves depth (µm)	Mean	Groove widths (µm)	Mean	Mask lines width
	49.7	**48.40**	208.49	**200.77**	**200**
	38.8		185.33		
	56.7		208.49		

Table 19: Development results for the Multilayer sample.

The third and the fourth set of grooves seemed to be fully developed. More time was spent with these grooves because the development seemed effective there. The SBX film was very thin though. Moreover, the difference between the lines widths in the mask and the grooves widths reached minimum values (compared to previous samples), which meant a good transfer of the pattern with this designed mask. An example of this good transferring is shown in Figure 46, where it may be appreciated the straight grooves edges.

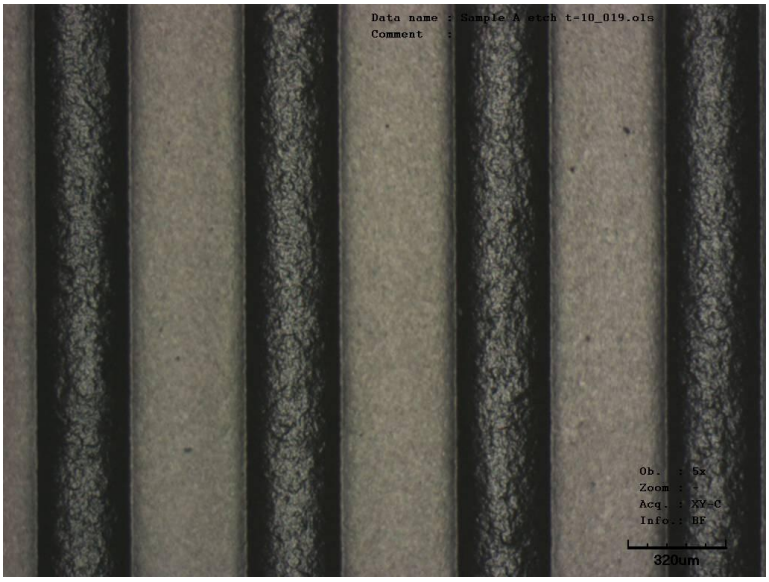

Figure 46: Second set of grooves developed on the multilayer sample. Confocal microscope image

4.5 Conclusions of the development process

- The old SBX was partially cured, dried or even spoiled before use.
- The new SBX clearly shows a relationship between rotational speed and SBX film thickness which can be used as a model.

- Water may not be a developer but a physical remover for the SBX and thus pressure is crucial.

- All the effective development methods for SBX tried were not homogeneous over the surface; it was always focused in a region of the surface. An even development would be desirable.

- Developing the SBX through its thickness would allow placing one IDE in each side of the fibres permitting to pole the composite either along the fibres axis or in thickness direction. However, though it can be achieved as in sample 60, the pressure needed in order to do so was too much that caused grooves distortion. In the case of the samples cured under the features mask development through the thickness can be achieved for certain thicknesses and features sizes.

- A water jet seems to be the most effective way to develop SBX which confirms the information from the user instructions.

- Ultrasound baths were definitely not helpful and promoted SBX removal in pits as well as helping the SBX layer to come off the substrate. In Figure 40 the mentioned effect provoked by the ultrasound bath vibrations is shown. It can be noticed that the edge of the feature is extremely distorted as well as the pits generated by the vibrations.

- Although ultrasound baths dissolved SBX, it had non-desired effects on the grooves quality (definition) and on the film.

- The definition of partially developed features and grooves widths were good enough to position and align the PZT fibres.

- The definition of fully developed features was very poor, especially looking at the edges where some SBX was still attached to the film.

- A multilayer film seems the best option to achieve good width transfer from the pattern on the mask to the SBX. Nevertheless, a shallow thickness was obtained in the case of the multilayer sample.

- Exposure times between 1 minute and 2 minutes seemed fine for the range of thicknesses worked (around 100 micrometers).

4.6 Casting SBX

According to the instructions, the shrinkage factor (the ratio between the wet thickness and the final dry thickness) is 3.75. Some samples were prepared so as to ratify this value for both the old SBX (Table 20) and the new SBX (Table 21). As mentioned in section 3.4.2.2, each spacer (tape strip) was 130 µm thick. As a consequence, the wet thickness using 4 spacers was 4 times 130 µm, which is 390 µm. For 9 spacers, the wet thickness is 1170 µm.

Old SBX				
4 spacer				
Sample	Wet thickness (µm)	Dried thicknesses (µm)	Mean	Shrinkage factor
1	390	237	288	1.65
2	390	242	Standard deviation	1.61
5	390	385	68.62	1.01
9 spacer				
Sample	Wet thickness (µm)	Dried thicknesses (µm)	Mean	Shrinkage factor
5	1170	555	540.25	2.11
10	1170	377	Standard deviation	3.10
23	1170	596	98.21	1.96
26	1170	633		1.85

Table 20: Old SBX casting data

New SBX				
4 spacer				
Sample	Wet thickness (µm)	Dried thicknesses (µm)	Mean	Shrinkage factor
11	390	338	284	1.15
17	390	240	Standard deviation	1.63
18	390	289	35.71	1.35
19	390	269		1.45
9 spacer				
Sample	Wet thickness (µm)	Dried thicknesses (µm)	Mean	Shrinkage factor
14	1170	416	414.25	2.81
141	1170	383	Standard deviation	3.05
28	1170	478	39.42	2.45
30	1170	380		3.08

Table 21: New SBX casting data

The shrinkage factor was definitely not close to 3.75.The results show that the thicker the SBX film was the more shrinkage the film underwent. The dispersions of the manual casting (standard deviation of the samples) were much higher than for the spinning process shown in Table 11.

A plot of the data (Figure 47) has been done to compare old and new SBX and to show the dispersion of the data.

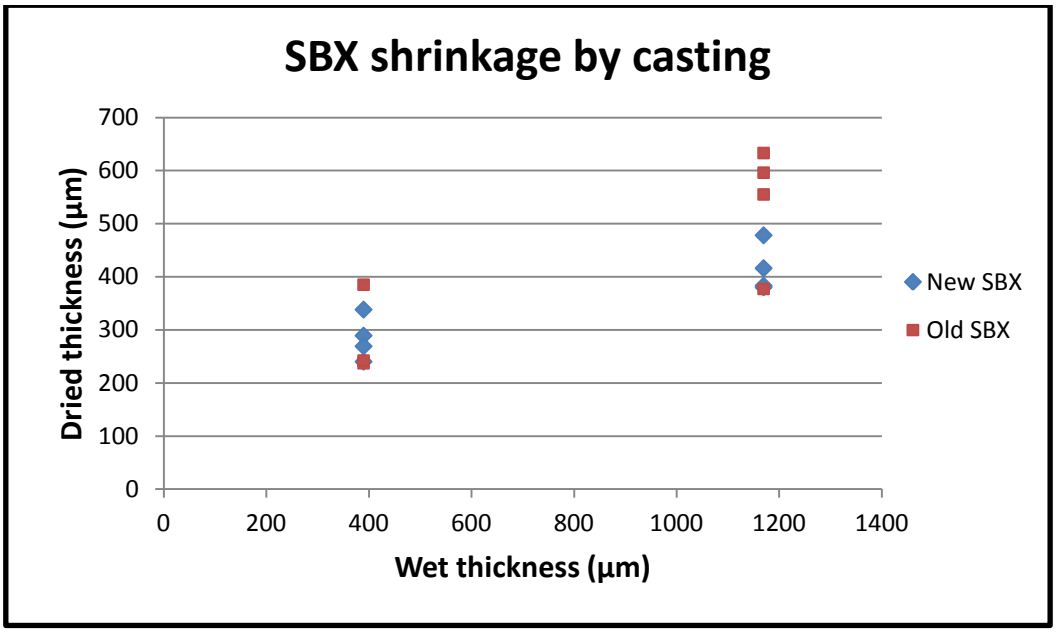

Figure 47: Casting data comparison for old and new SBX

The information extracted from this plot is that:

- The thickness dispersion of the casted samples was greater for the old SBX than for the new SBX.

- The new SBX shrank around a 25% for the thinner samples and around 63% for the thicker samples.

- Although this process is fast and easy, it gives too much thickness variation to be used to prepare samples with a certain film thickness. The surface profile may depend on the blade (glass slide) passed across it and the spacers (tape strips) span.

- It is possible to reach thicknesses around the fibres thickness.

4.7 IDEs results and discussion

During the developing sections it was conceived the idea that developing through the SBX thickness was a hard and risky task in order to obtain good and well defined grooves. However, when the samples were not fully developed the quality and definition were good. Consequently, the idea of doing grooves was still good but only to align the fibres and lay down an IDE in one side of them, not on both sides as it would have been possible with a full development.

Shadow mask done to deposit an IDE by evaporation

Figure 48 shows an image of the copper shadow mask prepare by the process described in section 3.7.2.1. Only the IDE patterns with the larger finger separation were fully etched in this sample. These particular IDEs were then separated and used to provide the masking in both the evaporation and the screen printing approaches the results of which are now discussed.
The thickness of the shadow mask, shown in Figure 48, was around 42 micrometers thick.

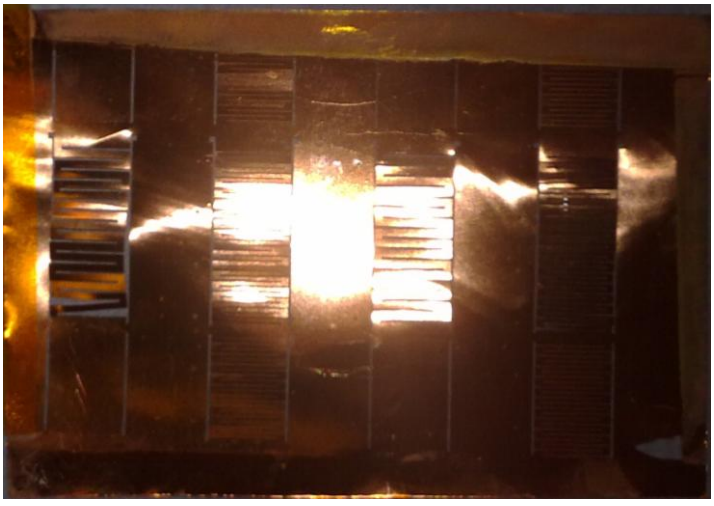

Figure 48: Copper shadow mask

4.7.1 Sample made by evaporating IDE (First approach)

The IDE surface was very bumpy because the SBX was less thick than the fibres were. The surface roughness can be appreciated in the right picture of Figure 49. Some electrical measurements were performed so as to measure track resistance. It was checked that there was no contact between the IDE sides. The track resistance values obtained between the extremes of each side were 39Ω and 38.5Ω.

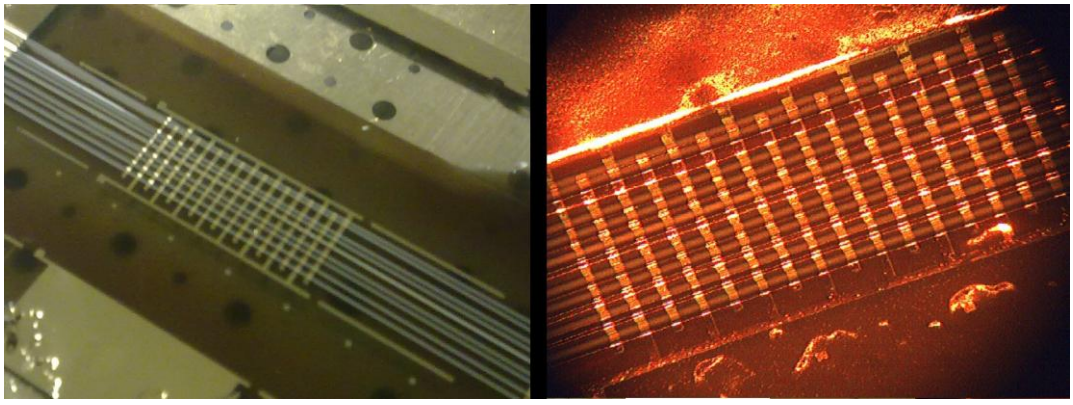

Figure 49: Evaporated IDE on a sample (left) and optical microscope picture (right)

4.7.2 Sputtered IDEs

The aluminium film thickness obtained was 100nm.

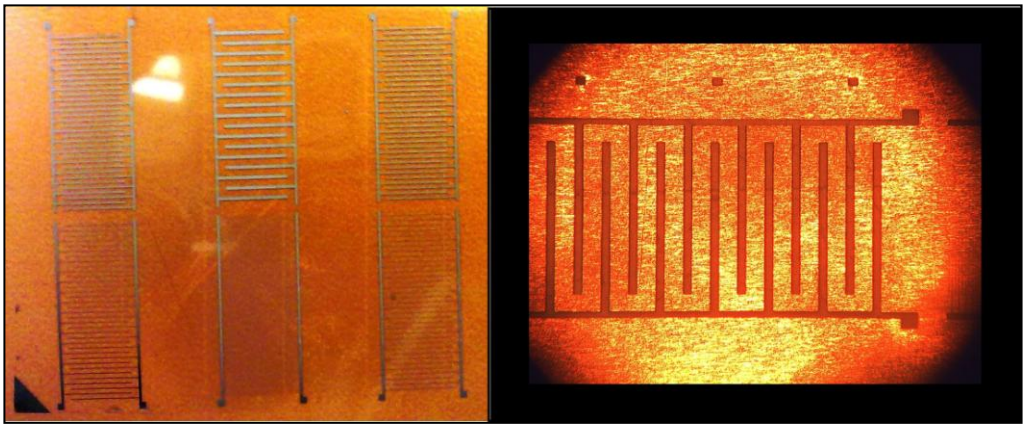

Figure 50: Al IDEs sputtered onto Polyimide film (left) and one of the Al IDEs under the optical microscope (right)

Some electrical tests were performed to have an idea of the resistance of the track between the electrical pad and the most extreme part of the fingers as well for the sputtered IDEs. It was also checked whether or not there were short-circuits between both sides of each IDE.

In Figure 30 the IDEs were numbered and the characteristics described in Table 4. It resulted that some of the IDE with the design of IDE 1 (the thinnest fingers) had short-circuits between both IDE sides so they were useless. The values of resistance obtained in different tests were 555Ω, 332Ω, 206Ω and 637Ω between sides. Resistance values for the IDEs without short-circuits are in Table 22. These measurements were taken from the electrical pad to the most extreme part of the same side.

IDE	Track resistance (Ω)	
IDE 1	144	--
IDE 2	150.8	--
IDE 3	185	115
IDE 4	179.5	133.5

Table 22: Resistance values for sputtered IDEs

4.7.3 Sample made with the sputtered IDEs and PDMS as adhesive (second approach)

Although it was tried to prevent bubbling by all means, some bubbles appeared in between and around the fibres at the moment of putting in contact both polyimide films with the PDMS. A picture was taken under the optical microscope to show it (Figure 51). These bubbles, as mentioned before, are a risk because they would act as stress concentrators and also because could affect the sample poling.

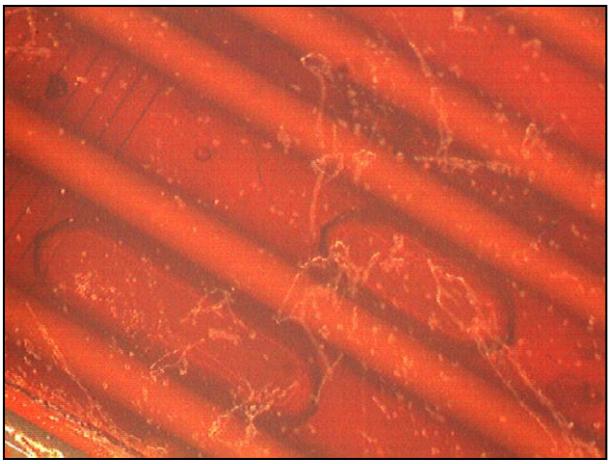

Figure 51: Bubbles appeared in between fibres

The final sample is shown in Figure 52.

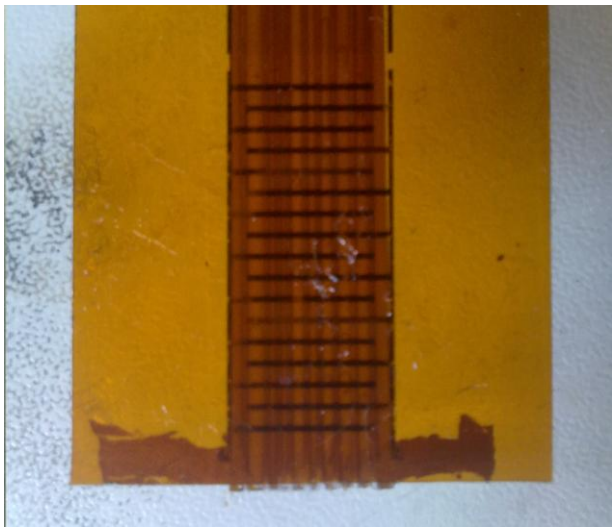

Figure 52: Sample made with two polyimide films and PDMS as adhesive

4.7.4 Screen printed IDEs

An attempt to screen print the IDE was done on a glass slide (Figure 53).

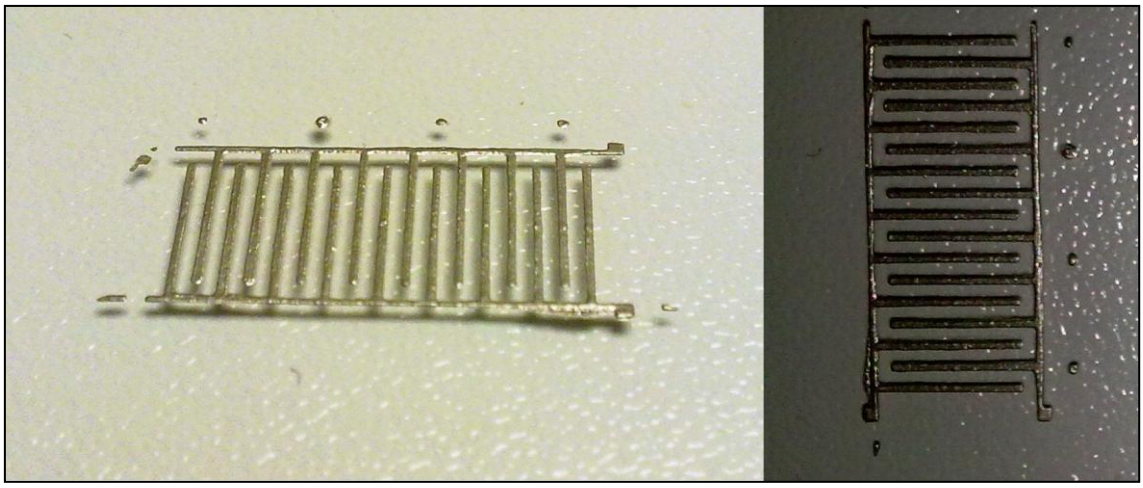

Figure 53: Screen-printed IDE onto glass slide

Some electrical tests were performed to measure the track resistance in this IDE as well. The resistance values were 6.9Ω and 5.4Ω between extremes of both sided. There was not short-circuiting between sides. The thickness of the screen-printed IDE was also checked in various fingers having values of 31.8, 29.9 and 31.9 micrometers. Obviously, the resistance is much lower (around 30 times) than for the sputtered IDE but, on the other hand the IDE was also much thicker (300 times). When the epoxy was too thick then a spring-back problem came across when it was tried to lift the mask (the resin stuck partially to the mask). This was another reason why the silver epoxy was thinned.

4.7.5 Sample made by screen printing (third approach)

The fibres were not perfectly aligned. Some of them had moved when they were pressed against the SBX. The IDE did not look very good and the quality was very poor due to the difficulty of making the epoxy to pass through the shadow mask (see Figure 54). It was experienced again the spring-back effect, previously commented, when lifting the shadow mask removing some of the epoxy just screen-printed. The rough surface caused by the thickness difference between the fibres and the SBX played a key role in order not has a good IDE screen-printing. There were zones where more epoxy had to be passed through provided the differences in thickness (more space to fill). All the electrical measurements obviously failed.

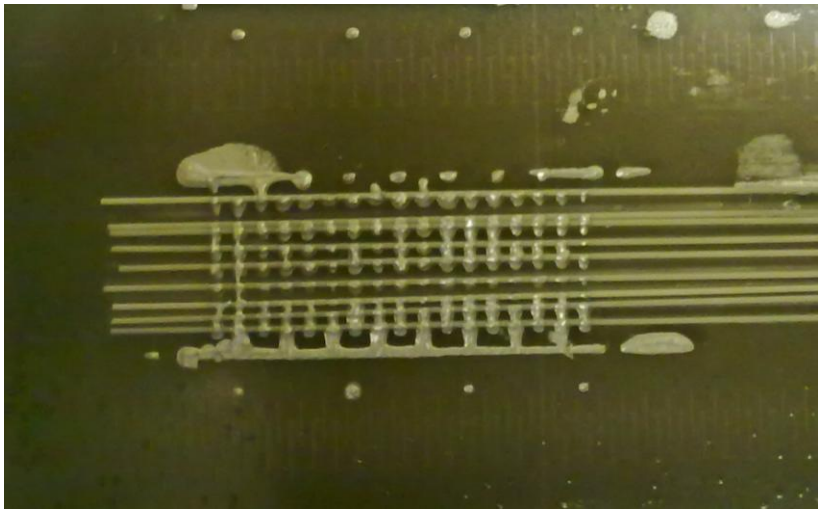

Figure 54: Sample with screen-printed IDE

4.7.6 Conclusions

First approach

- Surprisingly the SBX seemed not to be affected by the temperature in the evaporation chamber so apparently, it a viable process.
- The resistance obtained in the evaporated IDE was relatively low. However, it could be better if the surface had been flatter, in addition to contain less strain. Therefore, again, thickness control is very important to achieve the dry thickness near to the fibres thickness and so the desired flatness.

Second approach

- This method produced the best defined IDE electrodes. However it was the least reliable in achieving good electrical contact to the PZT fibres.
- The approach of putting together the two polyimide films, one with the IDE and other with the SBX plus fibres seems a good idea. However, the selection of the adhesive is a key thing. Bubbles appeared when using PDMS and it supposes a big issue. Besides, it was not tested whether PDMS was a good adhesive.

- It was not possible to check the conductivity of the IDE after fabricating the composite. This conductivity might have changed. Furthermore, there was no way to know how well the contact was between the fibres and the IDE. Again the flatter the surface of the SBX plus the fibres the better to prevent strains on the IDE.

- For this approach the carbon fibre arrays would apply the stress on the two polyimide films in the middle. These films would take away direct stress on the PZT fibres.

Third approach

- For the screen-printed IDE, flatness was a factor as vital and crucial as for the evaporating approach. The flatter the sample the easier to pass the silver epoxy through the shadow mask. The transferred IDE pattern was not good partly because of the roughness of the sample.

- The spring-back effect experienced when removing the shadow mask is directly related to the viscosity of the silver epoxy resin. Further trials to find a good compromise between the amount of acetone to thin the silver epoxy and the electrical conductivity of the resulting thinned silver epoxy should be done. In simple words viscosity optimisation of the silver epoxy resin would be required.

- This approach is the one in which more tasks were carried out by the individual and as a consequence, more errors may be committed. Some of these stresses could be alleviated using automated screen-printing set-ups though.

4.8 Mechanical tests

4.8.1 Horizontal test vs. vertical test

The curves from the data obtained are plotted in Figure 55 and as it can be seen all the tests were reporting the same data for forces lower than 1.5 N. A

very slight difference appeared in the end of the tests. This little difference could be due to some residual strains on the elastic band tested.

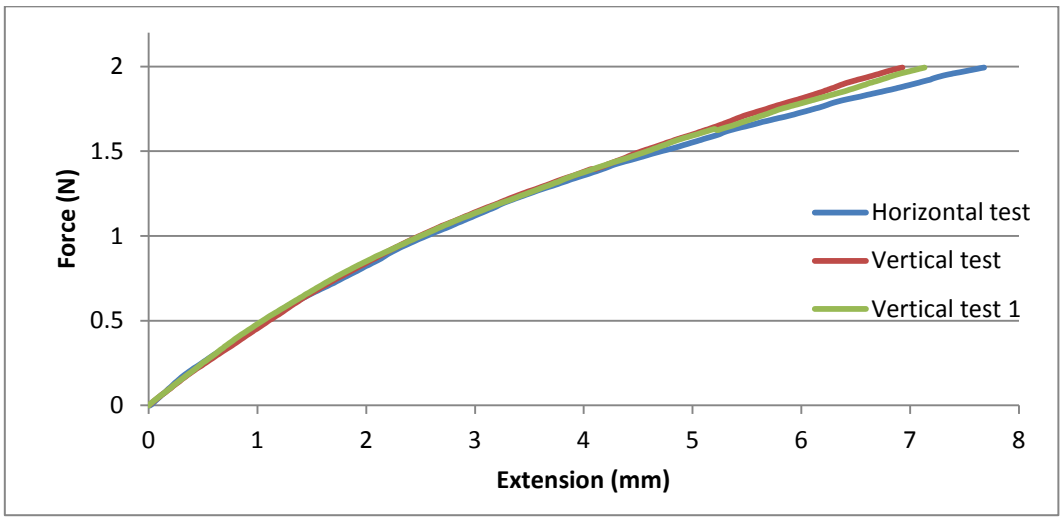

Figure 55: Comparison between vertical and horizontal test

4.8.2 Tests

The samples were casted as described in section 3.4.2.2 and cured under the sun 2 minutes. The size of all samples was 19 mm long by 5 mm wide except for the samples with carbon fibres in it that were 19mm long by 15mm wide. In Table 23 the thickness ranges have been written for the old and new SBX again as reminder.

SBX	4 SPACERS	9 SPACERS
NEW	284±40 µm	414.25±64 µm
OLD	288±97 µm	540.25±163 µm

Table 23: Dried thickness ranges

All samples were prepared using 4 spacers unless said the contrary. Also note that the word “extension” from the x axis in all plots refers to the distance that the tip bended the sample.

4.8.2.1 Fibres only tests

Four tests were performed to investigate the breaking point of the PZT fibres, shown in Figure 56.

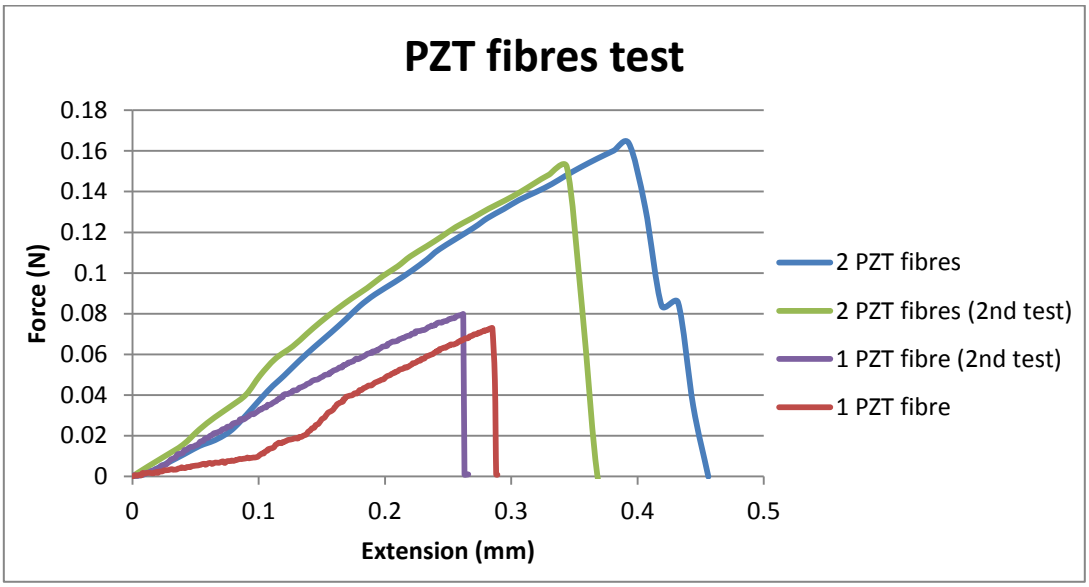

Figure 56: PZT fibre tests

The breaking point of a PZT fibre is somewhere around 0.07 N. Computing the flexural strength using Equation 6, it comes to be 24.086 MPa. In the case of two PZT fibres together the flexural strength turns out to be 51.61 MPa for a breaking point around 0.15 N, doubling the value of a single PZT fibre. It can be also seen that when two fibres where tested, the elastic part was longer than for the single PZT fibre and the breaking point occurred at more bending distance.

4.8.2.2 Old SBX

Here are presented the results obtained of the old SBX behaviour with and without fibres inside. The data was plotted in Figure 57

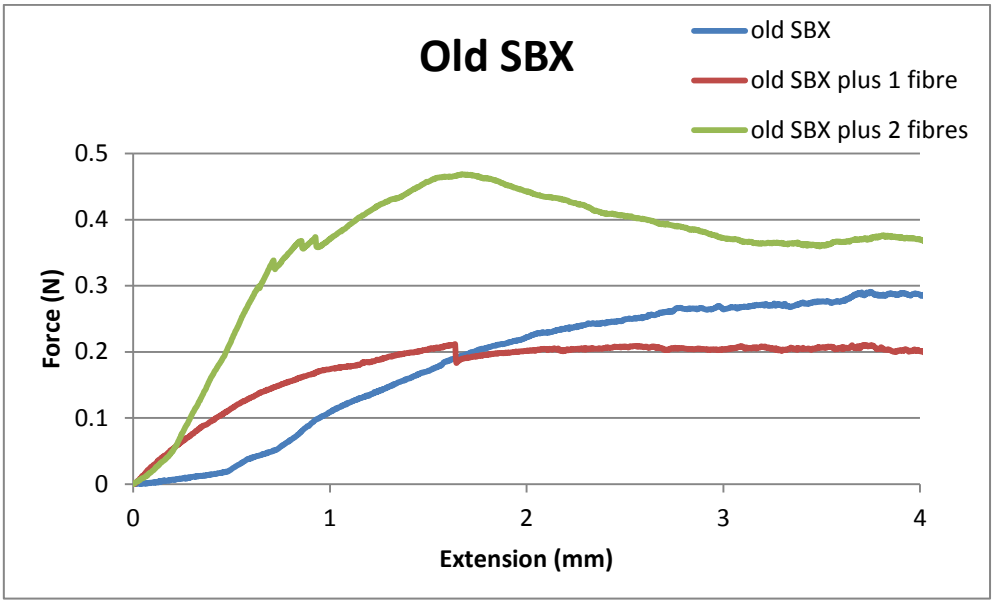

Figure 57: old SBX comparison

It can be observed that the fibres stiffen the composite. It is very clear the drop in the plot that occurs when the fibre breaks for the sample with one fibre. This drop was not so obvious. Besides, if the breaking point of the SBX plus one fibre of this graph (around 0.2N at 1.6mm) compared to the PZT fibre tested in previous graph (0.07N at 0.3mm), it is reasonable to think that the combination of the polymer matrix and the PZT fibre had a synergic effect.

In Figure 58 and Figure 59 are presented the tests done for SBX alone and for SBX plus a PZT fibre left one week under certain conditions explained in section 3.8.

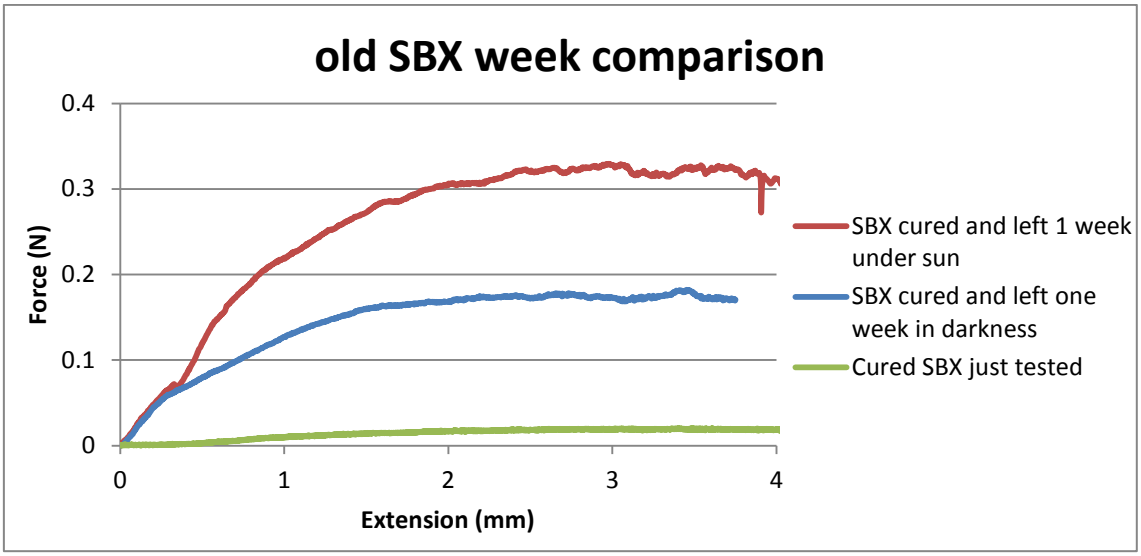

Figure 58: old SBX properties change with time

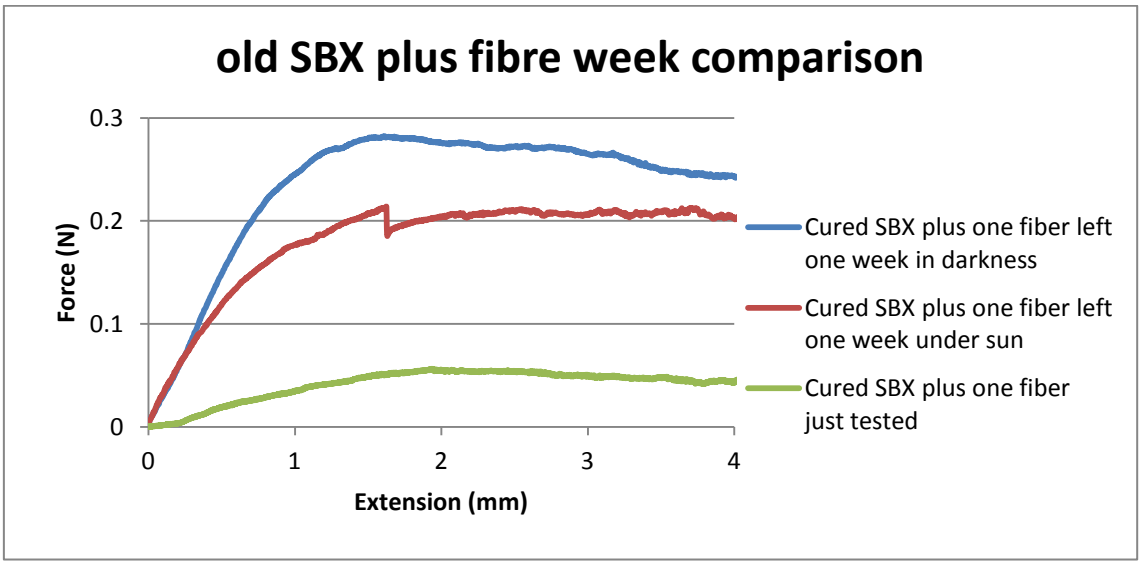

Figure 59: old SBX plus fibre change with time

It can be seen in Figure 58 that SBX changed its properties with time depending if it was left under the sun light or in darkness. Clearly, in both cases, after one week the SBX gained stiffness, being the stiffest the sample left under sun. An explanation for this could be that if two minutes were not enough for the SBX to fully cure, leaving the sample one week under sun light would have given it enough time to cure and consequently to fully cross-link.

On the other hand, for the samples with one fibre inside (Figure 59), although again the two samples left one week are stiffer than the SBX just tested, the stiffest was the sample left in darkness. In addition to this, it can be noticed that for the sample left under the sun it is possible to see the drop in the curve indicating that the fibre was broken but not for the sample left in darkness. This could be either because the fibre in the sample left in darkness was already broken somehow or because the sample was thick enough that the breaking drop was not appreciated by the machine.

Common sense says that samples left under sun should probably be stiffer than the ones left in darkness and that SBX plus a fibre should be stiffer than just SBX. However, it is not like this in these plots. An explanation to why the SBX plus a fibre would not be stiffer could be adhesion. Since supposedly the old SBX was already partially cured the fibre would not have adhered to it as well as it could do it for fresh and uncured SBX. In other words it could have been more difficult to have a good wetting of the fibres with the old SBX. Another explanation could be that overexposure may cause damage to the sample which weakens the structure.

The change of mechanical behaviour with relation to the thickness of the samples was something of interest so it was decided to compare samples with and without fibres for different sample thicknesses made out of 4 and 9 spacers. The plot of the data obtained is shown in Figure 60.

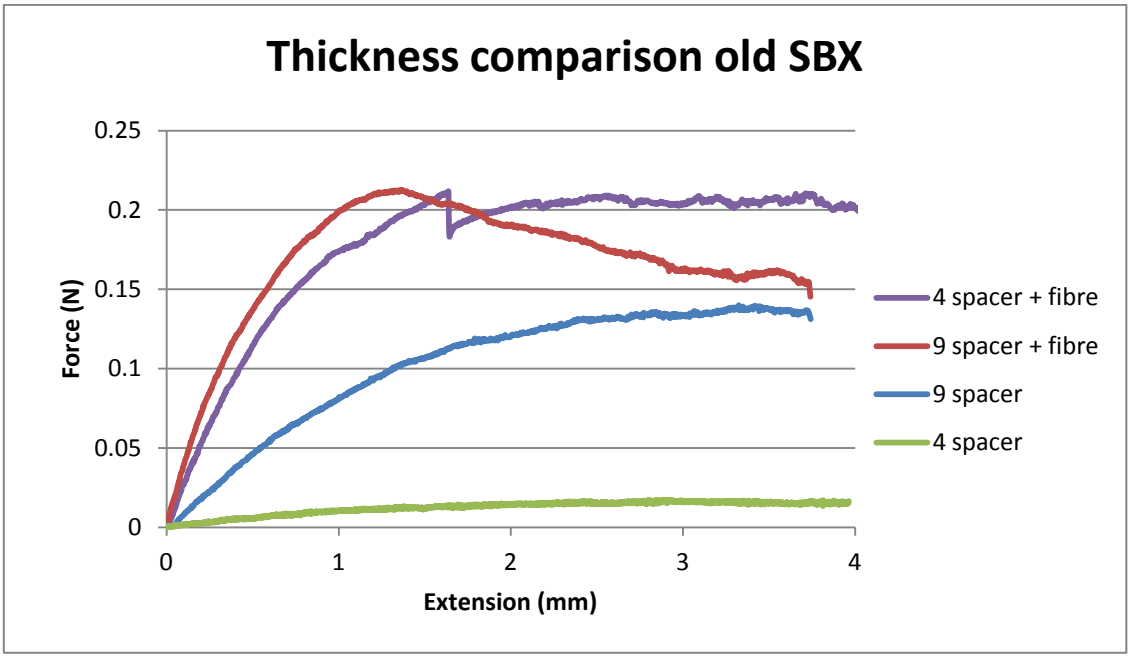

Figure 60: Thickness comparison

Thickness seemed to play a reasonable role when no fibre was in the SBX. In the case of having fibres inside there was almost no difference, at least for the thicknesses worked in this test. Another remarkable thing to notice is that for the 9 spacer SBX samples the breaking point is not clear on the curve. This could be because the SBX was thick enough to absorb all the energy of the breakage so that the machine could not appreciate it.

4.8.2.3 New SBX

Same tests as for the old SBX were done for the new SBX, adding some things thought to be interesting. The comparison of the SBX behaviour alone and with one and two fibres is shown in Figure 61 for samples made with the help of 4 and 9 spacers (different thicknesses).

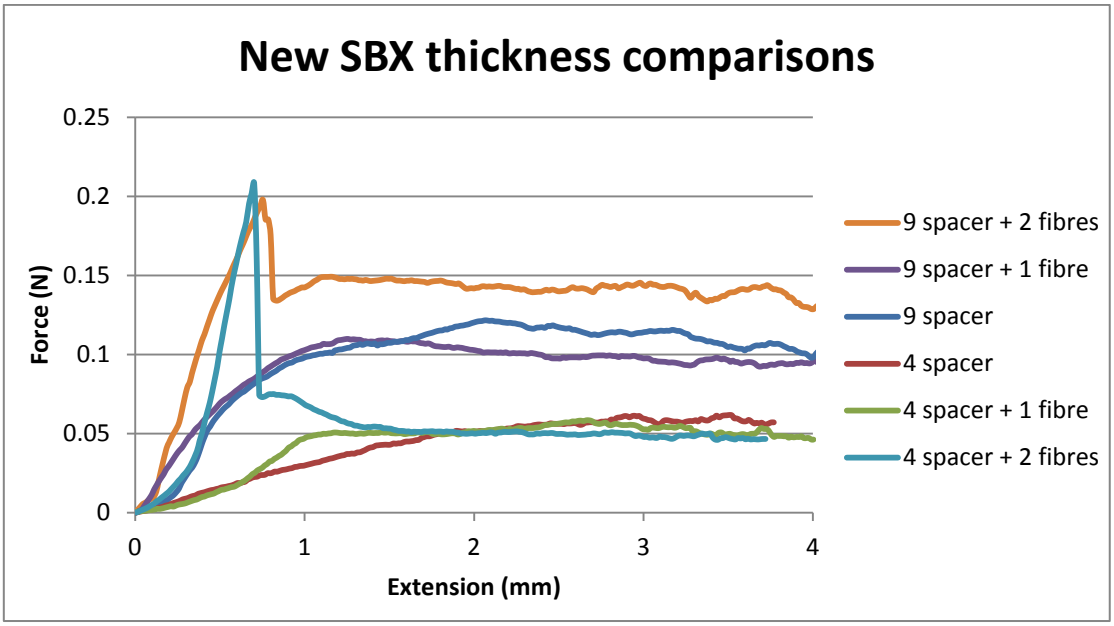

Figure 61: Different samples comparison made with 4 and 9 spacers

Firstly, comparing the thickness differences, the thicker samples offered more resistance to be bent. For the samples with two PZT fibres, the curves are pretty similar no matter the thickness. Before the breakage of the fibres, the SBX and SBX plus a fibre samples for the different thicknesses had a difference in performance of 0.05N. It can also be observed that 1 fibre is not enough to affect importantly the performance of the SBX and that all curves finally tend to the same force, the force needed to bend just SBX.

Again it was important to check how the mechanical behaviour of the SBX could change if it was left in darkness or under the sun in comparison with a sample just cured and tested (control sample). Figure 62 and Figure 63 shows these differences after 1 week time.

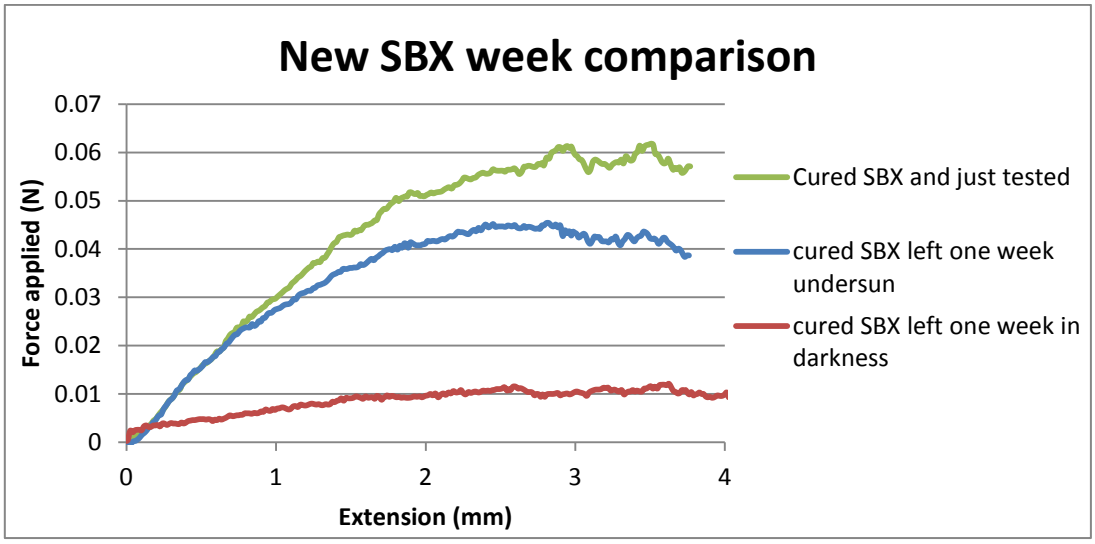

Figure 62: New SBX week comparison

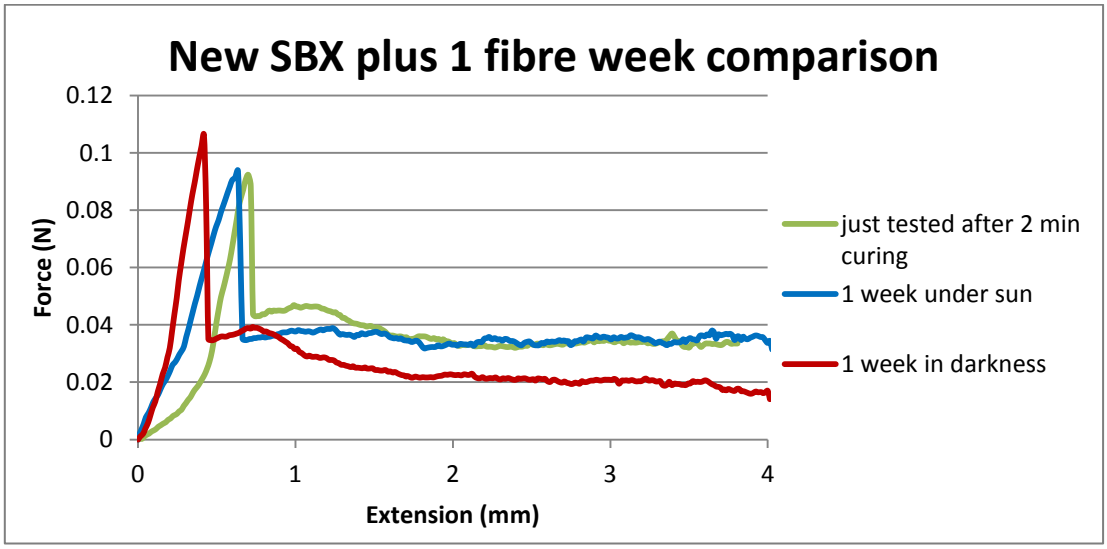

Figure 63 New SBX plus 1 fibre week comparison

For Figure 62, it is shown how the sample left in darkness had a poorer performance than the rest of the samples, even poorer than the SBX just tested after cured. It seems that its properties became worst. Surprisingly, the sample left under the sun did not perform better either. For the sample with 1 fibre, no big differences were noticed. All of them followed the same trend even for the breaking point (they broke at more or less 0.1 N). Therefore, the time and conditions at which the SBX is submitted have a great influence on its behaviour.

In Figure 64 a graph has been done in order to give an overview of the difference in performance from the fibres alone, the SBX alone and the combination of both of them.

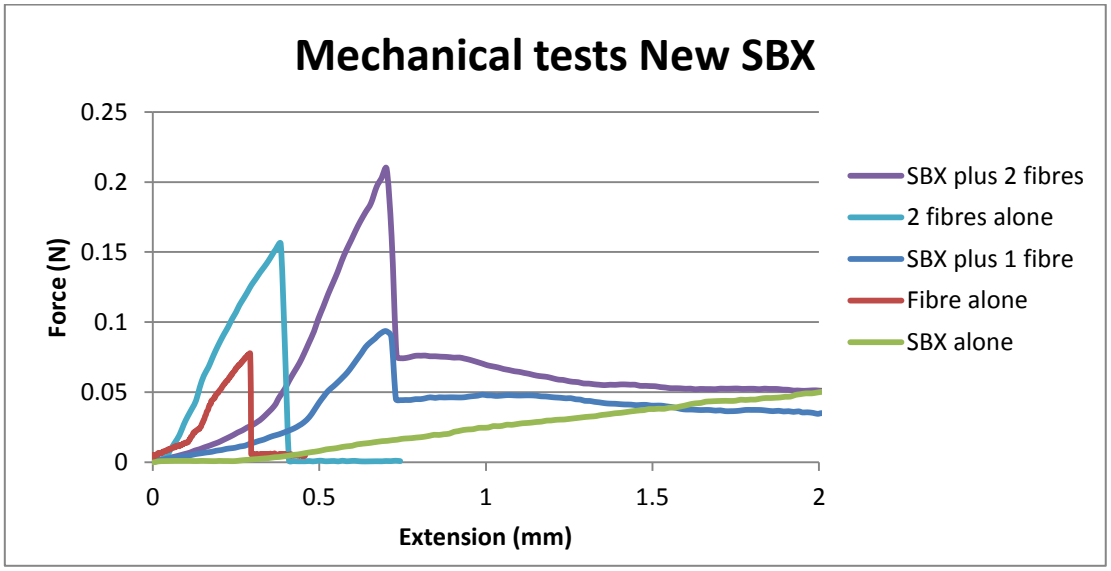

Figure 64: General comparison

The first thing that can be seen is that not only the PZT fibres alone broke in an earlier stage than the PZT fibres in SBX but they broke at higher forces applied. It is also very obvious the difference between just SBX, SBX plus a fibre and the SBX plus two fibres, increasing progressively the force needed to bend the samples.

4.8.2.4 Multi-fibre samples

The thickness of the samples was measured both on the on the carbon fibres and on the PZT fibres and are shown in Table 1.

Sample	Thickness on CF (µm)	Thickness on PZT (µm)
2CF+9PZT	478	738
6CF+2PZT	547	764
2PZT+2CF	380	718

Table 24: Multi-fibre thicknesses

The testing of some multi-fibre samples with the new SBX is shown in Figure 65. These multi-fibre samples were composed either by different PZTs, or combinations of PZTs fibres and carbon fibres (CF).

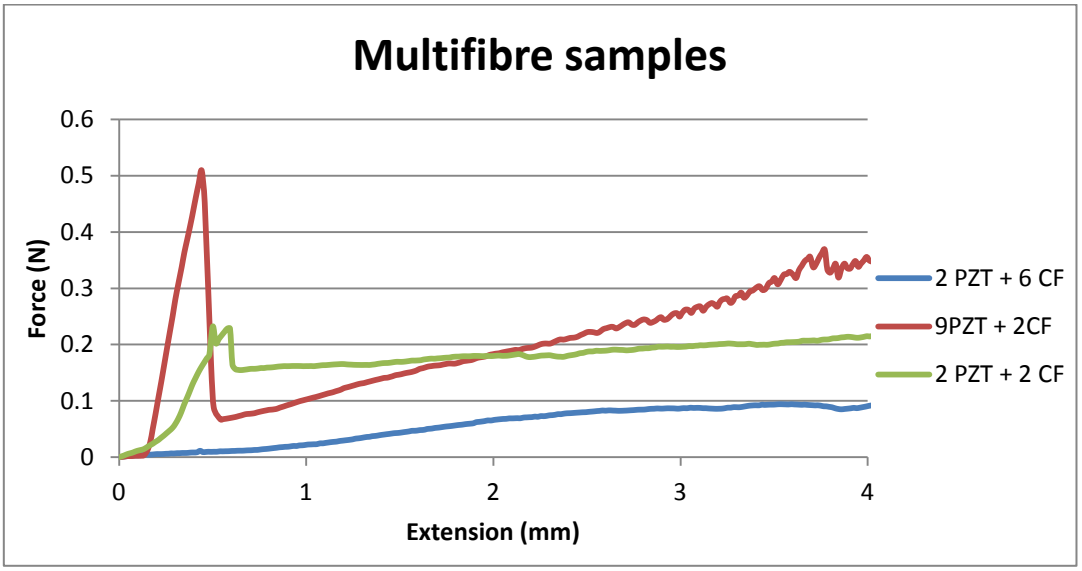

Figure 65: Multi-fibre tests with new SBX

The overall performance of all of them was much better than the simple samples tested previously. However, there is a high breaking peak at 0.5N for the 9 PZT fibres sample. It can also be noticed that layer of carbon fibres in a right angle on top of the PZT fibres is not enhancing any stress in the composite at all.

4.8.2.5 Old versus new SBX

A graph was done comparing two SBX samples, one with old and the other with new SBX, to check whether their behaviour were very different or, in the contrary they were similar.

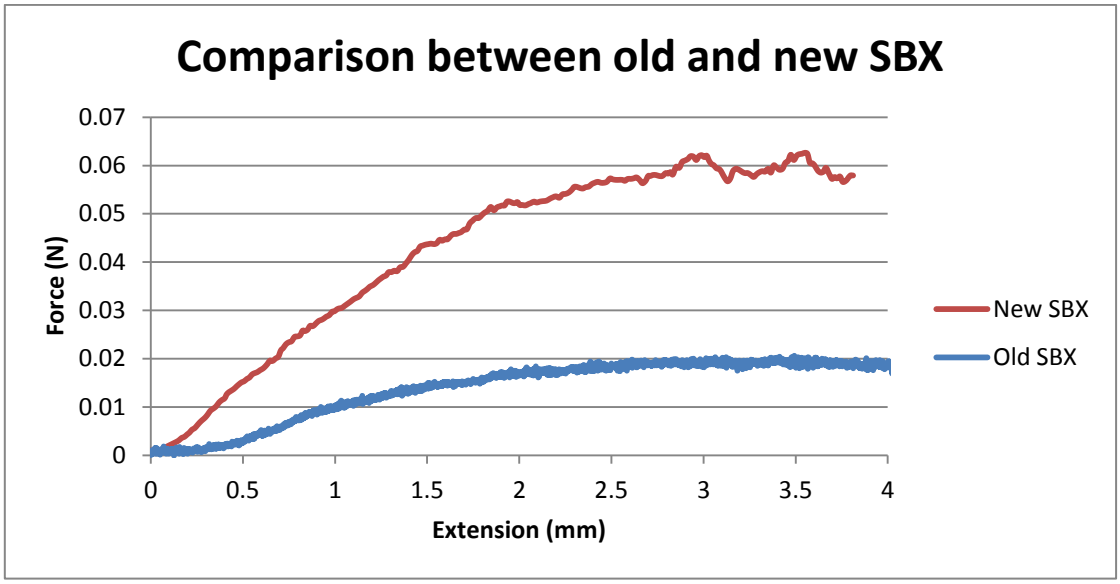

Figure 66: Comparison between old and new SBX

The new SBX visibly showed better mechanical behaviour, enabling to withstand more load for the same bending extension. This gives sense to the decision taken of having ordered a new SBX in the middle of the project.

Another comparison (Figure 67) was made for samples made out of two PZT fibres separated 0.7 mm and two carbon fibres in the right direction and on top which were separated 10mm and centred in the sample.

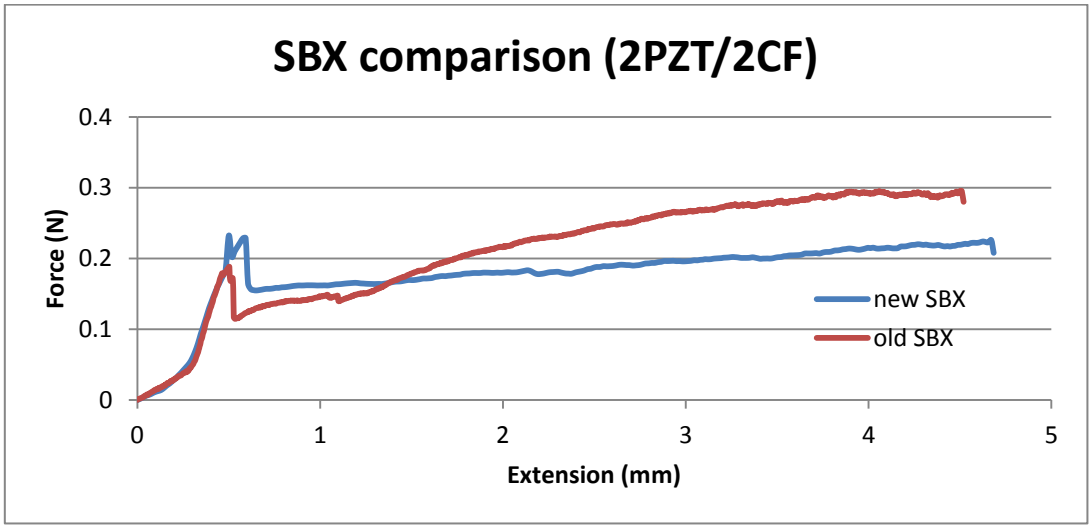

Figure 67: Comparison for the different SBX samples with carbon fibres

To begin with, the presence of carbon fibres definitely increased the force needed to bend the samples. Both curves seem to follow the same trend, especially in the beginning of the test. It is very easy to see the point at which the two PZT fibres were breaking in both cases. A curious thing is that old SBX appears to get stiffer the deeper the bending tip was going into the sample.

4.8.3 Overall conclusions

- One of reason on how sometimes there were inexplicable behaviours, for instance samples left under sun performing worst than the SBX just cured, was thought to be that the differences in thicknesses obtained for 4 and 9 spacers (the range in where thicknesses were). These differences had a big influence for such small forces and bending distances tested. Also defects like bubbles in the SBX might have influenced the results.

- The breaking points of the fibres obtained in the plots indicate that the composite should be located in a part of the body with not large vibrations as the breaking point was always around 0.5 and 2 millimetres of bending.

- These mechanical tests did not demonstrate any stress enhancement along the PZT fibres. The only way to check that would be monitoring the electricity obtained from the composite during the tests.

- The carbon fibres used for some samples tested were placed on one side of the PZT fibres instead of being in both sides and well aligned so as to enhance the stress of the PZT fibres as it would be the case of the final composite.

- The old SBX had a different behaviour than the new SBX and, although the fibres always broke before 2 millimetres of bending, which is a short range, the stress at which they broke was enhanced by adding more fibres or using carbon fibres as shown for instance in Figure 65 and Figure 67.

5 SUGGESTIONS AND FURTHER WORK

- Provided that the matrix thickness is crucial and critical to get the electrodes on the PZT fibres, other materials such as the negative resists SU-8 or Polyimide may be used for future investigations in order to have an easier thickness control than the obtained for SBX. Some more suggestions would be ORDYL, PerMX, TMMF S2030 DFR and MX5000. A good recommendation would be to use a resist which can be normally developed, instead of physically removed like the SBX

- Working with a polymer matrix such as PDMS would represent no shrinkage issues making thickness control more reliable as well as that is transparency even after cured would help for a manual alignment of the different arrays of fibres and IDEs.

- The relation of the SBX exposure time with the sample thickness could be studied to improve the development process.

- It would be interesting to do some experiments with multilayer SBX films aiming the thickness of 260 micrometers and check the development through-the-thickness as done for the sample of Table 19.

- Producing more samples like the ones made in the three approaches and poling them would be a next step. In addition to this the way to demonstrate the stress enhancing on the PZT fibre it should be monitored the electricity generated whilst testing in the microtester. Also another subsequent step would be to implement the carbon fibres in the composite.

- The method of how to align the carbon fibres between the IDE fingers and with respect to the PZT fibres has to be carefully designed so that it could be an accurate and reproducible method.

- Future mechanical tests could be compared with the result form the mechanical tests done in this thesis.

6 CONCLUSIONS

- It has not been demonstrated that the fibre arrangement thought for this application (Figure 3) enhances the stress along the PZT fibres.

- PDMS was not suitable because it was unable to absorb stresses and it was extremely flexible for this application. Some samples were made with fibres; however the fibres broke always when it was tried to remove the PDMS from the PTFE film. However, it may be that PDMS with some type of fillers probably in a polyimide film could be taken into consideration for further work.

- The thickness of the wet SBX layer plays a significant role. It was noticed during the project that if the samples were not dried on a flat surface, the thicker the samples were the more uneven they end up and hence thickness reproducibility was very much affected.

- The manual casting approach used is a proce**s**s that causes large variation in sample thicknesses and consequently it is not a good method in terms of reproducibility, especially because thicker samples were made by this method. However, for PDMS it should be fine.

- Spinning is an automatic process which could ensure reproducibility of the samples if they are spun enough time to reach the equilibrium of forces in it.

- An SBX model of the thickness in relation to the rotational spinner has been done.

- The physical development process for SBX using pressurised water seemed to be too harsh to achieve reliable resolution or continuity of the groove structure.

- Based on the mechanical tests, SBX properties changes with time depending if the sample is left under sun or left in darkness.

- Although the effect of more PZT fibre multiplies the strength of the composite within the range of forces thought for the composite to withstand (around 1 N) the limited flexibility shown would be a handicap for the composite to work if a large flexure is involved.

- The reliability of the results obtained from the old SBX emulsion samples should be viewed with caution due to the age and integrity of the emulsion.

- SBX does not seem a really suitable polymer matrix as it was first thought to be.

- A process has been design that may be implemented for another matrix material and fibres having designed even masks with mask alignments for grooves, carbon fibres and IDEs that are useful as well.

- Three feasible ways to make the IDE have been tried. Due to the rough surfaces obtained with the SBX, the deposition of the IDE in another polyimide film and then attaching it to the fibres in the SBX seemed to be the more reliable. However the electrical contact to the fibre was not good.

- A process to fabricate an active fibre composite has been given and it is shown in Figure 68.

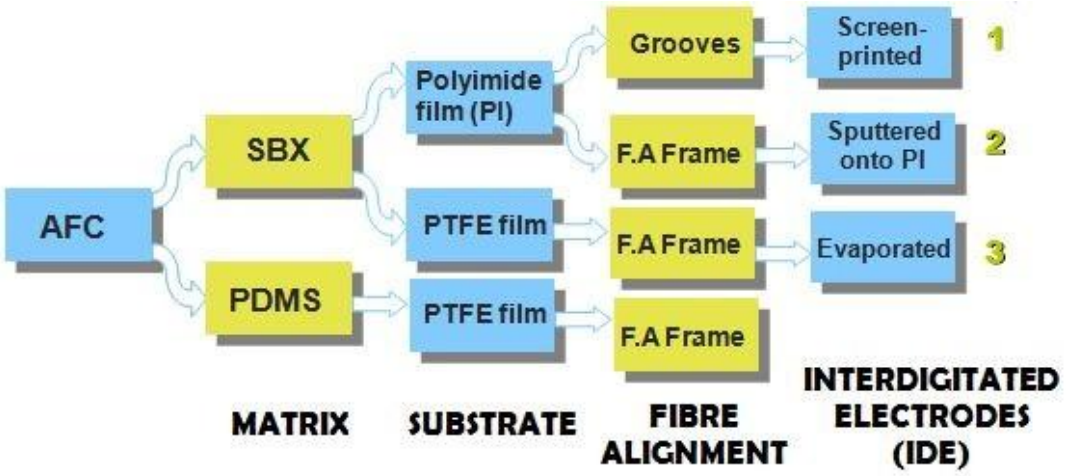

Figure 68: Process flow

REFERENCES

1. **Beeby, Stephen and White, Neil.** *Energy Harvesting for autonomous systems.* Norwood, MA, USA : Artech House, 2010.

2. *Ultra-Low-Voltage Input Power Ultra-Low-Voltage Input Power.* **Davis, Sam.** 2010, PET innovations, pp. 32-35.

3. **Kim, Sehwan and Chou, Pai H.** Energy Harvesting by Sweeping Voltage-Escalated Charging of a Reconfigurable Supercapacitor Array. [Online] July 2011. http://www.ece.uci.edu/~chou/islped11.pdf.

4. *Potential Ambient Energy-Harvesting Sources and Techniques.* **Yildiz, Faruk.** 2009, The Journal of Technology Studies, pp. 40-48.

5. **Featherston, C A, Holford, K M and Greaves, B.** *Harvesting Vibration Energy for Structural Health Monitoring in Aircraft.* Cardiff : Trans Tech Publivations, Switzerland, 2009.

6. **Blackstone-Key Ultrasonics.** Magnetostrictive Versus Piezoelectric Transducers for Power ultrasonic Applications. [Online] May 2011. http://www.blackstone-ney.com/pdfs/T_Mag_Vs_Piezo.pdf.

7. **Swiss Confereration. Federal Office ofr National Economic Supply FONES.** Energy consumption and body weight. [Online] May 2011. http://www.bwl.admin.ch/themen/00509/00528/index.html?lang=en.

8. *Human-powered wearable computing.* **Starner, T.** Riverton, NJ, USA : IBM Systems Journal., 1996, Vol. 35.

9. *Human Generated Power for Mobile Electronics.* **Starner, Thad and Paradiso, Joseph A.** Atlanta, USA : Mendeley, 2004, Low Power Electronics Design, Vol. 1990, pp. 1-35.

10. **Kazmierski, Tom J; Beeby, Steve.** *Energy Harvesting Systems, Principles Modeling and Applications.* South Hampton : Springer, New York, 2011.

11. **Callister, William D.** *Materials Science and Engineering. .* Utah : Wiley, 2007.

12. Green Energy. [Online] May 2011. [Cited: 25 May 2011.] http://www.greenenergyhelpfiles.com/piezoelectriccrystal.htm.

13. **Beeby, Stephen and White, Neil.** *Energy Harvesting for autonomous systems.* Norwood, MA, USA : Artech House, 2010.

14. **University of Cambridge.** Teaching and Learning Packages. [Online] June 2011. [Cited: 25 June 2011.] http://www.doitpoms.ac.uk/tlplib/piezoelectrics/pzt.php.

15. **Prof. Dr. J.W.M. Frenken, DR. ir. T.H. Oosterkamp nad Dr. M.J. Rost.** Interface Physics Group, Leiden Institute of Physics. *Chapter 9 Piezoelectric Scanner.* [Online] June 2011. http://www.physics.leidenuniv.nl/sections/cm/ip/Onderwijs/Scanning-Probe-Microscopy/Chapters/CHEN%20Chapter%209%20Piezoelectric%20scanner%20213-235.pdf.

16. Physik Instrumente (PI). *Fundamentals of Piezoelectric.* [Online] June 2010. http://www.physikinstrumente.com/en/products/prdetail.php?sortnr=400600.00.

17. *Nanotechnology-enabled flexible and biocompatible energy harvesting.* **Qi, Yi and McAlpine, Michael C.** Princeton, USA : Energy Environ. Sci., 2010.

18. **The Open university.** Learning Space. [Online] June 2011. http://openlearn.open.ac.uk/mod/oucontent/view.php?id=397865&section=4.3.

19. **Spom, Dieter, et al.** *Smart composites with integrated tiny piezoelectric fibers.* Germany : ICCM, 2009.

20. **Morgan Technical Ceramics.** Piezoelectric Actions. [Online] July 2011. http://www.morganelectroceramics.com/resources/piezo-ceramic-tutorials/piezoelectric-actions/.

21. *Effect of Poling Temperature on Piezoelectric Properties of 0-3 PZT-Portland Cement Composites.* **Jatianong, N and Chaipanich, A.** 1-2, Chiang Mai, Thailand : Taylor & Francis, 2008, Ferroelectric Letters, Vol. 35, pp. 17-23. DOI: 10.1080/07315170801992179.

22. *Influence of poling conditions on the piezoelectric properties of PZT ceramics.* **Takahiro, Yamakawa, Masako, Kataoka and Norikazu, Sashida.** 11, Tokyo, Japan : Kluwer Academic Publishers, 2000, Journal of amterials science: Materials in electronics, pp. 425-428.

23. **Dorey, Robert.** Electrical properties: Piezo-Pyroelectrics. MSc Advanced Materials. *Non-published.* Cranfield : Cranfield University, 2011.

24. Knowledgecenter from APC. [Online] APC International, Ltd., July 2011. http://www.americanpiezo.com/knowledge-center.html.

25. **California Institute of Technology.** Micromachining Laboratory notes. [Online] July 2011. http://mems.caltech.edu/courses/EE40%20Web%20Files/Class_Notes_Posted/08_Piezoelectricity.pdf.

26. *Polymer based interfaces as bioinspired "smart skins".* **De Rossi, Danilo, Carpi, Federico and Sciliengo, Enzo Pasquale.** 1-3, Pisa, Italy : Elsevier, 2005, Advances in Colloid and Interface Science, Vol. 116.

27. **Piezodevices.** Piezocomposites. [Online] July 2011. http://www.piezodevices.com/?page_id=14.

28. **Priya, Shashank and Inman, Daniel J.** *Energy Harvesting Technologies.* Blacksburg, VA : Springer, 2009.

29. *Monolithic Piezoelectric Actuators and Vibration Dampers with Interdigitated Electrodes.* **Yoshikawa, S, et al.** Newport Beach, CA, USA : SPIE, 1999. Smart Structures and Materials 1999: Smart Structures and Integrated Systems. p. 578.

30. *Piezoelectric Fiber Composites with Interdigitated Electrodes.* **Bent, Aaron A and Hagood, Nesbitt W.** Cambridge : J Int Mater. Syst. Struct, 1997.

31. *Recent advances in active fiber composites technology.* **Rossetti, George A, Pizzochero, Alessandro and Bent, Aaron A.** Honolulu, HI , USA : Continuum Control Corp., 2002, Vols. (2) Applications of Ferroelectrics, 2000. ISAF 2000. Proceedings of the 2000 12th IEEE International Symposium, pp. 753-756. ISBN: 0-7803-5940-2 , D.O.I: 10.1109/ISAF.2000.942429.

32. **Bowen, C R, et al.** *Failure and volume fraction dependent mechanical properties of composite sensors and actuators.* Bath & Teddington, UK : Professional Engineering Publishing, 2006. pp. 1655-1663. DOI: 10.1243/09544062JMES255.

33. **Nelson, L J.** *Smart piezoelectric fibre composites.* Bath : Maney for the Institute of Materials, Minerals and Mining., 2002.

34. *Development of piezoelectric composites for transducers.* **Safari, A.** 4, New Jersey : Mendeley, 1994, J. Phys. III Fiance, pp. l129-1149 .

35. *An experimental investigation on the effect of environmental stress on Active Fiber Composite actuators.* **Morris, Donald G, Hagood, Nesbitt and Pizzochero, Alessandro.** Newport Beach, California : SPIE Digital Library, 1999. SPIE Conference on Industrial and Commercial Applications of Smart Structures. Vol. 3674.

36. *Low-Cost Piezocomposite Actuator for Structural Control Applications.* **Keats Wilkie, W, et al.** Langley, Hampton, USA : SPIE, 2000. Smart Structures adn Materials 2000: Industrial and commercial Applications of Smart Structures Technologies. p. 12.

37. *Piezoelectric Composites as Bender Actuators.* **Mossi, Karla, Bryant, Robert and Mane, Poorna.** Hampton, Virgina, USA : Taylor & Francis Inc, 2005, Vol. 71, pp. 221-232. DOI: 10.1080/10584580590964673.

38. **Emery, Chris.** Energy-harvesting rubber sheets could power pacemakers, mobile phones. *News at Princeton University.* [Online] January 2010. http://www.princeton.edu/main/news/archive/S26/47/03A23/index.xml?section=topstories.

39. *Enhanced Piezoelectricity and Stretchability in Energy Harvesting Devices Fabricated from Buckled PZT Ribbons.* **Qi, Yi, et al.** 3, 2011, Nano Letters, Vol. 11, pp. 1331-1336.

40. **Centeno, Anthony.** *Available Power from Piezoelectric Energy Harvesters.* London : Department of Materials. Imperial College London, 2010.

41. CTS electronic Components. *PZT5A & 5H Materials Technical Data (Typical Values).* [Online] July 2011. http://www.ctscorp.com/components/pzt/downloads/PZT_5Aand5H.pdf.

42. *Analysis of power generating performance for unimorph cantilever piezoelectric beams with interdigitated electrodes.* **Mo, Changki, Kim, Sunghwan and Clark, William W.** s.l. : ASME Digital Library, 2006. ASME 2005 International Design Engineering Technical Conferences and Computers and Information in Engineering Conference (IDETC/CIE2005). Vol. 1, pp. 2449-2454. DOIi:10.1115/DETC2005-85657.

43. *An experimental comparison between several active composite actuators for power generation.* **Sodano, Henry, Lloyd, Justin and Inman, Daniel.** Blacksburg, Virginia, USA : IOP Science, 2006, Smart Materials and Structures.

44. *Energy scavenging sources for biomedical sensors.* **Neuman, M R, Warrington, R O and Romero, E.** 8, Michigan, USA : IOP Science, 2009, Physiological Measurement, Vol. 32.

45. **Kendall, Clyde Jake.** *Parasitic Power collection in Shoe Mounted Devices.* Massachusetts : Massachusetts Institute of Technology, 1998.

46. **Shenck, Nathan S.** *A demonstration of Useful Electric Energy Generation from Piezoceramics in a Shoe.* Massachusetts : Massachusetts Institute of Technology, 1999.

47. *Harvested power and sensitivity analysis of vibrating shoe-mounted piezoelectric cantilevers.* **Moro, L and Benasciutti, D.** 19, Udine, Italy : IOP publishing, 2010, Smart Materials and Structures.

48. *Energy scavenging with shoe-mounted piezoelectrics.* **Shenck, Nathan S and Paradiso, Joseph A.** Media Lab., MIT, Cambridge, MA. : IEEE Computer Society , 2001. IEEE Micro. Vol. 21 Issue 3, pp. 30-42.

49. *Generating Electricity While Walking with Loads.* **Rome, Lawrence C, et al.** 5741, s.l. : Science, 2005, Vol. 309, pp. 1725-1728.

50. *Converting biomechanical energy into electricity by a muscle-movement-driven nanogenerator.* **Yang, Rusen, et al.** 3, Atlanta, Georgia, USA : Nanoletters, 2009, Vol. 9, pp. 1201-1205.

51. *Muscle-Driven In Vivo Nanogenerator.* **Li, Zhou, et al.** 23, s.l. : Wiley InterScience, 2010, Advanced Materials, Vol. 22, pp. 2534–2537. DOI: 10.1002/adma.200904355.

52. *Air/Liquid-Pressure and Heartbeat-Driven Flexible Fiber Nanogenerators as a Micro/Nano-Power Source or Diagnostic Sensor.* **Li, Zetang and Wang, Zhong Lin.** Weinheim : WILEY-VCH Verlag GmbH & Co, 2011, Advanced Materials, Vol. 23, pp. 84-89.

53. *Piezoelectric Ribbons Printed onto Rubber for Flexible Energy Conversion.* **QI, Yi, et al.** 2, s.l. : American Chemical Society, 2010, Nano Letters, Vol. 10, pp. 524-528. DOI: 10.1021/nl903377u.

54. *Using Piezoelectric Materials for Wearable Electronic Textiles.* **Edmison, Joshua, et al.** Blackburg, Virginia, USA : Ieee. Proceedings Sixth International Symposium on Wearable Computers (2002). Vol. 7, pp. 41-48. 10.1109/ISWC.2002.1167217.

55. *Overview Using Piezoelectric Materials for Wearable Electronic Textiles Related work : E-textiles Our e-Textile Viewpoint Related work : E-textiles Piezoelectric materials Piezoelectric materials : Uses Piezoelectric materials : Form factors Piezoelectric.* **Edmison, Joshua, et al.** Blackburg, Virginia, USA : Mendeley, 2002. pp. 6-9.

56. *Inclusion of Fabric Properties in the Design of Electronic Textiles.* **Quirk, Meghan M.** Blacksburg, Virginia, USA : s.n., 2009.

57. *Architectures for e-Textiles.* **Nakad, Zahi S.** Blacksburg, Virginia, USA : s.n., 2003. Proceedings of the Sixth International Symposium on Wearable Computing. ISWC 2002.

58. *Analyzing the Use of E-textiles to Improve Application Performance.* **Jones, Mark, et al.** Blacksburg, VA, USA : s.n., 2003, IEEE Vehicular Technology Conference 2003, Symposium on Wireless Adhoc, Sensor, and Wearable Networks , Vol. 5, pp. 2875-2880. 10.1109/VETECF.2003.1286137 .

59. **Barron, Chris.** RushPC News. *Research may make screen scrollable.* [Online] http://www.rushpc.com/shownews.php?docid=392.

60. **Soldier Systems Center (Natick).** Active fabric. [Online] April 2003. http://www.natick.army.mil/about/pao/pubs/warrior/02/janfeb/smartclo.htm.

61. **Kenyon, Henry S.** AFCEA International. *Dressing the Wired Warrior.* [Online] November 2001. http://www.afcea.org/signal/articles/anmviewer.asp?a=475&print=yes.

62. **Rangeresque.** Project Horizon. [Online] July 2011. http://www.tacticalwarfightergear.com/tacticalgear/catalog/Army_Technology.php.

63. *E-broidery: Design and fabrication of textile-based computing .* **Post, E R, et al.** 3&4, 2000, IBM Systems Journal, Vol. 39.

64. *Electrostatic power harvesting for material computing.* **Post, E Rehmi and Waal, Kit.** 2, London : Springer , 2011, Personal and Ubiquitous Computing, Vol. 15, pp. 115-121. DOI: 10.1007/s00779-010-0313-9.

65. **Guillot, François M, Becham, Haskell W and Leisen, Johannes.** *Piezoelectric Fabrics for Energy Harvesting.* Georgia : National Textile Center, 2009.

66. **Defence Science and Technology Organization.** Energy harvesting journal. *Body vibration energy to power soldiers' electronics.* [Online] July 2011. http://www.energyharvestingjournal.com/articles/body-vibration-energy-to-power-soldiers-electronics-00003551.asp?sessionid=1.

67. **Instron.** Materials Testing Solution. *Literature.* [Online] July 2011. http://www.instron.co.uk/wa/applications/test_types/flexure/default.aspx.

68. **Kopeliovich, Dmitri.** SubsTech Substances & Technologies. *Flexural strength test of ceramics.* [Online] December 2010. http://www.substech.com/dokuwiki/doku.php?id=flexural_strength_tests_of_ceramics.

69. **IKONICS IMAGING.** IKONICS IMAGING. *Sandcarving systems.* [Online] July 2010. http://www.ikonicsimaging.com/pdf/priceinfo_sbx.pdf.

70. **MEMS&Nanotechnology Exchange (MNX).** MEMSnet. [Online] July 2011. http://www.memsnet.org/mems/processes/deposition.html.

71. **Components, Packaging and Manufacturing Technology Society.** IIEE. *Components, Packaging and Manufacturing Technology.* [Online] August 2011. http://www.cpmt.org/mm/pkglab/theory/spin_theory.html.

72. *Series connection of supercapacitors, with an active device for equalizing the voltages.* **Barrade, Philippe, Pittet, Serge and Rufer, Alfred.** 2010, Laboratory of Industrial Electroniucs. Swiss Federal Insittute of technology Lausanne.

73. *Mechanical Energy Harvester With Ultralow Threshold Rectification Based on SSHI Nonlinear Technique.* **Gaurbio, Lauric, et al.** 4, April 2009, IEEE TRANSACTIONS ON INDUSTRIAL ELECTRONICS, Vol. 56, pp. 1048-1054.

74. *The cellular response to curvature-induced stress.* **Biton, Y Y and Safran, S A.** 4, Rehovot, Israel : IOP Science, 2009, Phys. Biol., Vol. 6, pp. 1-8. doi:10.1088/1478-3975/6/4/046010.

75. **Apiezon.** Apiezon Wax W W40 & W100. *Vacuum Sealing and Mounting Waxes.* [Online] July 2011. http://www.tedpella.com/technote_html/891-81_891-85_Apiezon-Wax-TN.pdf.